Superfocusing modes of surface plasmon polaritons in a wedge-shaped geometry obtained by quasi-separation of variables

2008 J. Phys. A: Math. Theor. 41 295401

(http://iopscience.iop.org/1751-8121/41/29/295401)

IOP PUBLISHING JOURNAL OF PHYSICS A: MATHEMATICAL AND THEORETICAL

J. Phys. A: Math. Theor. **41** (2008) 295401 (48pp) doi:10.1088/1751-8113/41/29/295401

Superfocusing modes of surface plasmon polaritons in a wedge-shaped geometry obtained by quasi-separation of variables

Kazuyoshi Kurihara[1], **Kazuhiro Yamamoto**[1], **Junichi Takahara**[2] **and Akira Otomo**[1]

[1] Kobe Advanced ICT Research Center, National Institute of Information and Communications Technology (NICT), Kobe 651-2492, Japan
[2] Department of Systems Innovation, Graduate School of Engineering Science, Osaka University, Toyonaka 560-8531, Japan

E-mail: k-kuri@nict.go.jp

Received 11 January 2008, in final form 30 May 2008
Published 24 June 2008
Online at stacks.iop.org/JPhysA/41/295401

Abstract

Analytic solutions to the superfocusing modes of surface plasmon polaritons in the wedge-shaped geometry are theoretically studied by solving the Helmholtz wave equation for the magnetic field using quasi-separation of variables in combination with perturbation methods. The solutions are described as a product of radial and extended angular functions and are obtained for a lossless metallic wedge and V-groove by determining the separation quantities that satisfy the boundary conditions. For the metallic wedge and V-groove, we show that the radial functions of the zeroth order are approximately described by the imaginary Bessel and modified Whittaker functions, respectively, and that the extended angular functions have odd and even symmetries, respectively, for reflection in the central plane of the wedge-shaped geometry. Importantly, we show that the wave numbers of superfocusing surface plasmon polaritons in the metallic wedge and V-groove are clearly different in their radial dependence.

PACS numbers: 02.30.Mv, 41.20.Gz, 42.25.Bs, 78.20.−e, 78.20.Bh

1. Introduction

Superfocusing is a concept for waves of any nature to be confined to a length scale significantly smaller than the diffraction limit of the focused waves. The superfocusing phenomenon is being intensively investigated in the field of nano-optics [1] as a possible technique to focus electromagnetic radiation in a region of the order of a few nanometers beyond the diffraction limit of light and thereby causing an extraordinary enhancement of the electromagnetic field. Superfocusing in optics is technically feasible with tapered metal tips, in which the

surface plasmon polaritons (SPPs) [2] that freely propagate along the metallic surface are gradually slowed down as they approach the tapered tip and stopped at the extremity where they accumulate as localized SPPs. Plasmonic superfocusing provides a possible way of optical confinement for practical applications such as optical nanolithography [3–7], nano-optical integrated circuits [8–11], high-resolution near-field optical microscopy [12], high-density optical data storage [13] and optical nanospectroscopy-based surface-enhanced Raman scattering (SERS) [14–20]. Moreover, the investigations on another type of superfocusing, acoustic superfocusing [21], have been started.

The possibility of plasmonic superfocusing, as far as we know, was theoretically studied for the first time by Nerkararyan [22], who discussed the peculiarity of SPP propagation in metallic wedge-shaped structures by approximately solving the Helmholtz wave equation by separation of variables—this method cannot be applied to obtain an exact solution—and suggested that the same conclusion could be reached by using the geometrical-optics approximation (almost equivalently, the eikonal approximation). Until quite recently, the problem of plasmonic superfocusing in tapered metal tips has been theoretically attacked by either the separation of variables approximation [22–24] or the geometrical-optics approximation [25–32]. Although these methods appear quite different, they reach the same conclusion; therefore, they are approximations of the same level. Apart from analytic methods, numerical methods based on finite-difference time-domain (FDTD) algorithms have been frequently applied [9, 33–39], but these methods cannot provide as deep a physical insight as analytic methods can do. In a preceding paper [40], as an analytic method for solving the Helmholtz wave equation of plasmonic superfocusing, we proposed a new approach based on quasi-separation of variables, which implies an incomplete separation of variables in comparison with the conventional one. This new approach provides an approximation of a higher level than the previous approaches of separation of variables and geometrical optics.

The present paper reexamines plasmonic superfocusing in a wedge-shaped geometry, which was previously studied by Nerkararyan [22] and Gramotnev [26, 29], by using a new approach based on quasi-separation of variables in combination with the perturbation method. We investigate two wedge-shaped geometries, a lossless metallic wedge and V-groove, by solving the zeroth- and first-order perturbation equations obtained when the solutions obtained by quasi-separation of variables are assumed to satisfy the Helmholtz wave equation for magnetic field. Physically important results and concepts can be obtained by solving the zeroth-order perturbation equations. More accurate solutions can be obtained by solving the first- and higher-order perturbation equations. In order to understand the solutions intuitively, electric-field-line representations are very useful. Peculiarities of superfocusing SPPs are briefly characterized by the dependences of the wave numbers on the distance from the wedge apex, which are obtained by applying the Liouville–Green approximation [41, 42] to the zeroth-order radial equations. Surprisingly, the new approach based on quasi-separation of variables gives a new finding that the radial dependence of the wave numbers of the superfocusing SPPs in the metallic wedge is clearly different from those of the superfocusing SPPs in the metallic V-groove. This conclusion has never been reached by following the two previous approaches, although it was suggested by numerical analysis based on an FDTD algorithm[3].

The plan of this paper is as follows. In section 2, we begin by assuming solutions based on quasi-separation of variables to the Helmholtz wave equation for the magnetic field and introduce quasi-separation invariants, simply called separation quantities, in order to separate the Helmholtz equation and obtain the radial and extended angular equations.

[3] Superfocusing behavior in the metallic wedge was not observed as clearly as that for the metallic V-groove shown in [9].

The radial equations are linear, second-order, homogeneous, ordinary differential equations (ODEs), while the angular equations are differential equations that appear unsolvable at first glance. In section 3, we unify the radial equations separately described in the metallic and dielectric regions by considering two asymptotic boundary conditions at infinite and infinitesimal distances from the wedge apex. Accordingly, the separation quantities separately described in the metallic and dielectric regions are also unified. In section 4, we explicitly describe the boundary conditions for the unified radial and extended angular functions. In section 5, we introduce a perturbation parameter to solve the extended angular equations by means of perturbation methods and rewrite the extended angular equations, the unified radial equation and the boundary conditions according to the order of the perturbation parameter. In section 6, we discuss the zeroth-order perturbation equations for the metallic wedge and V-groove. First, the symmetries of the extended angular functions with respect to the central plane of the wedge-shaped geometry are determined by considering the existence conditions for the unified separation quantities as positive real numbers. Second, the unified separation quantities are numerically determined and fitted to suitable figure-of-merit functions used for analytically solving the zeroth-order radial equations. Third, solutions of the zeroth-order radial equations are approximately given by already-known special functions. Fourth, the zeroth-order amplitude reflection coefficients for plasmonic superfocusing are obtained. In sections 7 and 8, we discuss the first-order perturbation solutions for the metallic wedge and V-groove, respectively. In section 9, we describe electric-field-line representation to visually and intuitively express the solutions to the zeroth- and first-order perturbation equations. In section 10, we express the wave numbers of superfocusing SPPs as analytic formulas. In section 11, we briefly summarize the main points of this paper. In addition, four appendices are included. In appendix A, we fully explain the asymptotic expansions for the modified Whittaker functions used in section 10. In appendix B, we briefly explain the relations of Whittaker functions used in section 6. In appendices C and D, we give the second-order perturbation solutions for the metallic wedge and V-groove, respectively, which can be used in future plasmonic superfocusing research.

2. Quasi-separation of variables applied to the wave equation for a magnetic field

We consider two wedge-shaped structures: a metallic wedge surrounded by dielectric and a dielectric wedge surrounded by metal, which will simply be called the metallic wedge and the metallic V-groove, respectively. As shown in figure 1, the cylindrical coordinates (ρ, ϕ, z) can be used to describe an infinite wedge with an angle 2α $(0 < \alpha < \pi/2)$ and permittivity ε_1, surrounded by matter with permittivity ε_2. In case where the imaginary parts of the permittivities are ignored, we have the conditions $\varepsilon_1 < 0$, $\varepsilon_2 > 0$ for the metallic wedge and the conditions $\varepsilon_1 > 0$, $\varepsilon_2 < 0$ for the metallic V-groove. We consider simple superfocusing of SPPs with translational symmetry about the z-axis, whose magnetic field at time t at the point located by the coordinate vector $\boldsymbol{x}$ is $\boldsymbol{H}(\boldsymbol{x}, t)$ that is directed along the z-axis and depends on ρ and ϕ; therefore, it is written as

$$\boldsymbol{H}(\boldsymbol{x}, t) = (0, 0, H_z(\rho, \phi, t)). \tag{1}$$

Beginning with the Maxwell equations in the absence of sources, we assume that the time dependence of all the fields is given by $\mathrm{e}^{-\mathrm{i}\omega t}$; hence, we can write

$$H_z(\rho, \phi, t) = \mathrm{Re}[H_z(\rho, \phi)\,\mathrm{e}^{-\mathrm{i}\omega t}]. \tag{2}$$

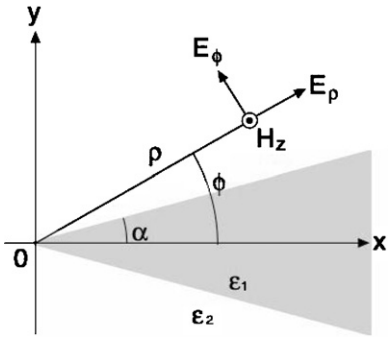

Figure 1. Geometry for a metallic wedge or V-groove where superfocusing of SPPs takes place at the tip. α is half the wedge angle. ε_1 and ε_2 are the permittivities inside and outside the wedge, respectively. H_z is the magnetic field of superfocusing SPPs with translational symmetry about the z-axis. E_ρ and E_ϕ are the electric fields of the radial and angular components, respectively, induced by H_z.

The two Maxwell curl equations can be combined to give the Helmholtz wave equation for the magnetic field in equation (2), namely,

$$\frac{1}{\rho}\frac{\partial}{\partial\rho}\left(\rho\frac{\partial H_{zj}(\rho,\phi)}{\partial\rho}\right)+\frac{1}{\rho^2}\frac{\partial^2 H_{zj}(\rho,\phi)}{\partial\phi^2}+\varepsilon_j\frac{\omega^2}{c^2}H_{zj}(\rho,\phi)=0, \qquad j=1,2 \tag{3}$$

with the definition of the magnetic field $H_z(\rho,\phi)$ in the metallic and dielectric regions given as

$$H_z(\rho,\phi)=\begin{cases}H_{z1}(\rho,\phi), & |\phi|\leqslant\alpha\\ H_{z2}(\rho,\phi), & \alpha\leqslant|\phi|\leqslant\pi,\end{cases} \tag{4}$$

where ω is the angular frequency of interest and c is the velocity of light in vacuum. The magnetic field $H_z(\rho,\phi)$ in equation (4) may be classified into even (+) or odd (−) symmetries with respect to ϕ, because the geometrical structure in figure 1 is invariant for reflection in the $\phi=0$ plane ($\rho\to\rho$, $\phi\to-\phi$, $z\to z$) and the differential operator of the Helmholtz wave equation (3) is even under the reflection transformation. As is done in the preceding paper [40], we look for the solutions of the following form by using quasi-separation of variables:

$$H_{zj}(\rho,\phi)=R_j(\rho)Q_j^s(\phi,\rho), \qquad j=1,2 \tag{5}$$

with the boundary conditions

$$Q_j^s(\alpha,\rho)=1, \qquad j=1,2 \tag{6}$$

to determine $Q_j^s(\phi,\rho)$ uniquely, where s indicates either the even (+) or odd (−) symmetry with respect to ϕ. Substituting equation (5) into equation (3), we get

$$\begin{aligned}&-\left(\frac{\rho}{R_j(\rho)}\frac{\partial}{\partial\rho}\left(\rho\frac{\partial R_j(\rho)}{\partial\rho}\right)+\varepsilon_j\frac{\omega^2}{c^2}\rho^2\right)\\ &=\left(\begin{aligned}&\frac{1}{Q_j^s(\phi,\rho)}\frac{\partial^2 Q_j^s(\phi,\rho)}{\partial\phi^2}+\frac{\rho^2}{Q_j^s(\phi,\rho)}\frac{\partial^2}{\partial\rho^2}Q_j^s(\phi,\rho)\\ &+\frac{2\rho^2}{R_j(\rho)Q_j^s(\phi,\rho)}\left(\frac{\partial R_j(\rho)}{\partial\rho}\right)\frac{\partial Q_j^s(\phi,\rho)}{\partial\rho}+\frac{\rho}{Q_j^s(\phi,\rho)}\frac{\partial Q_j^s(\phi,\rho)}{\partial\rho}\end{aligned}\right), \qquad j=1,2.\end{aligned} \tag{7}$$

Since the left side of equation (7) depends on ρ alone, while the right side depends on both ρ and ϕ, both the sides must depend on ρ alone. Setting both the sides equal to $\zeta_j(\rho)$, we obtain

$$\frac{\rho}{R_j(\rho)}\frac{\partial}{\partial\rho}\left(\rho\frac{\partial R_j(\rho)}{\partial\rho}\right)+\varepsilon_j\frac{\omega^2}{c^2}\rho^2=-\zeta_j(\rho),\qquad j=1,2 \tag{8}$$

and

$$\begin{aligned}&\frac{1}{Q_j^s(\phi,\rho)}\frac{\partial^2 Q_j^s(\phi,\rho)}{\partial\phi^2}+\frac{\rho^2}{Q_j^s(\phi,\rho)}\frac{\partial^2}{\partial\rho^2}Q_j^s(\phi,\rho)\\&+\frac{2\rho^2}{R_j(\rho)Q_j^s(\phi,\rho)}\left(\frac{\partial R_j(\rho)}{\partial\rho}\right)\frac{\partial Q_j^s(\phi,\rho)}{\partial\rho}\\&+\frac{\rho}{Q_j^s(\phi,\rho)}\frac{\partial Q_j^s(\phi,\rho)}{\partial\rho}=\zeta_j(\rho),\qquad j=1,2.\end{aligned} \tag{9}$$

Here, $\zeta_j(\rho)$ for $j=1,2$ are called quasi-separation invariants, or simply separation quantities, in analogy with the separation constants in ordinary separation of variables. Multiplying equation (8) by $R_j(\rho)/\rho^2$ and rearranging terms, we find the following radial equations:

$$\frac{\partial^2 R_j(\rho)}{\partial\rho^2}+\frac{1}{\rho}\frac{\partial R_j(\rho)}{\partial\rho}+\left(\frac{\zeta_j(\rho)}{\rho^2}+\varepsilon_j\frac{\omega^2}{c^2}\right)R_j(\rho)=0,\qquad j=1,2. \tag{10}$$

Multiplying equation (9) by $Q_j^s(\phi,\rho)$ and rearranging terms, we obtain the following extended angular equations:

$$\frac{\partial^2 Q_j^s(\phi,\rho)}{\partial\phi^2}-\zeta_j(\rho)Q_j^s(\phi,\rho)=-F_j^s(\phi,\rho),\qquad j=1,2 \tag{11}$$

where

$$F_j^s(\phi,\rho)=\rho^2\frac{\partial^2}{\partial\rho^2}Q_j^s(\phi,\rho)+\frac{2\rho^2}{R_j(\rho)}\left(\frac{\partial R_j(\rho)}{\partial\rho}\right)\frac{\partial Q_j^s(\phi,\rho)}{\partial\rho}+\rho\frac{\partial Q_j^s(\phi,\rho)}{\partial\rho},\qquad j=1,2. \tag{12}$$

Now, we can replace equation (3) with equations (10) and (11) that satisfy the boundary conditions (6).

3. Unification of the radial equations

The radial equations (10), which are separately expressed in the two different regions $j=1,2$, are considered for two limiting cases of $\rho\to 0$ and $\rho\to\infty$, in order to find a unified form of these equations for SPPs propagating along a metal–dielectric interface.

For $\rho\to 0$, since the conditions

$$\frac{|\zeta_j(0)|}{\rho^2}\gg|\varepsilon_j|\frac{\omega^2}{c^2},\qquad j=1,2\qquad(\rho\to 0) \tag{13}$$

are acceptable unless $\zeta_j(0)=0$, the radial equations (10) become

$$\frac{\partial^2 R_j(\rho)}{\partial\rho^2}+\frac{1}{\rho}\frac{\partial R_j(\rho)}{\partial\rho}+\frac{\zeta_j(0)}{\rho^2}R_j(\rho)=0,\qquad j=1,2\qquad(\rho\to 0), \tag{14}$$

in which we lose the material terms ε_j for separately describing the radial equations (10) in the two regions. This suggests that we should use a unified notation for the two different regions in equation (14). Setting

$$\zeta_u(0) = \zeta_j(0), \qquad j = 1, 2 \tag{15}$$

$$R_u(\rho) = R_j(\rho), \qquad j = 1, 2 \qquad (\rho \to 0) \tag{16}$$

as the unified notation, we rewrite equations (14) as

$$\frac{\partial^2 R_u(\rho)}{\partial \rho^2} + \frac{1}{\rho}\frac{\partial R_u(\rho)}{\partial \rho} + \frac{\zeta_u(0)}{\rho^2} R_u(\rho) = 0 \qquad (\rho \to 0), \tag{17}$$

which gives asymptotic solutions for $R_u(\rho)$ as $\rho \to 0$. Two nontrivial linearly independent particular solutions to equation (17) are given by

$$R_u(\rho) = \exp\left(\mathrm{i}\nu \ln \rho\right), \qquad \exp\left(-\mathrm{i}\nu \ln \rho\right) \qquad (\rho \to 0) \tag{18}$$

where

$$\nu = \sqrt{\zeta_u(0)}. \tag{19}$$

Remembering the time dependence $\mathrm{e}^{-\mathrm{i}\omega t}$ in equation (2), we see that $\exp\left(\mathrm{i}\nu \ln \rho\right)$ and $\exp\left(-\mathrm{i}\nu \ln \rho\right)$ in equation (18) correspond to the outgoing and incoming waves, respectively, involving a logarithmic phase singularity that can express the superfocusing process in the limiting case $\rho \to 0$ when ν in equation (19) is a positive real number,

$$\nu > 0. \tag{20}$$

For $\rho \to \infty$, since the physical situation is considered to be the same as for SPPs in the planar geometry, the radial equations (10) can be described with a unified notation for the two regions in the form

$$R_u(\rho) = R_j(\rho), \qquad j = 1, 2 \qquad (\rho \to \infty) \tag{21}$$

and this equation satisfies the Sommerfeld radiation conditions [43]

$$\lim_{\rho\to\infty} R_u(\rho) = O\left(\frac{1}{\sqrt{\rho}}\right), \qquad \lim_{\rho\to\infty} \sqrt{\rho}\left(\frac{\partial R_u(\rho)}{\partial \rho} \pm \mathrm{i}k_p R_u(\rho)\right) = 0 \tag{22}$$

where k_p is the wave number of SPPs in the planar geometry, given by [44, 45]

$$k_p = \frac{\omega}{c}\sqrt{\frac{\varepsilon_1\varepsilon_2}{\varepsilon_1 + \varepsilon_2}} \tag{23}$$

with the SPP existence conditions

$$\varepsilon_1\varepsilon_2 < 0, \tag{24}$$

$$\varepsilon_1 + \varepsilon_2 < 0 \tag{25}$$

for permittivities $\varepsilon_1, \varepsilon_2$ being real numbers. The radiation conditions (22) yield two asymptotic solutions

$$R_u(\rho) = \frac{\exp(\mathrm{i}k_p\rho)}{\sqrt{\rho}}, \qquad \frac{\exp(-\mathrm{i}k_p\rho)}{\sqrt{\rho}} \qquad (\rho \to \infty), \tag{26}$$

which are two nontrivial linearly independent particular solutions of the following ODE:

$$\frac{\partial^2 R_u(\rho)}{\partial \rho^2} + \frac{1}{\rho}\frac{\partial R_u(\rho)}{\partial \rho} + \left(-\frac{1}{4\rho^2} + k_p^2\right) R_u(\rho) = 0 \qquad (\rho \to \infty), \tag{27}$$

or, equivalently,

$$\frac{\partial^2 R_u(\rho)}{\partial \rho^2} + \frac{1}{\rho}\frac{\partial R_u(\rho)}{\partial \rho} + k_p^2 R_u(\rho) = 0 \qquad (\rho \to \infty) \tag{28}$$

under the reasonable condition

$$k_p^2 \gg \frac{1}{4\rho^2} \qquad (\rho \to \infty)\,. \tag{29}$$

Comparing equation (28) with the radial equations (10) in the limiting case $\rho \to \infty$, we see that equations (10) can be transformed from the radial equations (28) when the conditions

$$\lim_{\rho\to\infty} \frac{\zeta_j(\rho)}{\rho^2} = \beta_j^2, \qquad j = 1, 2 \tag{30}$$

and

$$\beta_j = \sqrt{k_p^2 - \varepsilon_j \frac{\omega^2}{c^2}}, \qquad j = 1, 2 \tag{31}$$

are satisfied.

Now, we are ready to look for a unified form of the radial equations (10) for superfocusing SPPs. The unified form can be obtained from the inversion process of finding the limiting equations (17) and (28) as $\rho \to 0$ and $\rho \to \infty$, respectively. It is easy to find a simple candidate of the form

$$\frac{\partial^2 R_u(\rho)}{\partial\rho^2} + \frac{1}{\rho}\frac{\partial R_u(\rho)}{\partial\rho} + \left(k_p^2 + \frac{\zeta_u(0)}{\rho^2}\right) R_u(\rho) = 0 \qquad (0 \leqslant \rho < \infty)\,, \tag{32}$$

which approaches equations (17) and (28) under the reasonable conditions $\zeta_u(0)/\rho^2 \gg k_p^2$ as $\rho \to 0$ and $\zeta_u(0)/\rho^2 \ll k_p^2$ as $\rho \to \infty$, respectively. These algebraic procedures indicate that a more general candidate is

$$\frac{\partial^2 R_u(\rho)}{\partial\rho^2} + \frac{1}{\rho}\frac{\partial R_u(\rho)}{\partial\rho} + \left(k_p^2 + \frac{\zeta_u(0) + A(\rho)}{\rho^2}\right) R_u(\rho) = 0 \qquad (0 \leqslant \rho < \infty) \tag{33}$$

where $A(\rho)$ is arbitrary only if

$$\lim_{\rho\to 0} A(\rho) = 0, \qquad \lim_{\rho\to\infty} A(\rho)/\rho^2 = 0. \tag{34}$$

By setting

$$A(\rho) = \zeta_u(\rho) - \zeta_u(0), \tag{35}$$

we can rewrite equation (33) as

$$\frac{\partial^2 R_u(\rho)}{\partial\rho^2} + \frac{1}{\rho}\frac{\partial R_u(\rho)}{\partial\rho} + \left(k_p^2 + \frac{\zeta_u(\rho)}{\rho^2}\right) R_u(\rho) = 0 \qquad (0 \leqslant \rho < \infty) \tag{36}$$

where the condition

$$\lim_{\rho\to\infty} \zeta_u(\rho)/\rho^2 = 0 \tag{37}$$

is satisfied from equations (34) and (35). Comparing equation (36) with the radial equations (10), we find that the unification conditions

$$\frac{\zeta_j(\rho)}{\rho^2} = \beta_j^2 + \frac{\zeta_u(\rho)}{\rho^2}, \qquad j = 1, 2 \qquad (0 \leqslant \rho < \infty) \tag{38}$$

allow the radial functions in equation (10) to be unified as follows:

$$R_u(\rho) = R_j(\rho), \qquad j = 1, 2 \qquad (0 \leqslant \rho < \infty)\,. \tag{39}$$

Equation (36) is the modified form of the radial equations (10) for superfocusing SPPs, in which the separation quantities and the radial functions are described in the unified notation for the metallic and dielectric regions. Further discussion on the unified radial equation (36) would require more detailed information on the unified separation quantity $\zeta_u(\rho)$, which can be determined from the boundary conditions.

4. Boundary conditions for the radial and extended angular functions

Here, as a preparation for considering the extended angular equations (11), we examine the boundary conditions for the radial and extended angular functions. Let us first investigate the radial function. In the preceding section, we simplified the original radial equations (10) to the unified radial equation (36), which is a linear, second-order, homogeneous ODE that possesses two nontrivial linearly independent particular solutions as a fundamental system of solutions. Indeed, the boundary conditions of the unified radial function depend on a situation of interest such as the incoming or outgoing solutions for $\rho \to 0$ or $\rho \to \infty$. In particular, a special boundary condition for the superfocusing process is the incoming solution for $\rho \to 0$ that expresses an extraordinary enhancement of the electromagnetic field coming from the outside; it is obtained from equation (18) and is given by

$$R_u(\rho) = H_0 \exp(-\mathrm{i}\nu \ln \rho) \qquad (\rho \to 0), \tag{40}$$

where H_0 is the complex amplitude of the magnetic field to be determined by the initial conditions. We shall choose equation (40) to be a boundary condition of the unified radial function.

To obtain the boundary conditions of the angular functions, we can use the continuity of the radial electric field at the metal–dielectric surface ($\phi = \alpha$). The Ampère–Maxwell equation in the absence of current density allows us to describe the electrical field as a function of the magnetic field. From this equation, together with the existence of the magnetic field $\boldsymbol{H}(\boldsymbol{x}, t) = (0, 0, H_z(\rho, \phi, t))$ assumed in equation (1), we see that the electric field $\boldsymbol{E}(\boldsymbol{x}, t)$ can be written as

$$\boldsymbol{E}(\boldsymbol{x}, t) = (E_\rho(\rho, \phi, t), E_\phi(\rho, \phi, t), 0) \tag{41}$$

where, with the following harmonic time dependence

$$E_\rho(\rho, \phi, t) = \mathrm{Re}[E_\rho(\rho, \phi)\, \mathrm{e}^{-\mathrm{i}\omega t}], \tag{42}$$

$$E_\phi(\rho, \phi, t) = \mathrm{Re}[E_\phi(\rho, \phi)\, \mathrm{e}^{-\mathrm{i}\omega t}], \tag{43}$$

and in terms of their following explicit expressions in the two regions:

$$E_\rho(\rho, \phi) = \begin{cases} E_{\rho 1}(\rho, \phi), & |\phi| \leqslant \alpha \\ E_{\rho 2}(\rho, \phi), & \alpha \leqslant |\phi| \leqslant \pi, \end{cases} \tag{44}$$

$$E_\phi(\rho, \phi) = \begin{cases} E_{\phi 1}(\rho, \phi), & |\phi| \leqslant \alpha \\ E_{\phi 2}(\rho, \phi), & \alpha \leqslant |\phi| \leqslant \pi, \end{cases} \tag{45}$$

we find that

$$E_{\rho j}(\rho, \phi) = \frac{\mathrm{i}c}{\omega \varepsilon_j} \frac{1}{\rho} \frac{\partial}{\partial \phi} H_{zj}(\rho, \phi), \qquad j = 1, 2, \tag{46}$$

$$E_{\phi j}(\rho, \phi) = -\frac{\mathrm{i}c}{\omega \varepsilon_j} \frac{\partial}{\partial \rho} H_{zj}(\rho, \phi), \qquad j = 1, 2. \tag{47}$$

Substituting equation (5) into equation (46), and using equation (39), we see that the radial electric fields become

$$E_{\rho j}(\rho, \phi) = \frac{\mathrm{i}c}{\omega \varepsilon_j} \frac{R_u(\rho)}{\rho} \frac{\partial}{\partial \phi} Q_j^s(\phi, \rho), \qquad j = 1, 2, \tag{48}$$

which are continuous at the metal–dielectric surface ($\phi = \alpha$). Hence, we find the following expression for the boundary conditions of the angular functions:

$$\frac{1}{\varepsilon_1} \lim_{\phi \to \alpha - 0} \frac{\partial}{\partial \phi} Q_1^s(\phi, \rho) = \frac{1}{\varepsilon_2} \lim_{\phi \to \alpha + 0} \frac{\partial}{\partial \phi} Q_2^s(\phi, \rho). \tag{49}$$

Note that the continuity of the radial electric field on the other metal–dielectric surface ($\phi = -\alpha$) is automatically satisfied when the magnetic field has either even (+) or odd (−) symmetries with respect to ϕ.

5. Application of perturbation methods for solving the extended angular equations

From equations (38) and (39), we see that the extended angular equations (11) and (12) simplify to

$$\frac{\partial^2 Q_j^s(\phi, \rho)}{\partial \phi^2} - \{(\beta_j \rho)^2 + \zeta_u(\rho)\} Q_j^s(\phi, \rho) = -F_j^s(\phi, \rho), \qquad j = 1, 2 \tag{50}$$

with

$$F_j^s(\phi, \rho) = \rho^2 \frac{\partial^2}{\partial \rho^2} Q_j^s(\phi, \rho) + \frac{2\rho^2}{R_u(\rho)} \left(\frac{\partial R_u(\rho)}{\partial \rho} \right) \frac{\partial Q_j^s(\phi, \rho)}{\partial \rho} + \rho \frac{\partial Q_j^s(\phi, \rho)}{\partial \rho}, \qquad j = 1, 2. \tag{51}$$

In spite of this simplification, we still face difficulty with the fact that equations (50) and (51) include the as-yet-to-be-determined unified radial function $R_u(\rho)$. Moreover, we still face a basic difficulty in solving such a complicated partial differential equation (PDE) containing first- and second-order partial derivatives with respect to ρ and a second-order partial derivative with respect to ϕ. In order to overcome these difficulties, let us apply perturbation methods [46] to the extended angular equations (50), treating $F_j^s(\phi, \rho)$ on the right side as a perturbing term because the left side can be solved exactly. According to the perturbation theory, we introduce the perturbation parameter $0 \leqslant \delta \leqslant 1$ into equations (50) and consider the perturbed equation

$$\frac{\partial^2 Q_j^s(\phi, \rho)}{\partial \phi^2} - \{(\beta_j \rho)^2 + \zeta_u(\rho)\} Q_j^s(\phi, \rho) = -\delta F_j^s(\phi, \rho), \qquad j = 1, 2, \tag{52}$$

which should have a solution of the form

$$Q_j^s(\phi, \rho) = Q_j^{s(0)}(\phi, \rho) + \delta Q_j^{s(1)}(\phi, \rho) + \delta^2 Q_j^{s(2)}(\phi, \rho) + \cdots, \qquad j = 1, 2. \tag{53}$$

Accordingly, $\zeta_u(\rho)$ and $R_u(\rho)$ should be described as

$$\zeta_u(\rho) = \zeta_u^{(0)}(\rho) + \delta \zeta_u^{(1)}(\rho) + \delta^2 \zeta_u^{(2)}(\rho) + \cdots \tag{54}$$

and

$$R_u(\rho) = R_u^{(0)}(\rho) + \delta R_u^{(1)}(\rho) + \delta^2 R_u^{(2)}(\rho) + \cdots, \tag{55}$$

respectively. Substituting equations (53)–(55) into equation (52), and setting the coefficients of the powers of δ equal to each other, we have a system of equations for $Q_j^{s(0)}(\phi, \rho)$, $Q_j^{s(1)}(\phi, \rho)$, $Q_j^{s(2)}(\phi, \rho)$, ..., in the power series (53):

Coefficient of δ^0

$$\frac{\partial^2 Q_j^{s(0)}(\phi, \rho)}{\partial \phi^2} - \{\eta_j(\rho)\}^2 Q_j^{s(0)}(\phi, \rho) = 0, \qquad j = 1, 2 \tag{56}$$

with the newly defined function

$$\eta_j(\rho) = \sqrt{(\beta_j \rho)^2 + \zeta_u^{(0)}(\rho)}, \qquad j = 1, 2. \tag{57}$$

Coefficient of δ^1

$$\frac{\partial^2 Q_j^{s(1)}(\phi, \rho)}{\partial \phi^2} - \{\eta_j(\rho)\}^2 Q_j^{s(1)}(\phi, \rho) = -N_j^{s(1)}(\phi, \rho), \qquad j = 1, 2 \tag{58}$$

with the nonhomogeneous term

$$N_j^{s(1)}(\phi, \rho) = \rho^2 \frac{\partial^2}{\partial \rho^2} Q_j^{s(0)}(\phi, \rho) + \frac{2\rho^2}{R_u^{(0)}(\rho)} \left(\frac{\partial R_u^{(0)}(\rho)}{\partial \rho} \right) \frac{\partial Q_j^{s(0)}(\phi, \rho)}{\partial \rho} + \rho \frac{\partial Q_j^{s(0)}(\phi, \rho)}{\partial \rho} - \zeta_u^{(1)}(\rho) Q_j^{s(0)}(\phi, \rho), \qquad j = 1, 2. \tag{59}$$

Coefficient of δ^2

$$\frac{\partial^2 Q_j^{s(2)}(\phi, \rho)}{\partial \phi^2} - \{\eta_j(\rho)\}^2 Q_j^{s(2)}(\phi, \rho) = -N_j^{s(2)}(\phi, \rho), \qquad j = 1, 2 \tag{60}$$

with the nonhomogeneous term

$$N_j^{s(2)}(\phi, \rho) = \rho^2 \frac{\partial^2}{\partial \rho^2} Q_j^{s(1)}(\phi, \rho) + \frac{2\rho^2}{R_u^{(0)}(\rho)} \left(\frac{\partial R_u^{(0)}(\rho)}{\partial \rho} \right) \frac{\partial Q_j^{s(1)}(\phi, \rho)}{\partial \rho} + \frac{2\rho^2}{R_u^{(0)}(\rho)} \left(\frac{\partial R_u^{(1)}(\rho)}{\partial \rho} \right) \frac{\partial Q_j^{s(0)}(\phi, \rho)}{\partial \rho} - \frac{2\rho^2 R_u^{(1)}(\rho)}{\left\{ R_u^{(0)}(\rho) \right\}^2} \left(\frac{\partial R_u^{(0)}(\rho)}{\partial \rho} \right) \frac{\partial Q_j^{s(0)}(\phi, \rho)}{\partial \rho} + \rho \frac{\partial Q_j^{s(1)}(\phi, \rho)}{\partial \rho} - \zeta_u^{(1)}(\rho) Q_j^{s(1)}(\phi, \rho) - \zeta_u^{(2)}(\rho) Q_j^{s(0)}(\phi, \rho), \qquad j = 1, 2. \tag{61}$$

Setting equation (53) for $\phi = \alpha$ equal to the one from equation (6), we have

$$Q_j^s(\alpha, \rho) = Q_j^{s(0)}(\alpha, \rho) + \delta Q_j^{s(1)}(\alpha, \rho) + \delta^2 Q_j^{s(2)}(\alpha, \rho) + \cdots = 1, \qquad j = 1, 2, \tag{62}$$

which lead to the following Dirichlet boundary conditions [47]:

$$Q_j^{s(0)}(\alpha, \rho) = 1, \qquad Q_j^{s(1)}(\alpha, \rho) = 0, \qquad Q_j^{s(2)}(\alpha, \rho) = 0, \ldots, \qquad j = 1, 2, \tag{63}$$

by setting the coefficients of the powers of δ equal to each other in equation (62). In a similar manner, substituting equation (53) into equation (49), and setting the coefficients of the powers of δ equal to each other, we have the following Neumann boundary conditions [47]:

$$\frac{1}{\varepsilon_1} \lim_{\phi \to \alpha - 0} \frac{\partial}{\partial \phi} Q_1^{s(n)}(\phi, \rho) = \frac{1}{\varepsilon_2} \lim_{\phi \to \alpha + 0} \frac{\partial}{\partial \phi} Q_2^{s(n)}(\phi, \rho), \qquad n = 0, 1, 2, \ldots. \tag{64}$$

Note that imposing both the Dirichlet (63) and Neumann boundary conditions (64) is referred to as the Cauchy boundary conditions [47]; that is, we specify the values and normal derivatives of the functions $Q_j^{s(0)}(\phi, \rho)$, $Q_j^{s(1)}(\phi, \rho)$, $Q_j^{s(2)}(\phi, \rho)$, ... in the power series (53) along the metal–dielectric boundary ($\phi = \alpha$).

Perturbation methods should be also applied to the unified radial equation (36). Substituting equations (54) and (55) into the unified radial equation (36) and equating the coefficients of like powers of δ on both the sides, we have the following:

Coefficient of δ^0

$$\frac{\partial^2 R_u^{(0)}(\rho)}{\partial \rho^2} + \frac{1}{\rho} \frac{\partial R_u^{(0)}(\rho)}{\partial \rho} + \left(k_p^2 + \frac{\zeta_u^{(0)}(\rho)}{\rho^2} \right) R_u^{(0)}(\rho) = 0 \qquad (0 < \rho < \infty). \tag{65}$$

Coefficient of δ^1

$$\frac{\partial^2 R_u^{(1)}(\rho)}{\partial\rho^2} + \frac{1}{\rho}\frac{\partial R_u^{(1)}(\rho)}{\partial\rho} + \left(k_p^2 + \frac{\zeta_u^{(0)}(\rho)}{\rho^2}\right) R_u^{(1)}(\rho)$$
$$= -\frac{\zeta_u^{(1)}(\rho)}{\rho^2} R_u^{(0)}(\rho) \qquad (0 < \rho < \infty)\,. \tag{66}$$

Coefficient of δ^2

$$\frac{\partial^2 R_u^{(2)}(\rho)}{\partial\rho^2} + \frac{1}{\rho}\frac{\partial R_u^{(2)}(\rho)}{\partial\rho} + \left(k_p^2 + \frac{\zeta_u^{(0)}(\rho)}{\rho^2}\right) R_u^{(2)}(\rho)$$
$$= -\frac{\zeta_u^{(1)}(\rho)}{\rho^2} R_u^{(1)}(\rho) - \frac{\zeta_u^{(2)}(\rho)}{\rho^2} R_u^{(0)}(\rho) \qquad (0 < \rho < \infty)\,. \tag{67}$$

Substituting equation (55) into equation (40), and setting the coefficients of the powers of δ equal to each other, we have the following Dirichlet boundary conditions:

$$R_u^{(0)}(\rho) = H_0 \exp(-\mathrm{i}\nu\, \ln\rho) \qquad (\rho \to 0), \tag{68}$$

$$R_u^{(1)}(\rho) = R_u^{(2)}(\rho) = \cdots = 0 \qquad (\rho \to 0). \tag{69}$$

Summing up the points we have discussed in this section, we arrive at the following sequence of problems from which we can find the function sets $\left\{\zeta_u^{(n)}(\rho),\, R_u^{(n)}(\rho),\, Q_1^{s(n)}(\phi,\rho),\, Q_2^{s(n)}(\phi,\rho)\right\}$ for $n = 0, 1, 2, \ldots$ in sequence:

$$P_0 \begin{cases} \dfrac{\partial^2 Q_j^{s(0)}(\phi,\rho)}{\partial\phi^2} - \{\eta_j(\rho)\}^2 Q_j^{s(0)}(\phi,\rho) = 0, \qquad j = 1,2 \\ Q_j^{s(0)}(\alpha,\rho) = 1, \qquad j = 1,2 \\ \dfrac{1}{\varepsilon_1}\lim\limits_{\phi\to\alpha-0}\dfrac{\partial}{\partial\phi} Q_1^{s(0)}(\phi,\rho) = \dfrac{1}{\varepsilon_2}\lim\limits_{\phi\to\alpha+0}\dfrac{\partial}{\partial\phi} Q_2^{s(0)}(\phi,\rho) \\ \dfrac{\partial^2 R_u^{(0)}(\rho)}{\partial\rho^2} + \dfrac{1}{\rho}\dfrac{\partial R_u^{(0)}(\rho)}{\partial\rho} + \left(k_p^2 + \dfrac{\zeta_u^{(0)}(\rho)}{\rho^2}\right) R_u^{(0)}(\rho) = 0 \\ R_u^{(0)}(\rho)\big|_{\rho\to 0} \sim H_0 \exp(-\mathrm{i}\nu\, \ln\rho), \end{cases} \tag{70}$$

$$P_1 \begin{cases} \dfrac{\partial^2 Q_j^{s(1)}(\phi,\rho)}{\partial\phi^2} - \{\eta_j(\rho)\}^2 Q_j^{s(1)}(\phi,\rho) = -N_j^{s(1)}(\phi,\rho), \qquad j = 1,2 \\ Q_j^{s(1)}(\alpha,\rho) = 0, \qquad j = 1,2 \\ \dfrac{1}{\varepsilon_1}\lim\limits_{\phi\to\alpha-0}\dfrac{\partial}{\partial\phi} Q_1^{s(1)}(\phi,\rho) = \dfrac{1}{\varepsilon_2}\lim\limits_{\phi\to\alpha+0}\dfrac{\partial}{\partial\phi} Q_2^{s(1)}(\phi,\rho) \\ \dfrac{\partial^2 R_u^{(1)}(\rho)}{\partial\rho^2} + \dfrac{1}{\rho}\dfrac{\partial R_u^{(1)}(\rho)}{\partial\rho} + \left(k_p^2 + \dfrac{\zeta_u^{(0)}(\rho)}{\rho^2}\right) R_u^{(1)}(\rho) = -\dfrac{\zeta_u^{(1)}(\rho)}{\rho^2} R_u^{(0)}(\rho) \\ R_u^{(1)}(\rho)\big|_{\rho\to 0} = 0, \end{cases} \tag{71}$$

$$P_2 \begin{cases} \dfrac{\partial^2 Q_j^{s(2)}(\phi,\rho)}{\partial\phi^2} - \{\eta_j(\rho)\}^2 Q_j^{s(2)}(\phi,\rho) = -N_j^{s(2)}(\phi,\rho), & j=1,2 \\ Q_j^{s(2)}(\alpha,\rho) = 0, & j=1,2 \\ \dfrac{1}{\varepsilon_1}\lim\limits_{\phi\to\alpha-0}\dfrac{\partial}{\partial\phi}Q_1^{s(2)}(\phi,\rho) = \dfrac{1}{\varepsilon_2}\lim\limits_{\phi\to\alpha+0}\dfrac{\partial}{\partial\phi}Q_2^{s(2)}(\phi,\rho) \\ \dfrac{\partial^2 R_u^{(2)}(\rho)}{\partial\rho^2} + \dfrac{1}{\rho}\dfrac{\partial R_u^{(2)}(\rho)}{\partial\rho} + \left(k_p^2 + \dfrac{\zeta_u^{(0)}(\rho)}{\rho^2}\right) R_u^{(2)}(\rho) \\ = -\dfrac{\zeta_u^{(1)}(\rho)}{\rho^2} R_u^{(1)}(\rho) - \dfrac{\zeta_u^{(2)}(\rho)}{\rho^2} R_u^{(0)}(\rho) \\ R_u^{(1)}(\rho)\big|_{\rho\to 0} = 0. \end{cases} \tag{72}$$

Finally, it is useful to indicate that as $\rho \to 0$ the perturbation term in the perturbed equation (52) vanishes; that is,

$$\lim_{\rho\to 0} F_j^s(\phi,\rho) = 0, \qquad j=1,2, \tag{73}$$

which can be verified by calculating equations (51) under the condition that $R_u(\rho)$ ($\rho \to 0$) has a logarithmic phase singularity in equation (18) and $Q_j^s(\phi,\rho)$ remains finite at $\rho = 0$. Then, from equation (53), we find that

$$Q_j^s(\phi,0) = Q_j^{s(0)}(\phi,01), \qquad j=1,2, \tag{74}$$

$$Q_j^{s(1)}(\phi,0) = Q_j^{s(2)}(\phi,0) = \cdots = 0, \qquad j=1,2 \tag{75}$$

and from equation (54), we find that

$$\zeta_u(0) = \zeta_u^{(0)}(0), \tag{76}$$

$$\zeta_u^{(1)}(0) = \zeta_u^{(2)}(0) = \cdots = 0. \tag{77}$$

Substituting equation (76) into equation (19), we obtain

$$\nu = \sqrt{\zeta_u^{(0)}(0)} = \sqrt{\zeta_u(0)}. \tag{78}$$

6. Zeroth-order approximate solutions

We are to solve problem P_0 (70), which is composed of the zeroth-order perturbation equations that give the fundamental properties of the superfocusing modes in the metallic wedge and V-groove. In the metallic wedge, it will be shown that only the odd symmetry with respect to ϕ is allowed and that the zeroth-order unified radial equation closely approximates the Bessel differential equation of an imaginary order. In contrast, for the metallic V-groove, it will be shown that only the even symmetry is allowed and that the zeroth-order unified radial equation roughly approximates the modified form of the Whittaker differential equation.

6.1. Extended angular functions of the zeroth order

The zeroth-order extended angular equations (56) have two nontrivial linearly independent particular solutions,

$$\cosh\{\phi\eta_j(\rho)\}, \qquad \sinh\{\phi\eta_j(\rho)\}, \qquad j=1,2, \tag{79}$$

so that by taking account of the boundary conditions (6), we obtain a solution for the odd (−) symmetry with respect to ϕ, i.e.,

$$Q_1^{-(0)}(\phi, \rho) = \sinh\{\phi\eta_1(\rho)\}/\sinh\{\alpha\eta_1(\rho)\}, \qquad 0 \leqslant |\phi| \leqslant \alpha, \tag{80}$$

$$Q_2^{-(0)}(\phi, \rho) = \mathrm{sgn}(\phi)\sinh\{(\pi - |\phi|)\eta_2(\rho)\}/\sinh\{(\pi - \alpha)\eta_2(\rho)\}, \qquad \alpha \leqslant |\phi| \leqslant \pi \tag{81}$$

and a solution for the even (+) symmetry with respect to ϕ, i.e.,

$$Q_1^{+(0)}(\phi, \rho) = \cosh\{\phi\eta_1(\rho)\}/\cosh\{\alpha\eta_1(\rho)\}, \qquad 0 \leqslant |\phi| \leqslant \alpha, \tag{82}$$

$$Q_2^{+(0)}(\phi, \rho) = \cosh\{(\pi - |\phi|)\eta_2(\rho)\}/\cosh\{(\pi - \alpha)\eta_2(\rho)\}, \qquad \alpha \leqslant |\phi| \leqslant \pi. \tag{83}$$

6.2. Characteristic equations for determining the unified separation quantity of the zeroth order

Substituting equations (80) and (81) into the boundary condition (64), we obtain

$$\frac{\eta_1(\rho)}{\varepsilon_1}\coth\{\alpha\eta_1(\rho)\} = -\frac{\eta_2(\rho)}{\varepsilon_2}\coth\{(\pi - \alpha)\eta_2(\rho)\} \tag{84}$$

or

$$\frac{\tanh\{\alpha\eta_1(\rho)\}}{\tanh\{(\pi - \alpha)\eta_2(\rho)\}} + \frac{\varepsilon_2\eta_1(\rho)}{\varepsilon_1\eta_2(\rho)} = 0 \qquad \text{(odd symmetry)}, \tag{85}$$

which is the characteristic equation to determine the zeroth-order unified separation quantity $\zeta_u^{(0)}(\rho)$ for the odd symmetry.

In contrast, substituting equations (82) and (83) into the boundary condition (64), we get

$$\frac{\eta_1(\rho)}{\varepsilon_1}\tanh\{\alpha\eta_1(\rho)\} = -\frac{\eta_2(\rho)}{\varepsilon_2}\tanh\{(\pi - \alpha)\eta_2(\rho)\} \tag{86}$$

or

$$\frac{\tanh\{\alpha\eta_1(\rho)\}}{\tanh\{(\pi - \alpha)\eta_2(\rho)\}} + \frac{\varepsilon_1\eta_2(\rho)}{\varepsilon_2\eta_1(\rho)} = 0 \qquad \text{(even symmetry)}, \tag{87}$$

which is the characteristic equation for the even symmetry.

Symmetry properties of the superfocusing modes in the wedge-shaped geometry can be easily obtained by considering characteristic equations (85) and (87) at $\rho = 0$:

$$\frac{\tanh\left\{\alpha\sqrt{\zeta_u^{(0)}(0)}\right\}}{\tanh\left\{(\pi - \alpha)\sqrt{\zeta_u^{(0)}(0)}\right\}} + \frac{\varepsilon_2}{\varepsilon_1} = 0 \qquad \text{(odd symmetry)}, \tag{88}$$

$$\frac{\tanh\left\{\alpha\sqrt{\zeta_u^{(0)}(0)}\right\}}{\tanh\left\{(\pi - \alpha)\sqrt{\zeta_u^{(0)}(0)}\right\}} + \frac{\varepsilon_1}{\varepsilon_2} = 0 \qquad \text{(even symmetry)}, \tag{89}$$

which are the same in the first term but different in the second term. The first term in equations (88) and (89) satisfies the condition

$$0 < \frac{\tanh\left\{\alpha\sqrt{\zeta_u^{(0)}(0)}\right\}}{\tanh\left\{(\pi - \alpha)\sqrt{\zeta_u^{(0)}(0)}\right\}} < 1 \tag{90}$$

from the inequality

$$0 < \tanh\left\{\alpha\sqrt{\zeta_u^{(0)}(0)}\right\} < \tanh\left\{(\pi - \alpha)\sqrt{\zeta_u^{(0)}(0)}\right\} \qquad \left(0 < \alpha < \frac{\pi}{2}\right) \tag{91}$$

for $\sqrt{\zeta_u^{(0)}(0)}$ being a positive real number, which, from equations (20) and (78), is satisfied when the superfocusing takes place. Substituting equation (90) into equations (88) and (89), we have the conditions

$$-1 < \frac{\varepsilon_2}{\varepsilon_1} < 0 \qquad \text{(odd symmetry)}, \tag{92}$$

$$-1 < \frac{\varepsilon_1}{\varepsilon_2} < 0 \qquad \text{(even symmetry)}, \tag{93}$$

which can be respectively transformed using equations (24) and (25) into the forms

$$0 < \varepsilon_2 < -\varepsilon_1 \qquad \text{(odd symmetry)}, \tag{94}$$

$$0 < \varepsilon_1 < -\varepsilon_2 \qquad \text{(even symmetry)}. \tag{95}$$

Equations (94) and (95) tell us the symmetry properties of the superfocusing mode in which the odd (−) and even (+) symmetries are, respectively, allowed for the metallic wedge ($\varepsilon_1 < 0$, $\varepsilon_2 > 0$) and the metallic V-groove ($\varepsilon_1 > 0$, $\varepsilon_2 < 0$). Therefore, we find that, in determining the zeroth-order unified separation quantity, the characteristic equation of odd symmetry (85) is used for the metallic wedge, while the characteristic equation of even symmetry (87) is used for the metallic V-groove.

6.3. Approximately analytic determination of the zeroth-order unified separation quantity based on a figure-of-merit function

A minutely detailed description of the magnetic fields for superfocusing needs not a numeric but an analytic determination of the zeroth-order unified separation quantity $\zeta_u^{(0)}(\rho)$ because of the characteristic equations (85) and (87). Obviously, it is very difficult to express $\zeta_u^{(0)}(\rho)$ by solving equations (85) and (87) by using ordinary methods in terms of already-known analytic functions; however, it is easily possible to estimate $\zeta_u^{(0)}(\rho)$ fairly accurately by carefully choosing a figure-of-merit function whose parameters can be determined by fitting it to a numerically calculated curve from equations (85) or (87) with specific values of ε_1, ε_2 and α.

We will use the metallic permittivity $\varepsilon_m = -20$ and the dielectric permittivity $\varepsilon_d = 1$ as specific values of ε_1 and ε_2 in producing numerically calculated curves. We choose the specific values by assuming that the dielectric matter is air with a permittivity of $\varepsilon_d = 1$ and the metallic matter is gold with a permittivity of $\varepsilon_m = -20.6+1.57\mathrm{i}$ at the 750 nm wavelength; the imaginary part of ε_m is much smaller than the real part and thus can be ignored for the sake of simplicity.

Figure 2 shows $\zeta_u^{(0)}(0)$ as a function of the wedge angle 2α for the metallic wedge and V-groove, as calculated by

$$\frac{\tanh\left\{\alpha\sqrt{\zeta_u^{(0)}(0)}\right\}}{\tanh\left\{(\pi-\alpha)\sqrt{\zeta_u^{(0)}(0)}\right\}} + \frac{\varepsilon_d}{\varepsilon_m} = 0, \tag{96}$$

which was obtained from equations (88) and (89) for the metallic wedge ($\varepsilon_1 = \varepsilon_m$, $\varepsilon_2 = \varepsilon_d$) and the metallic V-groove ($\varepsilon_1 = \varepsilon_d$, $\varepsilon_2 = \varepsilon_m$). Although it seems surprising that $\zeta_u^{(0)}(0)$ is common to the metallic wedge and V-groove, this fact is implicit in Nerkararyan [22]. The dominant characteristics of figure 1 are that $\zeta_u^{(0)}(0)$ is positive when $2\alpha \leqslant 17.14$ and $\zeta_u^{(0)}(0)$ increases as the cone angle 2α decreases. With equations (18) and (19), this means that the superfocusing effects become stronger as the cone angle 2α decreases. Specific values in figure 1 are listed in table 1.

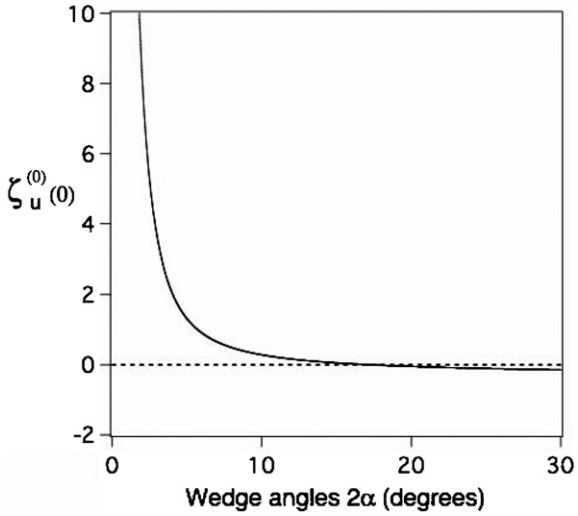

Figure 2. Numerical calculations of the zeroth-order unified separation quantities at $\rho = 0$, $\zeta_u^{(0)}(0)$, as a function of wedge angle 2α when $\varepsilon_m = -20$ and $\varepsilon_d = 1$ are used in equation (96). Note that $\zeta_u^{(0)}(0)$ is equal to $\zeta_u(0)$ and ν^2 from equation (78).

Table 1. Values of the solution $\zeta_u^{(0)}(0)$ in equation (96) for specific wedge angles 2α with $\varepsilon_d = 1$ and $\varepsilon_m = -20$. From equation (78), ν equals $\sqrt{\zeta_u^{(0)}(0)}$.

2α (degrees)	$\zeta_u^{(0)}(0)$	ν
1	32.88	5.734
3	3.654	1.912
5	1.311	1.145
10	0.2810	0.5301
15	0.05128	0.2265

From here onwards, to avoid a clash of notations between the metallic wedge and V-groove expressions of $\zeta_u^{(0)}(\rho)$, we use $\hat{\zeta}_u^{(0)}(\rho)$ and $\tilde{\zeta}_u^{(0)}(\rho)$ for the metallic wedge and V-groove, respectively. Generally, in the case of a clash of notation, let us use a circumflex ($\hat{}$) for the metallic wedge and a tilde ($\tilde{}$) for the metallic V-groove. However, $\hat{\zeta}_u^{(0)}(0)$ and $\tilde{\zeta}_u^{(0)}(0)$ are exceptional; they can both be replaced by $\zeta_u^{(0)}(0)$ as determined by equation (96). Since $\zeta_u^{(0)}(0)$ is well described by figure 2, we will freely replace $\hat{\zeta}_u^{(0)}(0)$ and $\tilde{\zeta}_u^{(0)}(0)$ with $\zeta_u^{(0)}(0)$.

In the metallic wedge, $\hat{\zeta}_u^{(0)}(\rho)$ is determined by solving equation (85) under the conditions $\varepsilon_1 = \varepsilon_m$ and $\varepsilon_2 = \varepsilon_d$. In figure 3, the solid lines show $\hat{\zeta}_u^{(0)}(\rho)/\zeta_u^{(0)}(0)$ for specific wedge angles as a function of ρ/λ_0, where λ_0 ($=2\pi c/\omega$) is the wavelength in vacuum; the broken lines are fitting curves for the respective solid lines and they are consequently unclear due to their overlap with the solid lines. In the curve fitting, we choose a figure-of-merit function with two parameters, p_1 and p_2, of the form

$$\frac{\hat{\zeta}_u^{(0)}(\rho)}{\zeta_u^{(0)}(0)} = \exp\left[(p_1\lambda_0)\left((\rho/\lambda_0) + (p_2/\lambda_0)\left\{\exp\left(-\frac{(\rho/\lambda_0)}{(p_2/\lambda_0)}\right) - 1\right\}\right)\right]$$
$$= \exp[p_1(\rho + p_2\{\exp(-\rho/p_2) - 1\})]. \tag{97}$$

Here, the term $p_1(\rho + p_2\{\exp(-\rho/p_2) - 1\})$ is the same as the one describing free-fall motion with air resistance proportional to the velocity, behaving as a square increase around

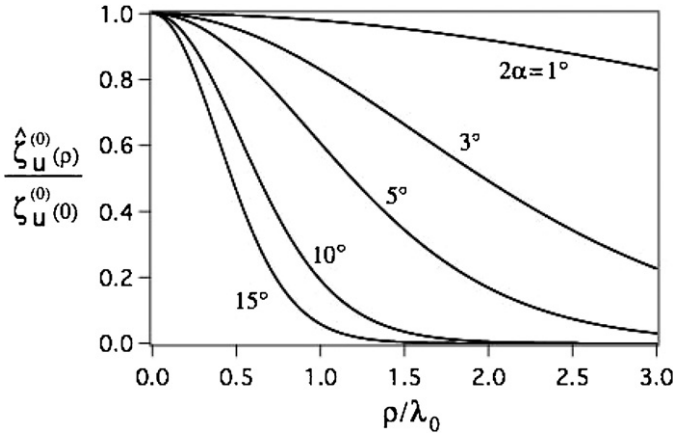

Figure 3. Numerical calculations of the zeroth-order unified separation quantities $\hat{\zeta}_u^{(0)}(\rho)$ for the metallic wedge as a function of the radius ρ for various wedge angles 2α when $\varepsilon_1 = -20$ and $\varepsilon_2 = 1$ are used in equation (85). For convenience of explanation, $\hat{\zeta}_u^{(0)}(\rho)/\zeta_u^{(0)}(0)$ is shown, where $\hat{\zeta}_u^{(0)}(0) = \zeta_u^{(0)}(0)$. Broken lines are fitting curves based on equation (97) and are not clearly visible because of their overlap with the solid lines that represent the results of numerical calculations.

Table 2. Values of the parameters in equation (97) obtained by fitting the curves in figure 3. The parameters are normalized by the wavelength in vacuum, λ_0.

2α (degrees)	$p_1\lambda_0$	p_2/λ_0
1	−1.551	36.45
3	−2.045	5.109
5	−2.961	2.620
10	−8.752	2.329
15	−15.67	2.381

ρ and a linear increase for larger ρ. Table 2 shows several values of p_1 and p_2 normalized to the wavelength in vacuum, λ_0, in equation (97) for specific wedge angles.

In the metallic V-groove, $\tilde{\zeta}_u^{(0)}(\rho)$ is determined by solving equation (87) under the conditions $\varepsilon_1 = \varepsilon_d$ and $\varepsilon_2 = \varepsilon_m$. In figure 4(*a*), the solid lines show $\tilde{\zeta}_u^{(0)}(\rho)/\zeta_u^{(0)}(0)$ for specific wedge angles as a function of ρ/λ_0. Their behavior is very different from the behavior of the solid lines plotting $\hat{\zeta}_u^{(0)}(\rho)/\zeta_u^{(0)}(0)$ in figure 3. In order to find a figure-of-merit function suitable for $\tilde{\zeta}_u^{(0)}(\rho)$, we draw a new graph in figure 4(*b*) showing $\left\{\tilde{\zeta}_u^{(0)}(\rho) - \hat{\zeta}_u^{(0)}(\rho)\right\}\big/\zeta_u^{(0)}(0)$ as a function of ρ/λ_0, where $\hat{\zeta}_u^{(0)}(\rho)\big/\zeta_u^{(0)}(0)$ is already shown in figure 3. All the solid lines in figure 4(*b*) approach zero as $\rho \to 0$ and $\rho \to \infty$. These properties allow us to choose a figure-of-merit function with three parameters, q_1, q_2 and q_3, of the form

$$\frac{\tilde{\zeta}_u^{(0)}(\rho) - \hat{\zeta}_u^{(0)}(\rho)}{\zeta_u^{(0)}(0)} = (q_1\lambda_0)\,(\rho/\lambda_0)\exp\left[-(q_2\lambda_0)(\rho/\lambda_0) - \left(q_3\lambda_0^2\right)(\rho/\lambda_0)^2\right]$$
$$= q_1\rho\exp[-q_2\rho - q_3\rho^2] \tag{98}$$

for fitting the solid lines in figure 4(*b*). The fitting curves are shown in figure 4(*b*) as broken lines, which overlap with the solid lines. Table 3 shows several values of q_1, q_2 and q_3 normalized to the wavelength in vacuum, λ_0, in equation (98) for specific wedge angles.

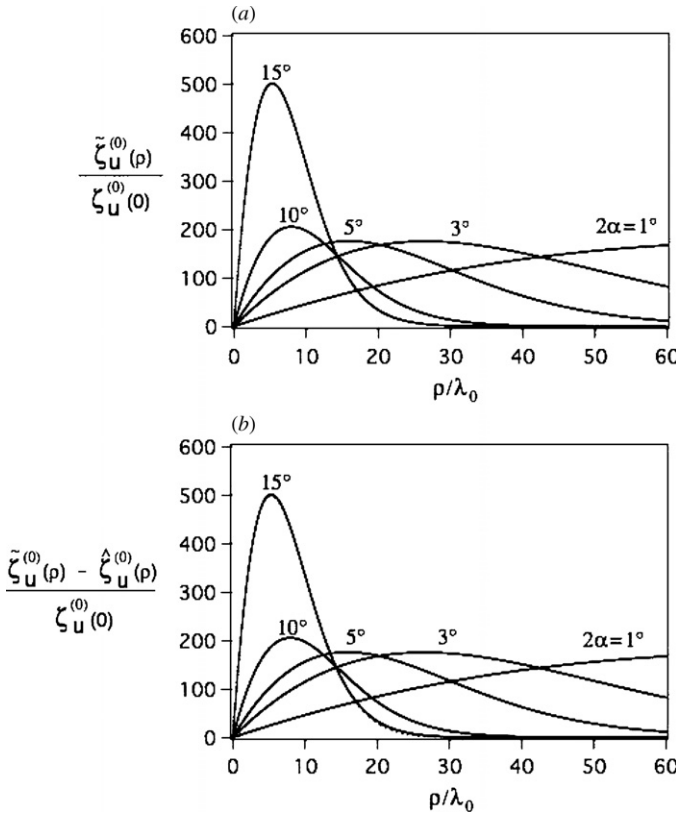

Figure 4. Numerical calculations of the zeroth-order unified separation quantities $\tilde{\zeta}_u^{(0)}(\rho)$ for the metallic V-groove as a function of the radius ρ for various wedge angles 2α when $\varepsilon_1 = 1$ and $\varepsilon_2 = -20$ are used in equation (87). Part (*a*) shows $\tilde{\zeta}_u^{(0)}(\rho)/\zeta_u^{(0)}(0)$, where $\tilde{\zeta}_u^{(0)}(0) = \zeta_u^{(0)}(0)$. For convenience of fitting the curves, part (*b*) shows $\{\tilde{\zeta}_u^{(0)}(\rho) - \hat{\zeta}_u^{(0)}(\rho)\}/\zeta_u^{(0)}(0)$ as a solid line, where $\hat{\zeta}_u^{(0)}(0)/\zeta_u^{(0)}(0)$ is shown in figure 3. Broken lines in part (*b*) are fitting curves based on equation (98) and are not clearly visible because of their overlap with the solid lines.

Table 3. Values of the parameters in equation (98) obtained by fitting the curves in figure 4(*b*). The parameters are normalized by the wavelength in vacuum, λ_0.

2α (degrees)	$q_1\lambda_0$	$q_2\lambda_0$	$q_3\lambda_0^2$
1	5.115	0.008 449	0.000 027 05
3	15.25	0.024 90	0.000 2499
5	25.66	0.042 25	0.000 6763
10	59.86	0.084 49	0.002 705
15	218.7	0.126 7	0.006 087

6.4. Unified radial functions of the zeroth order for the metallic wedge

In the metallic wedge, the zeroth-order unified separation quantity $\hat{\zeta}_u^{(0)}(\rho)$ determined by equation (85) is fairly accurately estimated by the figure-of-merit function in equation (97). However, even by using this quantity, we cannot solve the zeroth-order unified radial

equation (65) as an already-known differential equation. Nevertheless, we can show that the zeroth-order unified radial equation (65) closely approximates the imaginary Bessel differential equation [48] under the quasi-constant approximation condition. For the metallic wedge, let us write the zeroth-order unified radial equation (65) as

$$\frac{\partial^2 \hat{R}_u^{(0)}(\rho)}{\partial \rho^2} + \frac{1}{\rho}\frac{\partial \hat{R}_u^{(0)}(\rho)}{\partial \rho} + \left(k_p^2 + \frac{\hat{\zeta}_u^{(0)}(\rho)}{\rho^2}\right)\hat{R}_u^{(0)}(\rho) = 0. \tag{99}$$

Defining the modified wave number of SPPs in the planar geometry as

$$\hat{k}_{mp}(\rho) = \sqrt{k_p^2 + \frac{\hat{\zeta}_u^{(0)}(\rho) - \zeta_u^{(0)}(0)}{\rho^2}}, \tag{100}$$

we can write equation (99) as

$$\frac{\partial^2 \hat{R}_u^{(0)}(\rho)}{\partial \rho^2} + \frac{1}{\rho}\frac{\partial \hat{R}_u^{(0)}(\rho)}{\partial \rho} + \left(\{\hat{k}_{mp}(\rho)\}^2 + \frac{\zeta_u^{(0)}(0)}{\rho^2}\right)\hat{R}_u^{(0)}(\rho) = 0, \tag{101}$$

which can be approximately transformed into a Bessel differential equation if $\hat{k}_{mp}(\rho)$ varies smoothly and is approximately constant. This assumption is acceptable when the characteristic function

$$\chi(\rho) = \frac{\rho}{\hat{k}_{mp}(\rho)}\frac{\partial}{\partial \rho}\hat{k}_{mp}(\rho) \tag{102}$$

satisfies the condition

$$|\chi(\rho)| \ll 1 \tag{103}$$

because $\hat{k}_{mp}(\rho)$ can be treated as a quasi-constant in the variable transformation $\hat{r} = \rho\hat{k}_{mp}(\rho)$ as follows:

$$\frac{\partial}{\partial \rho} = \frac{\partial \hat{r}}{\partial \rho}\frac{\partial}{\partial \hat{r}} = \hat{k}_{mp}(\rho)\{1 + \chi(\rho)\}\frac{\partial}{\partial \hat{r}} \approx \hat{k}_{mp}(\rho)\frac{\partial}{\partial \hat{r}}, \tag{104}$$

in which equation (101) closely approximates the imaginary Bessel differential equation

$$\frac{\partial^2 \hat{R}_u^{(0)}}{\partial \hat{r}^2} + \frac{1}{\hat{r}}\frac{\partial \hat{R}_u^{(0)}}{\partial \hat{r}} + \left\{1 - \frac{(\mathrm{i}\nu)^2}{\hat{r}^2}\right\}\hat{R}_u^{(0)} = 0 \tag{105}$$

for $\nu = \sqrt{\zeta_u^{(0)}(0)}$ in equation (78). In our numerical calculations, condition (103) is satisfied as can be seen in figure 5; hence, these transformations are absolutely valid.

The general solution of equation (105) can be written in the form

$$\hat{R}_u^{(0)}(\rho) = aF_{\mathrm{i}\nu}(\rho\hat{k}_{mp}(\rho)) + bG_{\mathrm{i}\nu}(\rho\hat{k}_{mp}(\rho)), \tag{106}$$

where $F_{\mathrm{i}\nu}(x)$ and $G_{\mathrm{i}\nu}(x)$ are two real independent solutions for imaginary Bessel functions defined by Dunster [48] as

$$F_{\mathrm{i}\nu}(x) = \frac{1}{2}\left\{\mathrm{e}^{-\nu\pi/2}H_{\mathrm{i}\nu}^{(1)}(x) + \mathrm{e}^{\nu\pi/2}H_{\mathrm{i}\nu}^{(2)}(x)\right\} \tag{107}$$

and

$$G_{\mathrm{i}\nu}(x) = \frac{1}{2\mathrm{i}}\left\{\mathrm{e}^{-\nu\pi/2}H_{\mathrm{i}\nu}^{(1)}(x) - \mathrm{e}^{\nu\pi/2}H_{\mathrm{i}\nu}^{(2)}(x)\right\}. \tag{108}$$

Their behaviors for small values of x are described as

$$F_{\mathrm{i}\nu}(x) = \left(\frac{2\tanh(\nu\pi/2)}{\nu\pi}\right)^{1/2}\{\cos(\nu\ \ln(x/2) - \phi_{\nu,0}) + O(x^2)\}, \qquad x \to 0+, \tag{109}$$

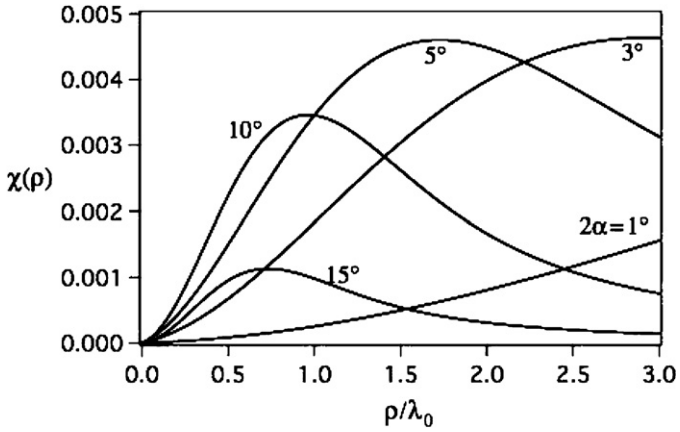

Figure 5. Numerical calculations of the characteristic function $\chi(\rho)$ defined in equation (102) for various wedge angles 2α in the metallic wedge with $\varepsilon_1 = -20$ and $\varepsilon_2 = 1$.

$$G_{i\nu}(x) = \left(\frac{2\coth(\nu\pi/2)}{\nu\pi}\right)^{1/2} \{\sin(\nu\ \ln(x/2) - \phi_{\nu,0}) + O(x^2)\}, \qquad x \to 0+, \tag{110}$$

where

$$\phi_{\nu,0} = \arg\{\Gamma(1 + i\nu)\}. \tag{111}$$

Substituting equations (109) and (110) into equation (106), we have

$$\hat{R}_u^{(0)}(\rho) = a\left(\frac{2\tanh(\nu\pi/2)}{\nu\pi}\right)^{1/2} \{\cos(\nu\ln(\rho\hat{k}_{mp}(\rho)/2) - \phi_{\nu,0})\}$$
$$+ b\left(\frac{2\coth(\nu\pi/2)}{\nu\pi}\right)^{1/2} \{\sin(\nu\ln(\rho\hat{k}_{mp}(\rho)/2) - \phi_{\nu,0})\}, \qquad \rho\hat{k}_{mp}(\rho) \to 0. \tag{112}$$

Comparing equation (112) with the boundary condition (68), we find

$$a = H_0 \exp\left[i\nu\ \ln\frac{\hat{k}_{mp}(\rho)}{2} - i\phi_{\nu,0}\right]\left(\frac{2\tanh(\nu\pi/2)}{\nu\pi}\right)^{-1/2}, \tag{113}$$

$$b = -iH_0 \exp\left[i\nu\ \ln\frac{\hat{k}_{mp}(\rho)}{2} - i\phi_{\nu,0}\right]\left(\frac{2\coth(\nu\pi/2)}{\nu\pi}\right)^{-1/2}. \tag{114}$$

The physical properties become clear when the general solution (106) is written using the Hankel functions of the first and second kinds, which express the outgoing and incoming waves, respectively, for $\rho \to \infty$. Substituting equations (113) and (114) into equation (106), and using equations (107) and (108), we find that $\hat{R}_u^{(0)}(\rho)$ is divided into an incoming part, $\hat{R}_{in}^{(0)}(\rho)$, and an outgoing part, $\hat{R}_{out}^{(0)}(\rho)$, as follows:

$$\hat{R}_u^{(0)}(\rho) = \hat{R}_{\rm in}^{(0)}(\rho) + \hat{R}_{\rm out}^{(0)}(\rho), \tag{115}$$

where

$$\hat{R}_{\rm in}^{(0)}(\rho) = H_0' \frac{\sqrt{\coth(\nu\pi/2)} + \sqrt{\tanh(\nu\pi/2)}}{2} e^{\nu\pi/2} H_{i\nu}^{(2)}(\rho\hat{k}_{mp}(\rho)), \tag{116}$$

$$\hat{R}_{\text{out}}^{(0)}(\rho) = H_0' \frac{\sqrt{\coth(\nu\pi/2)} - \sqrt{\tanh(\nu\pi/2)}}{2} \, \mathrm{e}^{-\nu\pi/2} H_{\mathrm{i}\nu}^{(1)}(\rho\hat{k}_{mp}(\rho)), \tag{117}$$

with

$$H_0' = H_0 \exp\left[\mathrm{i}\nu \, \ln \frac{\hat{k}_{mp}(\rho)}{2} - \mathrm{i}\phi_{\nu,0}\right] \left(\frac{2}{\nu\pi}\right)^{-1/2}. \tag{118}$$

Calculating from equations (116) and (117) the ratio

$$\frac{\hat{R}_{\text{out}}^{(0)}(\rho)}{\hat{R}_{\text{in}}^{(0)}(\rho)} = \mathrm{e}^{-2\nu\pi} \frac{H_{\mathrm{i}\nu}^{(1)}(\rho\hat{k}_{mp}(\rho))}{H_{\mathrm{i}\nu}^{(2)}(\rho\hat{k}_{mp}(\rho))} = \mathrm{e}^{-\nu\pi} \frac{F_{\mathrm{i}\nu}(\rho\hat{k}_{mp}(\rho)) + iG_{\mathrm{i}\nu}(\rho\hat{k}_{mp}(\rho))}{F_{\mathrm{i}\nu}(\rho\hat{k}_{mp}(\rho)) - iG_{\mathrm{i}\nu}(\rho\hat{k}_{mp}(\rho))}, \tag{119}$$

we obtain the zeroth-order amplitude reflection coefficient

$$\left|\frac{\hat{R}_{\text{out}}^{(0)}(\rho)}{\hat{R}_{\text{in}}^{(0)}(\rho)}\right| = \mathrm{e}^{-\nu\pi}. \tag{120}$$

This exponential ratio is described as a function of the imaginary Bessel index ν. We see that the incoming and the outgoing waves of the zeroth order are not balanced; the reflected outgoing wave is much smaller in amplitude than the incident incoming wave when ν is more than unity because the ratio in equation (120) is 0.043 for $\nu = 1$.

6.5. Unified radial functions of the zeroth order for the metallic V-groove

In the metallic V-groove, the zeroth-order unified separation quantity $\tilde{\zeta}_u^{(0)}(\rho)$ determined by equation (87) is fairly accurately estimated by the figure-of-merit function in equation (98). Even with it, though, we cannot solve the zeroth-order unified radial equation (65) as an already-known differential equation or to close approximation as an imaginary Bessel differential equation. However, we can show that the zeroth-order unified radial equation (65) roughly approximates the modified Whittaker differential equation [41, 42, 49, 50] through transformations. In the metallic V-groove, let us write the zeroth-order unified radial equation (65) as

$$\frac{\partial^2 \tilde{R}_u^{(0)}(\rho)}{\partial\rho^2} + \frac{1}{\rho}\frac{\partial \tilde{R}_u^{(0)}(\rho)}{\partial\rho} + \left(k_p^2 + \frac{\tilde{\zeta}_u^{(0)}(\rho)}{\rho^2}\right) \tilde{R}_u^{(0)}(\rho) = 0, \tag{121}$$

which can be rearranged as

$$\begin{aligned} &\frac{\partial^2 \tilde{R}_u^{(0)}(\rho)}{\partial\rho^2} + \frac{1}{\rho}\frac{\partial \tilde{R}_u^{(0)}(\rho)}{\partial\rho} \\ &+ \left(k_p^2 + \frac{\hat{\zeta}_u^{(0)}(\rho) - \zeta_u^{(0)}(0)}{\rho^2} + \frac{\tilde{\zeta}_u^{(0)}(\rho) - \hat{\zeta}_u^{(0)}(\rho)}{\rho^2} + \frac{\zeta_u^{(0)}(0)}{\rho^2}\right) \tilde{R}_u^{(0)}(\rho) = 0. \end{aligned} \tag{122}$$

From the figure-of-merit function in equation (98), we get the roughly approximate formula

$$\frac{\tilde{\zeta}_u^{(0)}(\rho) - \hat{\zeta}_u^{(0)}(\rho)}{\rho^2} = \frac{\zeta_u^{(0)}(0) q_1 \exp[-q_2\rho - q_3\rho^2]}{\rho} \approx \frac{\nu^2 q_1}{\rho} - \nu^2 q_1 q_2 \left(0 \leqslant \rho \ll \frac{1}{q_2}\right) \tag{123}$$

for $\nu = \sqrt{\zeta_u^{(0)}(0)}$ in equation (78). Substituting equation (123) into equation (122), we find that

$$\frac{\partial^2 \tilde{R}_u^{(0)}(\rho)}{\partial\rho^2} + \frac{1}{\rho}\frac{\partial \tilde{R}_u^{(0)}(\rho)}{\partial\rho} + \left(\{\tilde{k}_{mp}(\rho)\}^2 + \frac{\nu^2 q_1}{\rho} + \frac{\nu^2}{\rho^2}\right) \tilde{R}_u^{(0)}(\rho) = 0 \tag{124}$$

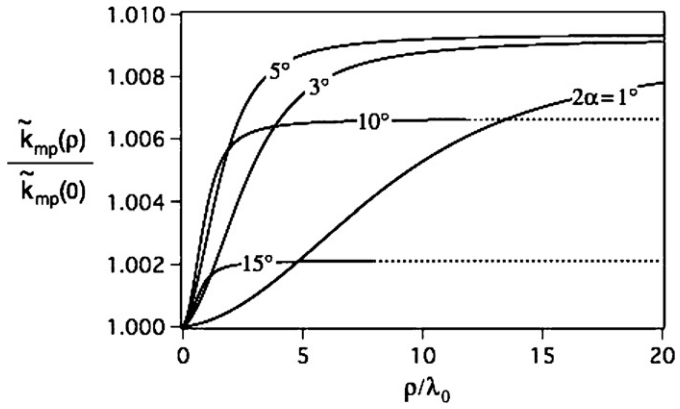

Figure 6. Numerical calculations of the ratio $\tilde{k}_{mp}(\rho)/\tilde{k}_{mp}(0)$ using equations (125) and (129) for various wedge angles 2α in the metallic V-groove with $\varepsilon_1 = 1$ and $\varepsilon_2 = -20$. The broken lines do not satisfy the approximation condition denoted by $0 \leqslant \rho \leqslant 1/q_2$ in equation (123) (specific values of q_2 are given in table 3).

with the definition

$$\tilde{k}_{mp}(\rho) = \sqrt{k_p^2 - \nu^2 q_1 q_2 + \frac{\hat{\zeta}_u^{(0)}(\rho) - \zeta_u^{(0)}(0)}{\rho^2}}. \tag{125}$$

We modify equation (124) by writing $\tilde{R}_u^{(0)}(\rho) = \rho^{-1/2} w^{(0)}(\rho)$ and obtain the differential equation

$$\frac{\partial^2 w^{(0)}(\rho)}{\partial \rho^2} + \left(\{\tilde{k}_{mp}(\rho)\}^2 + \frac{\nu^2 q_1}{\rho} + \frac{\nu^2 + \frac{1}{4}}{\rho^2} \right) w^{(0)}(\rho) = 0, \tag{126}$$

which could be transformed into the modified Whittaker differential equation if $\tilde{k}_{mp}(\rho)$ were constant. Here, let us solve the differential equation (126) under the rough approximation

$$\tilde{k}_{mp}(\rho) \approx \tilde{k}_{mp}(0), \tag{127}$$

in which the differential equation (126) approximates

$$\frac{\partial^2 w^{(0)}(\rho)}{\partial \rho^2} + \left(\{\tilde{k}_{mp}(0)\}^2 + \frac{\nu^2 q_1}{\rho} + \frac{\nu^2 + \frac{1}{4}}{\rho^2} \right) w^{(0)}(\rho) = 0, \tag{128}$$

where

$$\tilde{k}_{mp}(0) = \sqrt{k_p^2 - \nu^2 q_1 q_2 + \nu^2 p_1 / (2 p_2)} \tag{129}$$

from equations (78), (97) and (125). In our numerical calculations, condition (127) is satisfied in such a way that $\tilde{k}_{mp}(\rho)$ is numerically equal to $\tilde{k}_{mp}(0)$ within a range of 1% as shown in figure 6. Writing $\tilde{r} = 2\rho \tilde{k}_{mp}(0)$ in equation (128), we get the modified form of the Whittaker differential equation (see appendix A):

$$\frac{\partial^2 w^{(0)}}{\partial \tilde{r}^2} + \left(\frac{1}{4} - \frac{\kappa}{\tilde{r}} + \frac{\nu^2 + \frac{1}{4}}{\tilde{r}^2} \right) w^{(0)} = 0 \tag{130}$$

with the definition

$$\kappa = -\frac{\nu^2 q_1}{2\tilde{k}_{mp}(0)}. \tag{131}$$

Table 4. Values of the parameters calculated from equations (129) and (131) for specific values of the wedge angle 2α. The equations were solved using the values of ν, q_1, q_2, p_1 and p_2 given in tables 1–3. The parameters are normalized by the wavelength in vacuum, λ_0.

2α (degrees)	$\tilde{k}_{mp}(0)\lambda_0$	κ	$-\kappa/\nu$
1	6.280	−13.39	2.335
3	6.280	−4.437	2.321
5	6.276	−2.680	2.341
10	6.293	−1.336	2.521
15	6.322	−0.8870	3.917

Solutions to equation (130) are given by the (modified) Whittaker functions such as $M_{i\kappa,i\nu}(i\tilde{r})$, $M_{i\kappa,-i\nu}(i\tilde{r})$, $W_{i\kappa,i\nu}(i\tilde{r})$ and $W_{-i\kappa,i\nu}(-i\tilde{r})$. Their definitions, characteristics and connection formulas are briefly summarized in section 2 of [51]. Table 4 shows that specific values of κ in equation (131) are all negative in our numerical calculations.

We can now determine a rough approximate solution of the zeroth-order unified radial equation (121) satisfying the boundary condition (68). From (11.04) of chapter 7 [42], we see that the solution $M_{i\kappa,-i\nu}(i\tilde{r})$ to equation (130) has the asymptotic formula

$$M_{i\kappa,-i\nu}(i\tilde{r}) \sim (i\tilde{r})^{-i\nu+1/2} \qquad (\tilde{r} \to 0), \tag{132}$$

or

$$M_{i\kappa,-i\nu}(2i\rho\tilde{k}_{mp}(0)) \sim (2i\rho\tilde{k}_{mp}(0))^{-i\nu+1/2} \qquad (\rho \to 0), \tag{133}$$

whose behavior satisfies the boundary condition (68). Comparing equations (68) and (133), we find that

$$\tilde{R}_u^{(0)}(\rho) = H_0'' \rho^{-1/2} M_{i\kappa,-i\nu}(2i\rho\tilde{k}_{mp}(0)), \tag{134}$$

where

$$H_0'' = H_0\{2i\tilde{k}_{mp}(0)\}^{i\nu-1/2}. \tag{135}$$

The physical properties become clear when solution (134) is rewritten using the Whittaker functions $W_{-i\kappa,i\nu}(-2i\rho\tilde{k}_{mp}(0))$ and $W_{i\kappa,i\nu}(2i\rho\tilde{k}_{mp}(0))$, which express outgoing and incoming waves, respectively, for $\rho \to \infty$ (see appendix A). By applying relations (B.10) to equation (134), we find that $\tilde{R}_u^{(0)}(\rho)$ is divided into an incoming part, $\tilde{R}_{in}^{(0)}(\rho)$, and an outgoing part, $\tilde{R}_{out}^{(0)}(\rho)$, as follows:

$$\tilde{R}_u^{(0)}(\rho) = \tilde{R}_{in}^{(0)}(\rho) + \tilde{R}_{out}^{(0)}(\rho), \tag{136}$$

where

$$\tilde{R}_{in}^{(0)}(\rho) = iH_0'' \rho^{-1/2} \frac{\Gamma(1-2i\nu)\, e^{\pi(\nu+\kappa)}}{\Gamma\left(\frac{1}{2}-i\nu+i\kappa\right)} W_{i\kappa,i\nu}(2i\rho\tilde{k}_{mp}(0)), \tag{137}$$

$$\tilde{R}_{out}^{(0)}(\rho) = H_0'' \rho^{-1/2} \frac{\Gamma(1-2i\nu)\, e^{\pi\kappa}}{\Gamma\left(\frac{1}{2}-i\nu-i\kappa\right)} W_{-i\kappa,i\nu}(-2i\rho\tilde{k}_{mp}(0)). \tag{138}$$

From equations (137) and (138), we get the ratio

$$\frac{\tilde{R}_{out}^{(0)}(\rho)}{\tilde{R}_{in}^{(0)}(\rho)} = ie^{-\nu\pi} \frac{\Gamma\left(\frac{1}{2}-i\nu+i\kappa\right) W_{-i\kappa,i\nu}(-2i\rho\tilde{k}_{mp}(0))}{\Gamma\left(\frac{1}{2}-i\nu-i\kappa\right) W_{i\kappa,i\nu}(2i\rho\tilde{k}_{mp}(0))}, \tag{139}$$

in which $W_{\mathrm{i}\kappa,\mathrm{i}\nu}(2\mathrm{i}\rho\tilde{k}_{mp}(0))$ and $W_{-\mathrm{i}\kappa,\mathrm{i}\nu}(-2\mathrm{i}\rho\tilde{k}_{mp}(0))$ form a complex conjugate pair (see appendix B). By using the formula [41, 43, 53]

$$\left|\Gamma\left(\frac{1}{2}+\mathrm{i}y\right)\right| = \sqrt{\frac{\pi}{\cosh \pi y}} \tag{140}$$

for real y, we find from equation (139) that

$$\left|\frac{\tilde{R}^{(0)}_{\mathrm{out}}(\rho)}{\tilde{R}^{(0)}_{\mathrm{in}}(\rho)}\right| = \mathrm{e}^{-\nu\pi}\sqrt{\frac{\cosh \pi\ (\nu+\kappa)}{\cosh \pi\ (\nu-\kappa)}}, \tag{141}$$

which will be referred to as the zeroth-order amplitude reflection coefficient for the metallic V-groove. The specific values of $-\kappa/\nu$ in table 4 suggest the condition

$$-\kappa \gg \nu(>0), \tag{142}$$

which makes equation (141) close to

$$\left|\frac{\tilde{R}^{(0)}_{\mathrm{out}}(\rho)}{\tilde{R}^{(0)}_{\mathrm{in}}(\rho)}\right| \approx \mathrm{e}^{-2\nu\pi} \tag{143}$$

through the approximations

$$\cosh \pi(\nu+\kappa) \approx \tfrac{1}{2}\,\mathrm{e}^{-\pi(\nu+\kappa)}, \qquad \cosh \pi(\nu-\kappa) \approx \tfrac{1}{2}\,\mathrm{e}^{\pi(\nu-\kappa)}. \tag{144}$$

The exponential ratio (143) is much smaller than the ratio (120) for positive ν. We see that the incoming and outgoing waves of the zeroth order in the metallic V-groove are much less balanced than those in the metallic wedge.

7. First-order perturbation solutions for the metallic wedge

In the preceding section, we obtained the zeroth-order perturbation solutions for both the metallic wedge and V-groove by solving problem P_0 (70). In this and the following sections, we consider the first-order perturbation solutions for the metallic wedge and V-groove, respectively, by solving problem P_1 (71). The problem P_1 is involved in solving nonhomogeneous ODEs in which the homogeneous ODEs without the nonhomogeneous terms are already solved in problem P_0 (70). Specific solutions to the nonhomogeneous ODEs can be obtained by using the variation of parameters or the Green's function method.

For the metallic wedge, only the odd symmetry with respect to ϕ is allowed for the superfocusing modes. Accordingly, the half region $0 \leqslant \phi \leqslant \pi$ is all that needs to be considered. In this section, we shall write equation (57) as

$$\hat{\eta}_j(\rho) = \sqrt{(\beta_j\rho)^2 + \hat{\zeta}^{(0)}_u(\rho)}, \qquad j = 1, 2 \tag{145}$$

to clearly indicate functions for the metallic wedge.

7.1. Extended angular functions of the first order for the metallic wedge

From equations (58) and (59), we obtain the first-order extended angular equation for the odd symmetry:

$$\frac{\partial^2 Q^{-(1)}_j(\phi,\rho)}{\partial\phi^2} - \{\hat{\eta}_j(\rho)\}^2 Q^{-(1)}_j(\phi,\rho) = -N^{-(1)}_j(\phi,\rho), \qquad j = 1, 2 \tag{146}$$

with the nonhomogeneous term

$$N_j^{-(1)}(\phi,\rho)=\rho^2\frac{\partial^2}{\partial\rho^2}Q_j^{-(0)}(\phi,\rho)+\frac{2\rho^2}{\hat{R}_u^{(0)}(\rho)}\left(\frac{\partial\hat{R}_u^{(0)}(\rho)}{\partial\rho}\right)\frac{\partial Q_j^{-(0)}(\phi,\rho)}{\partial\rho}$$
$$+\rho\frac{\partial Q_j^{-(0)}(\phi,\rho)}{\partial\rho}-\hat{\zeta}_u^{(1)}(\rho)Q_j^{-(0)}(\phi,\rho),\qquad j=1,2, \tag{147}$$

where $Q_j^{-(0)}(\phi,\rho)$ and $\hat{R}_u^{(0)}(\rho)$ are as obtained in sections 6.1 and 6.4, respectively, and $\hat{\zeta}_u^{(1)}(\rho)$ is to be determined. The boundary conditions are given by

$$Q_j^{-(1)}(\alpha,\rho)=0,\qquad j=1,2, \tag{148}$$

$$Q_j^{-(1)}(0,\rho)=0,\qquad Q_j^{-(1)}(\pi,\rho)=0,\qquad j=1,2, \tag{149}$$

$$\frac{1}{\varepsilon_1}\lim_{\phi\to\alpha-0}\frac{\partial}{\partial\phi}Q_1^{-(1)}(\phi,\rho)=\frac{1}{\varepsilon_2}\lim_{\phi\to\alpha+0}\frac{\partial}{\partial\phi}Q_2^{-(1)}(\phi,\rho), \tag{150}$$

where equations (148) are obtained from equations (63), equations (149) are attributed to the characteristics of the odd symmetry and equation (150) is obtained from equations (64). In order to solve the nonhomogeneous ODEs (146), by reference to chapter 10.5 in [52], let us use the Green's function method based on the self-adjoint homogeneous differential equation

$$\frac{\mathrm{d}}{\mathrm{d}x}\left(p(x)\frac{\mathrm{d}}{\mathrm{d}x}\right)y(x)+q(x)y(x)=0,\qquad a\leqslant x\leqslant b, \tag{151}$$

in which the nonhomogeneous differential equation

$$\frac{\mathrm{d}}{\mathrm{d}x}\left(p(x)\frac{\mathrm{d}}{\mathrm{d}x}\right)y(x)+q(x)y(x)=-f(x) \tag{152}$$

has the solution

$$y(x)=\int_a^b G(x,t)f(t)\,\mathrm{d}t \tag{153}$$

with the Green's function

$$G(x,t)=\begin{cases}-\dfrac{u(x)v(t)}{p(t)W(t)}, & a\leqslant x<t\\[2ex] -\dfrac{u(t)v(x)}{p(t)W(x)}, & t<x\leqslant b\end{cases} \tag{154}$$

where $u(x)$ and $v(x)$ are two independent solutions of the homogenous differential equation (151) and satisfy the boundary conditions at $x=a$ and $x=b$, respectively, and

$$W(t)=u(t)v'(t)-v(t)u'(t) \tag{155}$$

is the Wronskian.

For the metallic region $j=1$, according to the Green's function method, the nonhomogeneous ODE (146) has the solution

$$Q_1^{-(1)}(\phi,\rho)=\int_0^{\alpha}\hat{G}_1(\phi,\phi')N_1^{-(1)}(\phi',\rho)\,d\phi'\quad(0\leqslant\phi\leqslant\alpha) \tag{156}$$

with the Green's function

$$\hat{G}_1(\phi,\phi')=\begin{cases}-\dfrac{\hat{u}_1(\phi)\hat{v}_1(\phi')}{\hat{p}_1(\phi')\hat{W}_1(\phi')}, & 0\leqslant\phi<\phi'\\[2ex] -\dfrac{\hat{u}_1(\phi')\hat{v}_1(\phi)}{\hat{p}_1(\phi')\hat{W}_1(\phi')}, & \phi'<\phi\leqslant\alpha\end{cases} \tag{157}$$

where by choosing

$$\hat{u}_1(\phi) = \sinh\{\phi\hat{\eta}_1(\rho)\}, \tag{158}$$

$$\hat{v}_1(\phi) = \sinh\{(\phi-\alpha)\hat{\eta}_1(\rho)\}, \tag{159}$$

we obtain the Wronskian

$$\hat{W}_1(\phi') = \hat{\eta}_1(\rho)\sinh\{\alpha\hat{\eta}_1(\rho)\} \tag{160}$$

and by comparing equations (146) and (152), we can take

$$\hat{p}_1(\phi') = 1. \tag{161}$$

It follows that

$$\begin{aligned}
Q_1^{-(1)}(\phi,\rho) = &-\frac{\sinh\{(\phi-\alpha)\hat{\eta}_1(\rho)\}}{\hat{\eta}_1(\rho)}\int_0^{\phi}\frac{\sinh\{\phi'\hat{\eta}_1(\rho)\}}{\sinh\{\alpha\hat{\eta}_1(\rho)\}}N_1^{-(1)}(\phi',\rho)\,\mathrm{d}\phi' \\
&-\frac{\sinh\{\phi\hat{\eta}_1(\rho)\}}{\hat{\eta}_1(\rho)}\int_{\phi}^{\alpha}\frac{\sinh\{(\phi'-\alpha)\hat{\eta}_1(\rho)\}}{\sinh\{\alpha\hat{\eta}_1(\rho)\}}N_1^{-(1)}(\phi',\rho)\,\mathrm{d}\phi' \\
= &-\frac{\sinh\{(\phi-\alpha)\hat{\eta}_1(\rho)\}}{\hat{\eta}_1(\rho)} \\
&\times\left[\begin{array}{l}
\rho^2\displaystyle\int_0^{\phi}Q_1^{-(0)}(\phi',\rho)\frac{\partial^2}{\partial\rho^2}Q_1^{-(0)}(\phi',\rho)\,\mathrm{d}\phi' \\
+\left\{\dfrac{2\rho^2}{\hat{R}_u^{(0)}(\rho)}\left(\dfrac{\partial\hat{R}_u^{(0)}(\rho)}{\partial\rho}\right)+\rho\right\}\displaystyle\int_0^{\phi}Q_1^{-(0)}(\phi',\rho)\frac{\partial}{\partial\rho}Q_1^{-(0)}(\phi',\rho)\,\mathrm{d}\phi' \\
-\hat{\zeta}_u^{(1)}(\rho)\displaystyle\int_0^{\phi}\left\{Q_1^{-(0)}(\phi',\rho)\right\}^2\mathrm{d}\phi'
\end{array}\right] \\
&-\frac{\sinh\{\phi\hat{\eta}_1(\rho)\}}{\hat{\eta}_1(\rho)} \\
&\times\left[\begin{array}{l}
\rho^2\displaystyle\int_{\phi}^{\alpha}Q_1^{-(0)}(\phi'-\alpha,\rho)\frac{\partial^2}{\partial\rho^2}Q_1^{-(0)}(\phi',\rho)\,\mathrm{d}\phi' \\
+\left\{\dfrac{2\rho^2}{\hat{R}_u^{(0)}(\rho)}\left(\dfrac{\partial\hat{R}_u^{(0)}(\rho)}{\partial\rho}\right)+\rho\right\}\displaystyle\int_{\phi}^{\alpha}Q_1^{-(0)}(\phi'-\alpha,\rho)\frac{\partial}{\partial\rho}Q_1^{-(0)}(\phi',\rho)\,\mathrm{d}\phi' \\
-\hat{\zeta}_u^{(1)}(\rho)\displaystyle\int_{\phi}^{\alpha}Q_1^{-(0)}(\phi'-\alpha,\rho)Q_1^{-(0)}(\phi',\rho)\,\mathrm{d}\phi'
\end{array}\right].
\end{aligned} \tag{162}$$

For the dielectric region $j = 2$, in the same manner as above, the nonhomogeneous ODE (146) has the solution

$$Q_2^{-(1)}(\phi,\rho) = \int_{\alpha}^{\pi}\hat{G}_2(\phi,\phi')N_2^{-(1)}(\phi',\rho)\,\mathrm{d}\phi' \qquad (\alpha\leqslant\phi\leqslant\pi) \tag{163}$$

with the Green's function

$$\hat{G}_2(\phi,\phi') = \begin{cases}
-\dfrac{\hat{u}_2(\phi)\hat{v}_2(\phi')}{\hat{p}_2(\phi')\hat{W}_2(\phi')}, & \alpha\leqslant\phi<\phi' \\
-\dfrac{\hat{u}_2(\phi')\hat{v}_2(\varphi)}{\hat{p}_2(\phi')\hat{W}_2(\phi')}, & \phi'<\phi\leqslant\pi
\end{cases}$$

where by choosing

$$\hat{u}_2(\phi) = \sinh\{(\alpha - \phi)\hat{\eta}_2(\rho)\}, \tag{165}$$

$$\hat{v}_2(\phi) = \sinh\{(\pi - \phi)\hat{\eta}_2(\rho)\}, \tag{166}$$

we get the Wronskian

$$\hat{W}_2(\phi') = \hat{\eta}_2(\rho)\sinh\{(\pi - \alpha)\hat{\eta}_2(\rho)\} \tag{167}$$

and, as with equation (161), we can take

$$\hat{p}_2(\phi') = 1. \tag{168}$$

It follows that

$$\begin{aligned}
Q_2^{-(1)}(\phi,\rho) = & -\frac{\sinh\{(\pi-\phi)\hat{\eta}_2(\rho)\}}{\hat{\eta}_2(\rho)}\int_\alpha^\phi \frac{\sinh\{(\alpha-\phi')\hat{\eta}_2(\rho)\}}{\sinh\{(\pi-\alpha)\hat{\eta}_2(\rho)\}} N_2^{-(1)}(\phi',\rho)\,\mathrm{d}\phi' \\
& -\frac{\sinh\{(\alpha-\phi)\hat{\eta}_2(\rho)\}}{\hat{\eta}_2(\rho)}\int_\phi^\pi \frac{\sinh\{(\pi-\phi')\hat{\eta}_2(\rho)\}}{\sinh\{(\pi-\alpha)\hat{\eta}_2(\rho)\}} N_2^{-(1)}(\phi',\rho)\,\mathrm{d}\phi' \\
= & -\frac{\sinh\{(\pi-\phi)\hat{\eta}_2(\rho)\}}{\hat{\eta}_2(\rho)} \\
& \times \left[\begin{array}{l}
\rho^2\displaystyle\int_\alpha^\phi Q_2^{-(0)}(\phi'+\pi-\alpha,\rho)\frac{\partial^2}{\partial\rho^2}Q_2^{-(0)}(\phi',\rho)\,\mathrm{d}\phi' \\
+\left\{\dfrac{2\rho^2}{\hat{R}_u^{(0)}(\rho)}\left(\dfrac{\partial\hat{R}_u^{(0)}(\rho)}{\partial\rho}\right)+\rho\right\}\displaystyle\int_\alpha^\phi Q_2^{-(0)}(\phi'+\pi-\alpha,\rho)\frac{\partial}{\partial\rho}Q_2^{-(0)}(\phi',\rho)\,\mathrm{d}\phi' \\
-\hat{\zeta}_u^{(1)}(\rho)\displaystyle\int_\alpha^\phi Q_2^{-(0)}(\phi'+\pi-\alpha,\rho)Q_2^{-(0)}(\phi',\rho)\,\mathrm{d}\phi'
\end{array}\right] \\
& -\frac{\sinh\{(\alpha-\phi)\hat{\eta}_2(\rho)\}}{\hat{\eta}_2(\rho)} \\
& \times \left[\begin{array}{l}
\rho^2\displaystyle\int_\phi^\pi Q_2^{-(0)}(\phi',\rho)\frac{\partial^2}{\partial\rho^2}Q_2^{-(0)}(\phi',\rho)\,\mathrm{d}\phi' \\
+\left\{\dfrac{2\rho^2}{\hat{R}_u^{(0)}(\rho)}\left(\dfrac{\partial\hat{R}_u^{(0)}(\rho)}{\partial\rho}\right)+\rho\right\}\displaystyle\int_\phi^\pi Q_2^{-(0)}(\phi',\rho)\frac{\partial}{\partial\rho}Q_2^{-(0)}(\phi',\rho)\,\mathrm{d}\phi' \\
-\hat{\zeta}_u^{(1)}(\rho)\displaystyle\int_\phi^\pi \left\{Q_2^{-(0)}(\phi',\rho)\right\}^2\mathrm{d}\phi'
\end{array}\right].
\end{aligned} \tag{169}$$

7.2. Determination of the unified separation quantity of the first order for the metallic wedge

The boundary condition (150) can be used to determine the first-order unified separation quantity $\hat{\zeta}_u^{(1)}(\rho)$. Substituting equation (162) into the left side of equation (150), we get

$$\lim_{\phi\to\alpha-0}\frac{\partial}{\partial\phi}Q_1^{-(1)}(\phi,\rho) = -\int_0^\alpha Q_1^{-(0)}(\phi',\rho)N_1^{-(1)}(\phi',\rho)\mathrm{d}\phi'. \tag{170}$$

Substituting equation (169) into the right side of equation (150), we have

$$\lim_{\phi\to\alpha+0}\frac{\partial}{\partial\phi}Q_2^{-(1)}(\phi,\rho) = \int_\alpha^\pi Q_2^{-(0)}(\phi',\rho)N_2^{-(1)}(\phi',\rho)\,\mathrm{d}\phi'. \tag{171}$$

Setting equation (170) equal to equation (171) according to equation (150), we find

$$\frac{1}{\varepsilon_1}\int_0^\alpha Q_1^{-(0)}(\phi',\rho)N_1^{-(1)}(\phi',\rho)\,\mathrm{d}\phi' + \frac{1}{\varepsilon_2}\int_\alpha^\pi Q_2^{-(0)}(\phi',\rho)N_2^{-(1)}(\phi',\rho)\,\mathrm{d}\phi' = 0. \tag{172}$$

Substituting equations (147) into equation (172) and rearranging terms, we find for the first-order unified separation quantity that

$$\hat{\zeta}_u^{(1)}(\rho) = \frac{\left[\begin{array}{l}\rho^2\left\{\frac{1}{\varepsilon_1}\int_0^\alpha Q_1^{-(0)}(\phi,\rho)\frac{\partial^2}{\partial\rho^2}Q_1^{-(0)}(\phi,\rho)\,\mathrm{d}\phi+\frac{1}{\varepsilon_2}\int_\alpha^\pi Q_2^{-(0)}(\phi,\rho)\frac{\partial^2}{\partial\rho^2}Q_2^{-(0)}(\phi,\rho)\,\mathrm{d}\phi\right\}\\ +\left\{\frac{2\rho^2}{\hat{R}_u^{(0)}(\rho)}\left(\frac{\partial\hat{R}_u^{(0)}(\rho)}{\partial\rho}\right)+\rho\right\}\left\{\begin{array}{l}\frac{1}{\varepsilon_1}\int_0^\alpha Q_1^{-(0)}(\phi,\rho)\frac{\partial}{\partial\rho}Q_1^{-(0)}(\phi,\rho)\,\mathrm{d}\phi\\ +\frac{1}{\varepsilon_2}\int_\alpha^\pi Q_2^{-(0)}(\phi,\rho)\frac{\partial}{\partial\rho}Q_2^{-(0)}(\phi,\rho)\,\mathrm{d}\phi\end{array}\right\}\end{array}\right]}{\frac{1}{\varepsilon_1}\int_0^\alpha\left\{Q_1^{-(0)}(\phi,\rho)\right\}^2\mathrm{d}\phi+\frac{1}{\varepsilon_2}\int_\alpha^\pi\left\{Q_2^{-(0)}(\phi,\rho)\right\}^2\mathrm{d}\phi}, \tag{173}$$

where $\varepsilon_1 = \varepsilon_m$ and $\varepsilon_2 = \varepsilon_d$ are used for numerical calculations.

7.3. Unified radial function of the first order for the metallic wedge

The first-order unified radial equation (66) is written using equation (100) as

$$\frac{\partial^2\hat{R}_u^{(1)}(\rho)}{\partial\rho^2}+\frac{1}{\rho}\frac{\partial\hat{R}_u^{(1)}(\rho)}{\partial\rho}+\left(\{\hat{k}_{mp}(\rho)\}^2+\frac{\zeta_u^{(0)}(0)}{\rho^2}\right)\hat{R}_u^{(1)}(\rho)=-\frac{\hat{\zeta}_u^{(1)}(\rho)}{\rho^2}\hat{R}_u^{(0)}(\rho), \tag{174}$$

whose associated homogeneous ODE can be approximately solved as an imaginary Bessel differential equation under the quasi-constant approximation as discussed in section 6.4. To solve equation (174), let us recall a solution to a nonhomogeneous, linear, second-order ODE

$$\frac{\mathrm{d}^2y}{\mathrm{d}x^2}+P(x)\frac{\mathrm{d}y}{\mathrm{d}x}+Q(x)y=F(x). \tag{175}$$

The most general solution of equation (175) is

$$y(x)=c_1y_1(x)+c_2y_2(x)+y_p(x), \tag{176}$$

where $y_1(x)$ and $y_2(x)$ are two nontrivial linearly independent solutions to the associated homogeneous ODE

$$\frac{\mathrm{d}^2y}{\mathrm{d}x^2}+P(x)\frac{\mathrm{d}y}{\mathrm{d}x}+Q(x)y=0 \tag{177}$$

and $y_p(x)$ is a particular solution given by

$$y_p(x)=y_2(x)\int^x\frac{y_1(s)F(s)\,\mathrm{d}s}{W\{y_1(s),y_2(s)\}}-y_1(x)\int^x\frac{y_2(s)F(s)\,\mathrm{d}s}{W\{y_1(s),y_2(s)\}}, \tag{178}$$

where $W\{y_1(s), y_2(s)\}$ is the Wronskian of $y_1(s)$ and $y_2(s)$. Note that the particular solution (178) can be obtained from the variation of parameters method (see exercise 9.6.25 in [52]). Accordingly, for the nonhomogeneous ODE (174), under the quasi-constant approximation, choosing the Hankel functions $H_{\mathrm{i}\nu}^{(1)}(\rho\hat{k}_{mp}(\rho))$ and $H_{\mathrm{i}\nu}^{(2)}(\rho\hat{k}_{mp}(\rho))$ as two nontrivial linearly independent solutions to the associated homogeneous ODE, from the reference of (5.9.4) in [43] we obtain the Wronskian

$$W\left\{H_{\mathrm{i}\nu}^{(1)}(\rho\hat{k}_{mp}(\rho)),H_{\mathrm{i}\nu}^{(2)}(\rho\hat{k}_{mp}(\rho))\right\}\approx-\frac{4\mathrm{i}}{\pi\rho}. \tag{179}$$

Then by taking account of the following boundary condition from equation (69)

$$\hat{R}_u^{(1)}(\rho)=0 \qquad (\rho\to 0), \tag{180}$$

we find that the solution is

$$\hat{R}_u^{(1)}(\rho)=\hat{R}_{\mathrm{in}}^{(1)}(\rho)+\hat{R}_{\mathrm{out}}^{(1)}(\rho), \tag{181}$$

where

$$\hat{R}^{(1)}_{\rm in}(\rho) = -\frac{\pi \mathrm{i}}{4} H^{(2)}_{\mathrm{i}\nu}(\rho \hat{k}_{mp}(\rho)) \int_0^{\rho} \hat{\zeta}^{(1)}_u(\rho') \hat{R}^{(0)}_u(\rho') H^{(1)}_{\mathrm{i}\nu}(\rho' \hat{k}_{mp}(\rho')) \frac{\mathrm{d}\rho'}{\rho'} \tag{182}$$

and

$$\hat{R}^{(1)}_{\rm out}(\rho) = \frac{\pi \mathrm{i}}{4} H^{(1)}_{\mathrm{i}\nu}(\rho \hat{k}_{mp}(\rho)) \int_0^{\rho} \hat{\zeta}^{(1)}_u(\rho') \hat{R}^{(0)}_u(\rho') H^{(2)}_{\mathrm{i}\nu}(\rho' \hat{k}_{mp}(\rho')) \frac{\mathrm{d}\rho'}{\rho'}. \tag{183}$$

The functions $\hat{R}^{(1)}_{\rm in}(\rho)$ and $\hat{R}^{(1)}_{\rm out}(\rho)$ correspond to the incoming and outgoing waves, respectively, for $\rho \to \infty$.

The second-order perturbation solutions can be obtained in much the same manner as the first-order perturbation solutions. We give the second-order perturbation solutions for the metallic wedge in appendix C.

8. First-order perturbation solutions for the metallic V-groove

In this section, we consider the first-order perturbation solutions for the metallic V-groove by solving problem (71). For the metallic wedge, only the even symmetry with respect to ϕ is allowed for the superfocusing modes. Because of the symmetry, we only have to examine the half region $0 \leqslant \phi \leqslant \pi$. Let us write equation (57) as

$$\tilde{\eta}_j(\rho) = \sqrt{(\beta_j \rho)^2 + \tilde{\zeta}^{(0)}_u(\rho)}, \qquad j = 1, 2 \tag{184}$$

to clearly show functions used in the metallic V-groove.

8.1. Extended angular functions of the first order for the metallic V-groove

From equations (58) and (59), we obtain the first-order extended angular equations for the even symmetry:

$$\frac{\partial^2 Q^{+(1)}_j(\phi, \rho)}{\partial \phi^2} - \{\tilde{\eta}_j(\rho)\}^2 Q^{+(1)}_j(\phi, \rho) = -N^{+(1)}_j(\phi, \rho), \qquad j = 1, 2 \tag{185}$$

with the nonhomogeneous terms

$$N^{+(1)}_j(\phi, \rho) = \rho^2 \frac{\partial^2}{\partial \rho^2} Q^{+(0)}_j(\phi, \rho) + \frac{2\rho^2}{\tilde{R}^{(0)}_u(\rho)} \left(\frac{\partial \tilde{R}^{(0)}_u(\rho)}{\partial \rho} \right) \frac{\partial Q^{+(0)}_j(\phi, \rho)}{\partial \rho}$$
$$+ \rho \frac{\partial Q^{+(0)}_j(\phi, \rho)}{\partial \rho} - \tilde{\zeta}^{(1)}_u(\rho) Q^{+(0)}_j(\phi, \rho), \qquad j = 1, 2, \tag{186}$$

where $Q^{+(0)}_j(\phi, \rho)$ and $\tilde{R}^{(0)}_u(\rho)$ are as obtained in sections 6.1 and 6.5, while $\tilde{\zeta}^{(1)}_u(\rho)$ is to be determined. The boundary conditions are given by

$$Q^{+(1)}_j(\alpha, \rho) = 0, \qquad j = 1, 2, \tag{187}$$

$$\frac{\partial}{\partial \phi} Q^{+(1)}_j(\phi, \rho)\Big|_{\phi=0} = 0, \qquad \frac{\partial}{\partial \phi} Q^{+(1)}_j(\phi, \rho)\Big|_{\phi=\pi} = 0, \qquad j = 1, 2 \tag{188}$$

and

$$\frac{1}{\varepsilon_1} \lim_{\phi \to \alpha - 0} \frac{\partial}{\partial \phi} Q^{+(1)}_1(\phi, \rho) = \frac{1}{\varepsilon_2} \lim_{\phi \to \alpha + 0} \frac{\partial}{\partial \phi} Q^{+(1)}_2(\phi, \rho), \tag{189}$$

where equations (187) are obtained from equations (63), equations (188) are ascribed to the characteristics of the even symmetry and equation (189) is obtained from equation (64).

The nonhomogeneous ODEs (185) can be solved by using the Green's function method (see equations (151)–(155)).

For the dielectric region $j = 1$, the nonhomogeneous ODE (185) has the solution

$$Q_1^{+(1)}(\phi, \rho) = \int_0^{\alpha} \tilde{G}_1(\phi, \phi') N_1(\phi', \rho)\, \mathrm{d}\phi' \qquad (0 \leqslant \phi \leqslant \alpha) \tag{190}$$

with the Green's function

$$\tilde{G}_1(\phi, \phi') = \begin{cases} -\dfrac{\tilde{u}_1(\phi)\tilde{v}_1(\phi')}{\tilde{p}_1(\phi')\tilde{W}_1(\phi')}, & 0 \leqslant \phi < \phi' \\ -\dfrac{\tilde{u}_1(\phi')\tilde{v}_1(\phi)}{\tilde{p}_1(\phi')\tilde{W}_1(\phi')}, & \phi' < \phi \leqslant \alpha, \end{cases} \tag{191}$$

where by choosing

$$\tilde{u}_1(\phi) = \cosh\{\phi\tilde{\eta}_1(\rho)\} \tag{192}$$

and

$$\tilde{v}_1(\phi) = \sinh\{(\phi - \alpha)\tilde{\eta}_1(\rho)\} \tag{193}$$

we obtain the Wronskian

$$\tilde{W}_1(\phi') = \tilde{\eta}_1(\rho)\cosh\{\alpha\tilde{\eta}_1(\rho)\} \tag{194}$$

and obviously we have

$$\tilde{p}_1(\phi') = 1. \tag{195}$$

It follows that

$$\begin{aligned} Q_1^{+(1)}(\phi, \rho) &= -\frac{\sinh\{(\phi - \alpha)\tilde{\eta}_1(\rho)\}}{\tilde{\eta}_1(\rho)} \int_0^{\phi} \frac{\cosh\{\phi'\tilde{\eta}_1(\rho)\}}{\cosh\{\alpha\tilde{\eta}_1(\rho)\}} N_1^{+(1)}(\phi', \rho)\, \mathrm{d}\phi' \\ &\quad - \frac{\cosh\{\phi\tilde{\eta}_1(\rho)\}}{\tilde{\eta}_1(\rho)} \int_{\phi}^{\alpha} \frac{\sinh\{(\phi' - \alpha)\tilde{\eta}_1(\rho)\}}{\cosh\{\alpha\tilde{\eta}_1(\rho)\}} N_1^{+(1)}(\phi', \rho)\, \mathrm{d}\phi' \\ &= -\frac{\sinh\{(\phi - \alpha)\tilde{\eta}_1(\rho)\}}{\tilde{\eta}_1(\rho)} \\ &\quad \times \left[\begin{array}{l} \rho^2 \displaystyle\int_0^{\phi} Q_1^{+(0)}(\phi', \rho) \frac{\partial^2}{\partial\rho^2} Q_1^{+(0)}(\phi', \rho)\, \mathrm{d}\phi' \\ \quad + \left\{ \dfrac{2\rho^2}{\tilde{R}_u^{(0)}(\rho)} \left(\dfrac{\partial \tilde{R}_u^{(0)}(\rho)}{\partial\rho} \right) + \rho \right\} \displaystyle\int_0^{\phi} Q_1^{+(0)}(\phi', \rho) \frac{\partial}{\partial\rho} Q_1^{+(0)}(\phi', \rho)\, \mathrm{d}\phi' \\ -\tilde{\zeta}_u^{(1)}(\rho) \displaystyle\int_0^{\phi} \left\{ Q_1^{+(0)}(\phi', \rho) \right\}^2 \mathrm{d}\phi' \end{array} \right] \\ &\quad + \frac{\cosh\{\phi\tilde{\eta}_1(\rho)\}}{\tilde{\eta}_1(\rho)} \\ &\quad \times \left[\begin{array}{l} \rho^2 \displaystyle\int_{\phi}^{\alpha} \left\{ \frac{1}{\tilde{\eta}_1(\rho)} \frac{\partial}{\partial\phi'} Q_1^{+(0)}(\phi' - \alpha, \rho) \right\} \frac{\partial^2}{\partial\rho^2} Q_1^{+(0)}(\phi', \rho)\, \mathrm{d}\phi' \\ + \left\{ \dfrac{2\rho^2}{\tilde{R}_u^{(0)}(\rho)} \left(\dfrac{\partial \tilde{R}_u^{(0)}(\rho)}{\partial\rho} \right) + \rho \right\} \displaystyle\int_{\phi}^{\alpha} \left\{ \frac{1}{\tilde{\eta}_1(\rho)} \frac{\partial}{\partial\phi'} Q_1^{+(0)}(\phi' - \alpha, \rho) \right\} \frac{\partial}{\partial\rho} Q_1^{+(0)}(\phi', \rho)\, \mathrm{d}\phi' \\ -\tilde{\zeta}_u^{(1)}(\rho) \displaystyle\int_{\phi}^{\alpha} \left\{ \frac{1}{\tilde{\eta}_1(\rho)} \frac{\partial}{\partial\phi'} Q_1^{+(0)}(\phi' - \alpha, \rho) \right\} Q_1^{+(0)}(\phi', \rho)\, \mathrm{d}\phi' \end{array} \right] \end{aligned} \tag{196}$$

For the metallic region $j = 2$, equation (185) has the solution

$$Q_2^{+(1)}(\phi, \rho) = \int_\alpha^\pi \tilde{G}_2(\phi, \phi') N_2^{+(1)}(\phi', \rho)\, \mathrm{d}\phi' \qquad (\alpha \leqslant \phi \leqslant \pi) \tag{197}$$

with the Green's function

$$\tilde{G}_2(\phi, \phi') = \begin{cases} -\dfrac{\tilde{u}_2(\phi)\tilde{v}_2(\phi')}{\tilde{p}_2(\phi')\tilde{W}_2(\phi')}, & \alpha \leqslant \phi < \phi' \\ -\dfrac{\tilde{u}_2(\phi')\tilde{v}_2(\varphi)}{\tilde{p}_2(\phi')\tilde{W}_2(\phi')}, & \phi' < \phi \leqslant \pi, \end{cases} \tag{198}$$

where by choosing

$$\tilde{u}_2(\phi) = \sinh\{(\alpha - \phi)\tilde{\eta}_2(\rho)\} \tag{199}$$

and

$$\tilde{v}_2(\phi) = \cosh\{(\pi - \phi)\tilde{\eta}_2(\rho)\} \tag{200}$$

we get the Wronskian

$$W_2(\phi') = \tilde{\eta}_2(\rho)\cosh\{(\pi - \alpha)\tilde{\eta}_2(\rho)\} \tag{201}$$

and obviously we have

$$\tilde{p}_2(\phi') = 1. \tag{202}$$

It follows that

$$\begin{aligned} Q_2^{+(1)}(\phi, \rho) &= -\frac{\cosh\{(\pi - \phi)\tilde{\eta}_2(\rho)\}}{\tilde{\eta}_2(\rho)} \int_\alpha^\phi \frac{\sinh\{(\alpha - \phi')\tilde{\eta}_2(\rho)\}}{\cosh\{(\pi - \alpha)\tilde{\eta}_2(\rho)\}} N_2^{+(1)}(\phi', \rho)\, \mathrm{d}\phi' \\ &\quad - \frac{\sinh\{(\alpha - \phi)\tilde{\eta}_2(\rho)\}}{\tilde{\eta}_2(\rho)} \int_\phi^\pi \frac{\cosh\{(\pi - \phi')\tilde{\eta}_2(\rho)\}}{\cosh\{(\pi - \alpha)\tilde{\eta}_2(\rho)\}} N_2^{+(1)}(\phi', \rho)\, \mathrm{d}\phi' \\ &= \frac{\cosh\{(\pi - \phi)\tilde{\eta}_2(\rho)\}}{\tilde{\eta}_2(\rho)} \\ &\quad \times \left[\begin{array}{l} \rho^2 \displaystyle\int_\alpha^\phi \left\{ \frac{1}{\tilde{\eta}_2(\rho)} \frac{\partial}{\partial \phi'} Q_2^{+(0)}(\phi' + \pi - \alpha, \rho) \right\} \frac{\partial^2}{\partial \rho^2} Q_2^{+(0)}(\phi', \rho)\, \mathrm{d}\phi' \\ + \left\{ \dfrac{2\rho^2}{\tilde{R}_u^{(0)}(\rho)} \left(\dfrac{\partial \tilde{R}_u^{(0)}(\rho)}{\partial \rho} \right) + \rho \right\} \\ \times \displaystyle\int_\alpha^\phi \left\{ \frac{1}{\tilde{\eta}_2(\rho)} \frac{\partial}{\partial \phi'} Q_2^{+(0)}(\phi' + \pi - \alpha, \rho) \right\} \frac{\partial}{\partial \rho} Q_2^{+(0)}(\phi', \rho)\, \mathrm{d}\phi' \\ -\tilde{\zeta}_u^{(1)} \displaystyle\int_\alpha^\phi \left\{ \frac{1}{\tilde{\eta}_2(\rho)} \frac{\partial}{\partial \phi'} Q_2^{+(0)}(\phi' + \pi - \alpha, \rho) \right\} Q_2^{+(0)}(\phi', \rho)\, \mathrm{d}\phi' \end{array} \right] \\ &\quad - \frac{\sinh\{(\alpha - \phi)\tilde{\eta}_2(\rho)\}}{\tilde{\eta}_2(\rho)} \\ &\quad \times \left[\begin{array}{l} \rho^2 \displaystyle\int_\phi^\pi Q_2^{+(0)}(\phi', \rho) \frac{\partial^2}{\partial \rho^2} Q_2^{+(0)}(\phi', \rho)\, \mathrm{d}\phi' \\ + \left\{ \dfrac{2\rho^2}{\tilde{R}_u^{(0)}(\rho)} \left(\dfrac{\partial \tilde{R}_u^{(0)}(\rho)}{\partial \rho} \right) + \rho \right\} \displaystyle\int_\phi^\pi Q_2^{+(0)}(\phi', \rho) \frac{\partial}{\partial \rho} Q_2^{+(0)}(\phi', \rho)\, \mathrm{d}\phi' \\ -\tilde{\zeta}_u^{(1)} \displaystyle\int_\phi^\pi \left\{ Q_2^{+(0)}(\phi', \rho) \right\}^2 \mathrm{d}\phi' \end{array} \right]. \end{aligned} \tag{203}$$

8.2. Determination of the unified separation quantity of the first order for the metallic V-groove

The boundary condition (189) is used for determining the first-order unified separation quantity $\tilde{\zeta}_u^{(1)}$. Substituting equation (196) into the left side of equation (189), we get

$$\lim_{\phi\to\alpha-0}\frac{\partial}{\partial\phi}Q_1^{+(1)}(\phi,\rho)=-\int_0^{\alpha}Q_1^{+(0)}(\phi',\rho)N_1^{+(1)}(\phi',\rho)\,\mathrm{d}\phi'. \tag{204}$$

Substituting equation (203) into the right side of equation (189), we have

$$\lim_{\phi\to\alpha+0}\frac{\partial}{\partial\phi}Q_2^{+(1)}(\phi,\rho)=\int_{\alpha}^{\pi}Q_2^{+(0)}(\phi',\rho)N_2^{+(1)}(\phi',\rho)\,\mathrm{d}\phi'. \tag{205}$$

Setting equation (204) equal to equation (205) from equation (189), we find

$$\frac{1}{\varepsilon_1}\int_0^{\alpha}Q_1^{+(0)}(\phi',\rho)N_1^{+(1)}(\phi',\rho)\,\mathrm{d}\phi'+\frac{1}{\varepsilon_2}\int_{\alpha}^{\pi}Q_2^{+(0)}(\phi',\rho)N_2^{+(1)}(\phi',\rho)\,\mathrm{d}\phi'=0. \tag{206}$$

Substituting equations (186) into equation (206) and by rearranging terms, we find for the first-order unified separation quantity that

$$\tilde{\zeta}_u^{(1)}(\rho)=\frac{\left[\begin{array}{l}\rho^2\left\{\frac{1}{\varepsilon_1}\int_0^{\alpha}Q_1^{+(0)}(\phi,\rho)\frac{\partial^2}{\partial\rho^2}Q_1^{+(0)}(\phi,\rho)\,\mathrm{d}\phi+\frac{1}{\varepsilon_2}\int_{\alpha}^{\pi}Q_2^{+(0)}(\phi,\rho)\frac{\partial^2}{\partial\rho^2}Q_2^{+(0)}(\phi,\rho)\,\mathrm{d}\phi\right\}\\ +\left\{\frac{2\rho^2}{\tilde{R}_u^{(0)}(\rho)}\left(\frac{\partial\tilde{R}_u^{(0)}(\rho)}{\partial\rho}\right)+\rho\right\}\left\{\begin{array}{l}\frac{1}{\varepsilon_1}\int_0^{\alpha}Q_1^{+(0)}(\phi,\rho)\frac{\partial}{\partial\rho}Q_1^{+(0)}(\phi,\rho)\,\mathrm{d}\phi\\ +\frac{1}{\varepsilon_2}\int_{\alpha}^{\pi}Q_2^{+(0)}(\phi,\rho)\frac{\partial}{\partial\rho}Q_2^{+(0)}(\phi,\rho)\,\mathrm{d}\phi\end{array}\right\}\end{array}\right]}{\frac{1}{\varepsilon_1}\int_0^{\alpha}\left\{Q_1^{+(0)}(\phi,\rho)\right\}^2\mathrm{d}\phi+\frac{1}{\varepsilon_2}\int_{\alpha}^{\pi}\left\{Q_2^{+(0)}(\phi,\rho)\right\}^2\mathrm{d}\phi}, \tag{207}$$

where $\varepsilon_1=\varepsilon_d$ and $\varepsilon_2=\varepsilon_m$ are used for numerical calculations. Note that we can obtain equation (173) by replacing even (+) by odd (−), and tilde (˜) by circumflex (ˆ), in equation (207).

8.3. Unified radial function of the first order for the metallic V-groove

According to equations (121)–(125), the first-order unified radial equation (66) roughly approximates to

$$\frac{\partial^2\tilde{R}_u^{(1)}(\rho)}{\partial\rho^2}+\frac{1}{\rho}\frac{\partial\tilde{R}_u^{(1)}(\rho)}{\partial\rho}+\left(\{\tilde{k}_{mp}(\rho)\}^2+\frac{\nu^2q_1}{\rho}+\frac{\nu^2}{\rho^2}\right)\tilde{R}_u^{(1)}(\rho)=-\frac{\tilde{\zeta}_u^{(1)}(\rho)}{\rho^2}\tilde{R}_u^{(0)}(\rho). \tag{208}$$

On writing $\tilde{R}_u^{(1)}(\rho)=\rho^{-1/2}w^{(1)}(\rho)$ and using the rough approximation (127), we can transform equation (208) into

$$\frac{\partial^2w^{(1)}(\rho)}{\partial\rho^2}+\left(\{\tilde{k}_{mp}(0)\}^2+\frac{\nu^2q_1}{\rho}+\frac{\nu^2+\frac{1}{4}}{\rho^2}\right)w^{(1)}(\rho)=-\frac{\tilde{\zeta}_u^{(1)}(\rho)}{\rho^{3/2}}\tilde{R}_u^{(0)}(\rho), \tag{209}$$

whose associated homogeneous ODE has the pair of solutions, $W_{\mathrm{i}\kappa,\mathrm{i}\nu}(2\mathrm{i}\rho\tilde{k}_{mp}(0))$ and $W_{-\mathrm{i}\kappa,\mathrm{i}\nu}(-2\mathrm{i}\rho\tilde{k}_{mp}(0))$. By referring to section 2.7 in [50], we get the Wronskian

$$W\{W_{\mathrm{i}\kappa,\mathrm{i}\nu}(2\mathrm{i}\rho\tilde{k}_{mp}(0)),\,W_{-\mathrm{i}\kappa,\mathrm{i}\nu}(-2\mathrm{i}\rho\tilde{k}_{mp}(0))\}=2\mathrm{i}\tilde{k}_{mp}(0)\,\mathrm{e}^{-\kappa\pi}. \tag{210}$$

By taking account of the following boundary condition from equation (69),

$$\tilde{R}_u^{(1)}(\rho)=0\qquad(\rho\to0), \tag{211}$$

we can solve the nonhomogeneous ODE (209) by using the particular solution in equations (175)–(178). After some algebraic operations, we find the solution

$$\tilde{R}_u^{(1)}(\rho) = \tilde{R}_{\text{in}}^{(1)}(\rho) + \tilde{R}_{\text{out}}^{(1)}(\rho), \tag{212}$$

where

$$\begin{aligned}\tilde{R}_{\text{in}}^{(1)}(\rho) &= -\mathrm{i}\mathrm{e}^{\kappa\pi}\rho^{-1/2}W_{\mathrm{i}\kappa,\mathrm{i}\nu}(2\mathrm{i}\rho\tilde{k}_{mp}(0)) \\ &\times \int_0^{\rho} \tilde{\zeta}_u^{(1)}(\rho')\tilde{R}_u^{(0)}(\rho')W_{-\mathrm{i}\kappa,\mathrm{i}\nu}(-2\mathrm{i}\rho'\tilde{k}_{mp}(0))\frac{\mathrm{d}\rho'}{2\tilde{k}_{mp}(0)(\rho')^{3/2}}\end{aligned} \tag{213}$$

and

$$\begin{aligned}\tilde{R}_{\text{out}}^{(1)}(\rho) &= \mathrm{i}\mathrm{e}^{\kappa\pi}\rho^{-1/2}W_{-\mathrm{i}\kappa,\mathrm{i}\nu}(-2\mathrm{i}\rho\tilde{k}_{mp}(0)) \\ &\times \int_0^{\rho} \tilde{\zeta}_u^{(1)}(\rho')\tilde{R}_u^{(0)}(\rho')W_{\mathrm{i}\kappa,\mathrm{i}\nu}(2\mathrm{i}\rho'\tilde{k}_{mp}(0))\frac{\mathrm{d}\rho'}{2\tilde{k}_{mp}(0)(\rho')^{3/2}}.\end{aligned} \tag{214}$$

Note that $\tilde{R}_{\text{in}}^{(1)}(\rho)$ and $\tilde{R}_{\text{out}}^{(1)}(\rho)$ correspond to the incoming and outgoing waves, respectively, for $\rho \to \infty$.

We can obtain the second-order perturbation solutions for the metallic V-groove in much the same manner as the first-order perturbation solutions (see appendix D).

9. Electric-field-line representation

It is very important to understand superfocusing SPPs not only mathematically but also visually. In the present case where the electromagnetic field has only a z-component of the magnetic field in the cylindrical coordinates system, we can use a field-line pattern representation of the electric field, which is graphically simpler and more intuitive than the field-vector pattern representation.

Here, we describe the field-line pattern representation of an electric field in detail. The tangent at an arbitrary point on an electric field line indicates the direction of the electric field vector $\boldsymbol{E}(\rho, \phi, t)$ at that point. This fact can be described mathematically by using a line vector element $\mathrm{d}\boldsymbol{s}$ as follows:

$$\boldsymbol{E}(\rho, \phi, t) \times \mathrm{d}\boldsymbol{s} = 0 \tag{215}$$

which can be simplified into

$$\frac{\mathrm{d}\rho}{E_\rho(\rho, \phi, t)} - \frac{\rho\,\mathrm{d}\phi}{E_\phi(\rho, \phi, t)} = 0 \tag{216}$$

when

$$\boldsymbol{E}(\rho, \phi, t) = E_\rho(\rho, \phi, t)\boldsymbol{e}_\rho + E_\phi(\rho, \phi, t)\boldsymbol{e}_\phi, \tag{217}$$

$$\mathrm{d}\boldsymbol{s} = \mathrm{d}\rho\,\boldsymbol{e}_\rho + \rho\,\mathrm{d}\phi\,\boldsymbol{e}_\phi, \tag{218}$$

where $\boldsymbol{e}_\rho$ and $\boldsymbol{e}_\phi$ are the unit vectors along the ρ- and φ-axes, respectively. For the magnetic fields described in equations (1) and (2), from equations (41)–(47) and equation (4), we can get the ρ and φ components of the electric field as follows:

$$E_\rho(\rho, \phi, t) = \mathrm{Re}[E_\rho(\rho, \phi)\ \exp(-\mathrm{i}\omega t)] = \frac{c}{\omega\varepsilon_j}\frac{1}{\rho}\frac{\partial}{\partial\phi}H_z\left(\rho, \phi, t - \frac{\pi}{2\omega}\right), \tag{219}$$

$$E_\phi(\rho, \phi, t) = \mathrm{Re}[E_\phi(\rho, \phi)\ \exp(-\mathrm{i}\omega t)] = -\frac{c}{\omega\varepsilon_j}\frac{\partial}{\partial\rho}H_z\left(\rho, \phi, t - \frac{\pi}{2\omega}\right). \tag{220}$$

Substituting equations (219) and (220) into equation (216), we obtain a differential equation expressed in terms of total derivatives with respect to ρ and ϕ as follows:

$$\frac{\partial}{\partial\rho}\left(H_z\left(\rho,\phi,t-\frac{\pi}{2\omega}\right)\right)\mathrm{d}\rho+\frac{\partial}{\partial\phi}\left(H_z\left(\rho,\phi,t-\frac{\pi}{2\omega}\right)\right)\mathrm{d}\phi=0, \tag{221}$$

which can be described by the exact differential form

$$\mathrm{d}\psi(\rho,\theta)=\frac{\partial}{\partial\rho}\psi(\rho,\theta)\,\mathrm{d}\rho+\frac{\partial}{\partial\phi}\psi(\rho,\theta)\,\mathrm{d}\phi=0 \tag{222}$$

with the solution

$$\psi(\rho,\theta)=\text{constant}, \tag{223}$$

if we set

$$\psi(\rho,\theta)=H_z\left(\rho,\phi,t-\frac{\pi}{2\omega}\right). \tag{224}$$

Since the time-varying scalar field for the electric-field-line representation, denoted by $f(\rho,\phi,t)$, is proportional to the sinusoidal time dependence $\mathrm{e}^{-\mathrm{i}\omega t}$, by taking account of equation (2) in estimating equation (224), we can set

$$f(\rho,\phi,t)=\psi(\rho,\theta) \tag{225}$$

or

$$f(\rho,\phi,t)=H_z\left(\rho,\phi,t-\frac{\pi}{2\omega}\right). \tag{226}$$

The field-line pattern at time $t=t_0$ is described by a scalar field with the contour

$$f(\rho,\phi,t_0)=C, \tag{227}$$

where C is the contour level. The contour interval can be controlled by the interval value of the contour level. The evolution of field-line patterns can be investigated for different moments

$$t=t_0+n\tau, \qquad \text{with} \qquad n=0,1,2,3,\ldots \tag{228}$$

where τ is a suitably chosen duration between two neighboring snapshots.

For actual calculations, let us rewrite equation (226) into a form containing the unified radial function and the extended angular function. Substituting equations (2), (4), (5) and (39) into equation (226), we obtain the scalar field for the electric-field-line representation as follows:

$$f(\rho,\phi,t)=\mathrm{Re}\big[\mathrm{R}_u(\rho)Q_j^s(\phi,\rho)\,\exp(-\mathrm{i}\omega t+\mathrm{i}\pi/2)\big], \qquad j=1,2, \tag{229}$$

where s indicates the even (+) or odd (−) symmetry with respect to ϕ and $\mathrm{R}_u(\rho)$ is accordingly determined. The electric-field-line representation becomes more accurate when we use a higher-order approximate solution of the unified radial and extended angular functions in equation (229). When the zeroth-order approximated solution is used in equation (229), the scalar field for the electric-field-line representation becomes

$$f^{0\mathrm{th}}(\rho,\phi,t)=\mathrm{Re}\big[\mathrm{R}_u^{(0)}(\rho)Q_j^{s(0)}(\phi,\rho)\,\exp(-\mathrm{i}\omega t+\mathrm{i}\pi/2)\big], \qquad j=1,2. \tag{230}$$

For the first-order approximated solution, it becomes

$$\begin{aligned} f^{1\mathrm{st}}(\rho,\phi,t)=\mathrm{Re}\big[&\big\{\mathrm{R}_u^{(0)}(\rho)+\mathrm{R}_u^{(1)}(\rho)\big\}\big\{Q_j^{s(0)}(\phi,\rho)+Q_j^{s(1)}(\phi,\rho)\big\}\\ &\times\exp(-\mathrm{i}\omega t+\mathrm{i}\pi/2)\big], \qquad j=1,2. \end{aligned} \tag{231}$$

In the same manner, we can easily write the scalar field for the electric-field-line representation when given the second-order approximated solution.

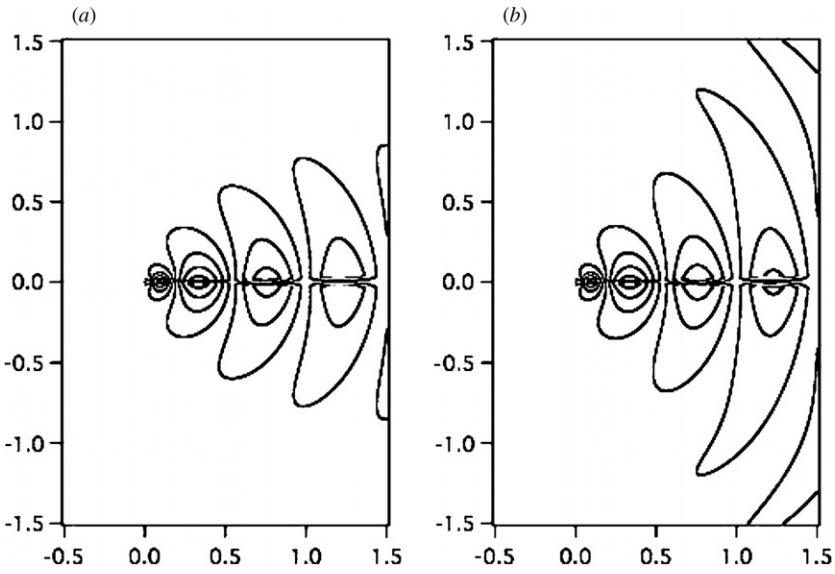

Figure 7. Electric field lines of superfocusing modes of SPPs in the metallic wedge with the wedge angle $2\alpha = 3^\circ$, obtained using the zeroth-order (a) and first-order (b) approximate solutions calculated for $\varepsilon_1 = -20$ and $\varepsilon_2 = 1$. Geometrical dimensions of the horizontal and vertical axes are $\rho/\lambda_0 = 1$.

Figure 7 shows the electric-field-line patterns of superfocusing modes for the metallic wedge with the angle $2\alpha = 3^\circ$ using the zeroth-order (a) and first-order (b) approximate solutions (equations (230) and (231)), where $\mathrm{R}_u^{(0)}(\rho)$, $\mathrm{R}_u^{(1)}(\rho)$, $Q_j^{s(0)}(\phi, \rho)$ and $Q_j^{s(1)}(\phi, \rho)$ are, respectively, replaced by $\hat{R}_u^{(0)}(\rho)$, $\hat{R}_u^{(1)}(\rho)$, $Q_j^{-(0)}(\phi, \rho)$ and $Q_j^{-(1)}(\phi, \rho)$. In the calculation, we used $\varepsilon_d = 1$, $\varepsilon_m = -20$, $t_0 = 0$ and $H_0 = 1$. Between parts (a) and (b) in the figure, the electric-field-line patterns look much the same near the origin and the wedge surface but become different farther from them. This behavior can be understood by the fact that the radial and extended angular functions of the first order are solved so as to equal zero at the origin and the wedge surface, respectively. Figure 7 suggests that around the origin, or the wedge apex, the zeroth-order approximate solution is sufficiently accurate to show the electric-field-line patterns for the metallic wedge.

Figure 8 shows the electric-field-line patterns of superfocusing modes for the metallic V-groove with the angle $2\alpha = 5^\circ$ for the zeroth-order (a) and first-order (b) approximate solutions (equations (230) and (231)), respectively, where $\mathrm{R}_u^{(0)}(\rho)$, $\mathrm{R}_u^{(1)}(\rho)$, $Q_j^{s(0)}(\phi, \rho)$ and $Q_j^{s(1)}(\phi, \rho)$ are, respectively, replaced by $\tilde{R}_u^{(0)}(\rho)$, $\tilde{R}_u^{(1)}(\rho)$, $Q_j^{+(0)}(\phi, \rho)$ and $Q_j^{+(1)}(\phi, \rho)$. In the calculations, we used $\varepsilon_d = 1$, $\varepsilon_m = -20$, $t_0 = 0$ and $H_0 = 1$, as in figure 7. The electric-field-line patterns between parts (a) and (b) in the figure look the same. This behavior can be understood from the following two facts: (i) the radial functions of the first order in equations (212)–(214) are estimated to have much smaller absolute values than those of the zeroth-order because of the small factor $\mathrm{e}^{\kappa\pi}$ in equations (213) and (214), where κ is negative and its specific values are shown in table 4 and (ii) the extended angular functions of the first order in equations (196) and (203) are estimated to have small absolute values because they are, respectively, inversely proportional to $\tilde{\eta}_1(\rho)$ and $\tilde{\eta}_2(\rho)$, which are much larger than unity (e.g., $\tilde{\eta}_1(0) = \tilde{\eta}_2(0) = 5.91$ for the wedge angle $2\alpha = 5^\circ$ in our calculation conditions).

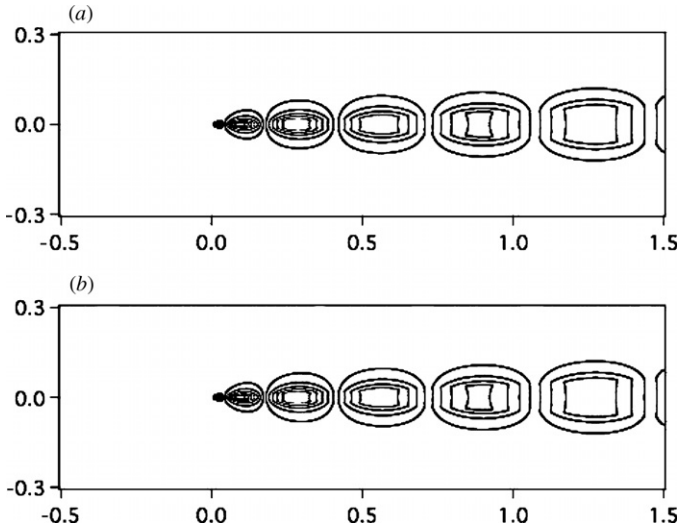

Figure 8. Electric field lines of the superfocusing modes of SPPs in the metallic V-groove with the wedge angle $2\alpha = 5^\circ$, obtained using the zeroth-order (*a*) and first-order (*b*) approximate solutions calculated for $\varepsilon_1 = 1$ and $\varepsilon_2 = -20$. Geometrical dimensions of the horizontal and vertical axes are $\rho/\lambda_0 = 1$.

Therefore, figure 8 suggests that the zeroth-order approximate solution can be used in place of the first-order approximate solution to show the electric-field-line patterns for the metallic V-groove.

Finally, it is highly important to point out that the electric-field-line patterns in figures 7 and 8 also represent their respective contour lines of the magnetic scalar field; it can be clearly understood from equation (226). Using equations (226)–(228), we could develop a computer-aided animation of the field-pattern evolution that would give a more intuitive understanding of the accumulation of superfocusing SPPs.

10. Wave numbers of superfocusing SPPs

Superfocusing modes of SPPs are briefly characterized by their wave numbers derived from their radial functions. In sections 6.4 and 6.5, we find that the zeroth-order radial functions for the metallic wedge and V-groove are described by the imaginary Bessel and modified Whittaker functions, respectively. This holds true for the first-order radial functions (see section 7.3 and 8.3 for the metallic wedge and V-groove, respectively) and the higher-order ones (see appendices C.3 and D.3 for the second-order). By approximately expressing the imaginary Bessel and modified Whittaker functions with exponential functions, we can determine the wave numbers of superfocusing SPPs for the metallic wedge and V-groove. The imaginary Bessel and modified Whittaker functions belong to the class of linear second-order homogeneous ODEs, for which asymptotic expansions based on exponential functions are categorized as the Liouville–Green approximation (also called the WKB approximation in relation with connection formulas). The Liouville transformation (see chapter 4.5 in [41]) is frequently used in the Liouville–Green approximation.

For the imaginary Bessel functions $H_{i\nu}^{(1)}(\nu z)$ and $H_{i\nu}^{(2)}(\nu z)$, from section 5 in [48], we have the Liouville–Green asymptotic approximation

$$H_{i\nu}^{(l)}(\nu z) \approx \mathrm{e}^{\pm\nu\pi/2}\left(\frac{2}{\pi\nu}\right)^{1/2}(1+z^2)^{-1/4}\,\exp[\pm\mathrm{i}(\nu\hat{\xi}(z)-\pi/4)](1+\cdots) \tag{232}$$

where

$$\hat{\xi}(z) = (1+z^2)^{1/2} + \ln\left(\frac{z}{1+(1+z^2)^{1/2}}\right) \tag{233}$$

and the upper and lower signs correspond to the case $l = 1$ and $l = 2$, respectively. In equation (232), by replacing z by $\rho\hat{k}_{mp}(\rho)/\nu$, we obtain an asymptotic approximation for $H_{i\nu}^{(1)}(\rho\hat{k}_{mp}(\rho))$ and $H_{i\nu}^{(2)}(\rho\hat{k}_{mp}(\rho))$, which appear in the zeroth-order radial functions for the metallic wedge (equations (116) and (117)). Therefore, the wave number of superfocusing SPPs for the metallic wedge, $\hat{k}_w(\rho)$, is given by

$$\hat{k}_w(\rho) = \nu\frac{\mathrm{d}}{\mathrm{d}\rho}\hat{\xi}\left(\frac{\rho\hat{k}_{mp}(\rho)}{\nu}\right). \tag{234}$$

Substituting equation (233) into equation (234) and using the quasi-constant condition for $\hat{k}_{mp}(\rho)$ in equations (102) and (103), we find that

$$\hat{k}_w(\rho) = \frac{\nu}{\rho}\sqrt{1+\frac{\{\hat{k}_{mp}(\rho)\}^2\rho^2}{\nu^2}}, \tag{235}$$

which can be expanded into a form appropriate for small ρ:

$$\hat{k}_w(\rho) \approx \frac{\nu}{\rho} + \frac{\{\hat{k}_{mp}(0)\}^2\rho}{2\nu} + \cdots. \tag{236}$$

Equation (236) clearly shows that the wave number of SPPs for the metallic wedge anomalously increases closer to the wedge apex. By using equations (97) and (100), the behavior of $\hat{k}_w(\rho)$ for large values of ρ can be described by the asymptotic formula

$$\hat{k}_w(\rho) \sim k_p \qquad (\rho\to\infty), \tag{237}$$

which is exactly the starting point of the unified radial function described by equations (21)–(23). Figure 9(*a*) shows $\hat{k}_w(\rho)/k_p$ as a function of ρ for specific wedge angles. This is a plot of $\hat{k}_w(\rho)$, calculated from equation (235) using equations (97) and (100), and divided by k_p in equation (23), where $k_p\lambda_0 = 6.446$. It is clear that the wave number of SPPs approaching the wedge apex increases more rapidly for the shaper wedge angle.

For the modified Whittaker functions $W_{-\mathrm{i}\kappa,\mathrm{i}\nu}(-\mathrm{i}\nu z)$ and $W_{\mathrm{i}\kappa,\mathrm{i}\nu}(\mathrm{i}\nu z)$ under the condition $-\kappa > \nu > 0$, according to appendix A, we have the Liouville–Green asymptotic approximation

$$\begin{aligned} W_{\mp\mathrm{i}\kappa,\mathrm{i}\nu}(\mp\mathrm{i}\nu z) &\approx 2^{-1/2}\,\mathrm{e}^{-\pi\kappa/2}\nu^{\mp\mathrm{i}(\nu+2\kappa)}(\nu-\kappa)^{\pm\mathrm{i}\nu}(2\nu-\kappa)^{\pm\mathrm{i}\kappa} \\ &\times\left(\frac{z^2-4\frac{\kappa}{\nu}z+z}{4z^2}\right)^{-\frac{1}{4}}\exp[\pm\mathrm{i}\nu\tilde{\xi}(z)](1+\cdots), \end{aligned} \tag{238}$$

where

$$\begin{aligned} \tilde{\xi}(z) &= \frac{1}{2}\left(z^2-4\frac{\kappa}{\nu}z+4\right)^{\frac{1}{2}} + \ln\left\{\frac{z}{2-\frac{\kappa}{\nu}z+\left(z^2-4\frac{\kappa}{\nu}z+4\right)^{\frac{1}{2}}}\right\} \\ &- \frac{\kappa}{\nu}\ln\left\{z-\frac{\kappa}{\nu}z+\left(z^2-4\frac{\kappa}{\nu}z+4\right)^{\frac{1}{2}}\right\}. \end{aligned} \tag{239}$$

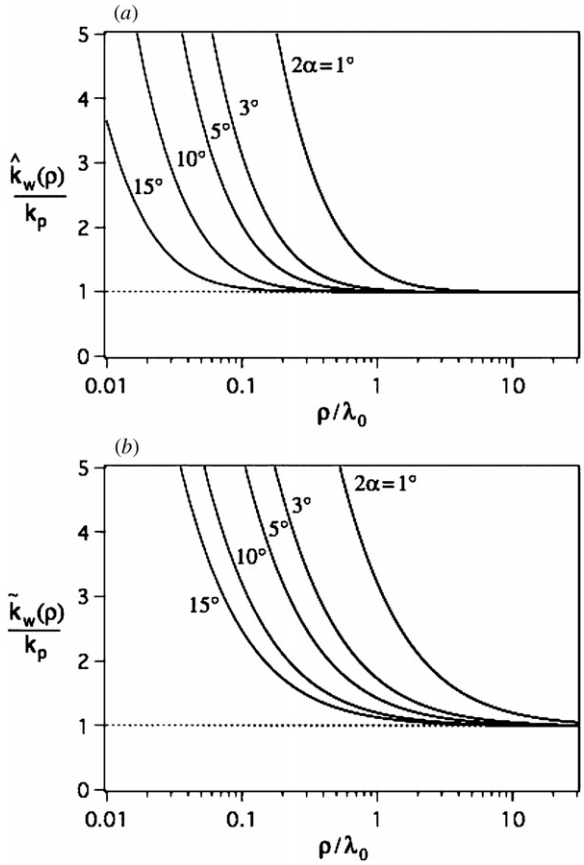

Figure 9. Numerical calculations of the wave numbers of superfocusing SPPs, $\hat{k}_w(\rho)$ and $\tilde{k}_w(\rho)$, in the metallic wedge (*a*) and V-groove (*b*), respectively, as calculated by equations (235) and (241), respectively. For convenience of explanation, $\hat{k}_w(\rho)/k_p$ and $\tilde{k}_w(\rho)/k_p$ are shown, where k_p is the wave number of planar SPPs given in equation (23).

In equation (238), by replacing z by $2\rho\tilde{k}_{mp}(0)/\nu$, we obtain the asymptotic approximation for $W_{-\mathrm{i}\kappa,\mathrm{i}\nu}(-2\mathrm{i}\rho\tilde{k}_{mp}(0))$ and $W_{\mathrm{i}\kappa,\mathrm{i}\nu}(2\mathrm{i}\rho\tilde{k}_{mp}(0))$, which appear in the zeroth-order radial functions for the metallic V-groove (equations (137) and (138)). Therefore, the wave number of superfocusing SPPs for the metallic V-groove, $\tilde{k}_w(\rho)$, is given by

$$\tilde{k}_w(\rho) = \nu \frac{\mathrm{d}}{\mathrm{d}\rho}\tilde{\xi}\left(\frac{2\rho\tilde{k}_{mp}(0)}{\nu}\right). \tag{240}$$

Substituting equation (239) into equation (240), we find that

$$\tilde{k}_w(\rho) = \frac{\nu}{\rho}B(\rho) + \frac{\kappa^2\tilde{k}_{mp}(0)\{\nu(1+B(\rho)) - \tilde{k}_{mp}(0)\rho\}}{\nu B(\rho)\{\nu^2 B(\rho) + \tilde{k}_{mp}(0)\rho(\nu-\kappa)\}}, \tag{241}$$

where

$$B(\rho) = \sqrt{1 + \frac{\tilde{k}_{mp}(0)\rho\{\tilde{k}_{mp}(0)\rho - 2\kappa\}}{\nu^2}}. \tag{242}$$

Note that equation (241) becomes equation (235) when setting $\kappa = 0$ and replacing tilde (˜) by circumflex (ˆ), which are the correspondence conditions for superfocusing SPPs between the metallic wedge and V-groove. Expanding equation (241) for small ρ, we find that

$$\tilde{k}_w(\rho) \approx \frac{\nu}{\rho} + \frac{\tilde{k}_{mp}(0)\kappa(2\kappa - \nu)}{\nu^2} + \frac{\{\tilde{k}_{mp}(0)\}^2(10\kappa^3 - 7\kappa^2\nu + \nu^3)\rho}{2\nu^4} + \cdots, \tag{243}$$

which is essentially different from equation (236) as it has a term $\rho^0(=1)$. The behavior of $\tilde{k}_w(\rho)$ in equation (241) for large values of ρ is described by the asymptotic formula

$$\tilde{k}_w(\rho) \sim \tilde{k}_{mp}(0) \qquad (\rho \to \infty), \tag{244}$$

in which $\tilde{k}_{mp}(0)$ given by equation (129) is nearly equal to k_p (compare specific values of $\tilde{k}_{mp}(0)\lambda_0$ in table 4 with $k_p\lambda_0 = 6.446$). Since the zeroth-order unified radial equation for the metallic V-groove is roughly approximately described by the modified Whittaker equation, equation (244) approximately satisfies $\tilde{k}_w(\rho) \sim k_p$ as $\rho \to \infty$ described in equations (21)–(23), which we assumed in order to introduce the unified radial equation. Figure 9(*b*) shows $\tilde{k}_w(\rho)/k_p$ as a function of ρ for specific wedge angles. This is a plot of equation (241) calculated with equation (242) and divided by k_p in equation (23). There are three appreciable differences between parts (*a*) and (*b*): first, the wave numbers for SPPs in the metallic V-groove increase farther from the wedge apex than those for the metallic wedge; second, the former's increase is slower than the latter's; third, the former always has a larger wave number at any point ρ. These behaviors are caused by the strengthening electric fields of SPPs for the metallic V-groove, which have the even symmetry in the magnetic field. In contrast, SPPs for the metallic wedge have a weakening electric field and the odd symmetry in the magnetic field. The extraordinary enhancement of the electromagnetic field results from the accumulation of SPPs due to the change from rapid to slow propagation, which is briefly characterized by the increase in the wave number. Figure 9 shows that compared with the odd symmetry of the metallic wedge, the even symmetry of the magnetic field for the metallic V-groove enables more superfocusing SPPs to be accumulated. This implies that the symmetry of the magnetic field plays a critical role in the accumulation of superfocusing SPPs.

11. Conclusions

We have studied the superfocusing modes of SPPs for the metallic wedge and V-groove by solving the Helmholtz wave equation for the magnetic field by using quasi-separation of variables in combination with perturbation methods. The zeroth- and first-order perturbation equations for radial and extended angular functions were solved analytically. The second-order perturbation solutions for the metallic wedge and V-groove are briefly described in appendices C and D. For the metallic wedge and V-groove, we showed that the radial equations of the zeroth order approximate the imaginary Bessel and modified Whittaker equations, respectively; the extended angular functions of the zeroth and higher order have odd and even symmetries, respectively, for reflection in the central plane of the wedge-shaped geometry. The radial and extended angular equations of the first order, which are nonhomogeneous, linear, second-order ODEs, were respectively solved by variation of parameters and Green's functions. In order to intuitively understand the zeroth- and first-order approximate solutions, we plotted their electric-field-line patterns for the metallic wedge and V-groove. The wave numbers of superfocusing SPPs were obtained as analytic formulas by using the Liouville–Green asymptotic approximation. We found that for the same wedge angle and the permittivities of metal and dielectric materials, the metallic V-groove has a much stronger superfocusing effect than the metallic wedge. We believe that the quasi-separation of variables method for

solving the Helmholtz wave equation is a powerful technique for theoretically understanding the plasmonic superfocusing in various geometries.

Acknowledgments

The authors are thankful to Professors M Haraguchi and M Fukui of the University of Tokushima for their useful discussions and comments.

Appendix A. Asymptotic expansions for the modified Whittaker functions $W_{\mathrm{i}\kappa,\mathrm{i}\mu}(\mathrm{i}z)$ and $W_{-\mathrm{i}\kappa,\mathrm{i}\mu}(-\mathrm{i}z)$

In this appendix, we study the asymptotic behavior of the modified Whittaker functions $W_{\mathrm{i}\kappa,\mathrm{i}\mu}(\mathrm{i}z)$ and $W_{-\mathrm{i}\kappa,\mathrm{i}\mu}(-\mathrm{i}z)$ for the case $\kappa < 0$, $\mu > 0$ and $z > 0$ with the condition $\kappa/\mu < -1$, for which, as far as we know [42, 51, 54, 55], the asymptotic expansions have not yet been considered. The definitions, characteristics and the connection formulas of Whittaker functions are summarized in section 2 in [51]. The modified Whittaker differential equation

$$\frac{\mathrm{d}^2 w}{\mathrm{d}z^2} = \left(-\frac{1}{4} + \frac{\kappa}{z} - \frac{\mu^2 + \frac{1}{4}}{z^2}\right) w \tag{A.1}$$

is obtained from the Whittaker differential equation

$$\frac{\mathrm{d}^2 w}{\mathrm{d}z^2} = \left(\frac{1}{4} - \frac{\kappa}{z} + \frac{\mu^2 - \frac{1}{4}}{z^2}\right) w \tag{A.2}$$

by replacing κ, μ and z by $\mathrm{i}\kappa$, $\mathrm{i}\mu$ and $\mathrm{i}z$, respectively. The modified Whittaker functions $W_{\mathrm{i}\kappa,\mathrm{i}\mu}(\mathrm{i}z)$ and $W_{-\mathrm{i}\kappa,\mathrm{i}\mu}(-\mathrm{i}z)$ satisfy equation (A.1). With the substitutions

$$x = z/\mu, \qquad \lambda = \kappa/\mu, \tag{A.3}$$

equation (A.1) becomes

$$\frac{\mathrm{d}^2 w}{\mathrm{d}x^2} = \{-\mu^2 f(x) + g(x)\} w, \tag{A.4}$$

where

$$f(x) = \frac{x^2 - 4\lambda x + 4}{4x^2} \tag{A.5}$$

and

$$g(x) = -\frac{1}{4x^2}. \tag{A.6}$$

The differential equation (A.4) is characterized by a regular singularity at $x = 0$, an irregular singularity at $x = \infty$ and turning points at $x = x_1$ and $x = x_2$, where

$$x_1 = 2\lambda - 2(\lambda^2 - 1)^{\frac{1}{2}}, \qquad x_2 = 2\lambda + 2(\lambda^2 - 1)^{\frac{1}{2}}. \tag{A.7}$$

For the present conditions

$$\lambda = \kappa/\mu < -1, \tag{A.8}$$

both x_1 and x_2 are real and negative, and $f(x)$ is positive throughout $0 < x < \infty$. By applying the Liouville transformation of section 2 in chapter 10 of [42],

$$W = \left(\frac{\mathrm{d}\xi}{\mathrm{d}x}\right)^{\frac{1}{2}} w, \qquad \left(\frac{\mathrm{d}\xi}{\mathrm{d}x}\right)^2 = f(x), \tag{A.9}$$

equation (A.4) can be transformed into the form

$$\frac{\mathrm{d}^2 W}{\mathrm{d}\xi^2} = (-\mu^2 + \psi(\xi))W, \tag{A.10}$$

where

$$\xi(x) = \int f^{1/2}(x)\,\mathrm{d}x = \frac{1}{2}(x^2 - 4\lambda x + 4)^{\frac{1}{2}} + \ln\left\{\frac{x}{2 - \lambda x + (x^2 - 4\lambda x + 4)^{\frac{1}{2}}}\right\}$$
$$-\lambda \ln\{x - \lambda x + (x^2 - 4\lambda x + 4)^{\frac{1}{2}}\}, \tag{A.11}$$

$$W(\xi) = f^{1/4}(x)w(x) = \left(\frac{x^2 - 4\lambda x + 4}{4x^2}\right)^{1/4} w(x) \tag{A.12}$$

and

$$\psi(\xi) = \frac{g(x)}{f(x)} - \frac{1}{f^{3/4}(x)}\frac{\mathrm{d}^2}{\mathrm{d}x^2}\left\{\frac{1}{f^{1/4}(x)}\right\} = -\frac{x\{x^3 + 16\lambda + 4z(-4 + \lambda^2)\}}{(x^2 - 4\lambda x + 4)^3}. \tag{A.13}$$

Note that the integration constant in equation (A.11) is taken to be zero for later convenience.

According to theorem 3.1 of chapter 10 [42], the transformed equation (A.10) has the following solutions:

$$W_{n,1}(\mu, \xi) = \mathrm{e}^{\mathrm{i}\mu\xi} \sum_{s=0}^{n-1} \frac{A_s(\xi)}{(\mathrm{i}\mu)^s} + \varepsilon_{n,1}(\mu, \xi), \tag{A.14}$$

$$W_{n,2}(\mu, \xi) = \mathrm{e}^{-\mathrm{i}\mu\xi} \sum_{s=0}^{n-1} (-1)^s \frac{A_s(\xi)}{(i\mu)^s} + \varepsilon_{n,2}(\mu, \xi), \tag{A.15}$$

where coefficients A_s are defined recursively by $A_0 = 1$ and

$$A_{s+1} = -\frac{x}{(x^2 - 4\lambda x + 4)^{1/2}}\frac{\mathrm{d}A_s}{\mathrm{d}x} - \frac{1}{4}\int \frac{\{x^3 + 16\lambda + 4x(-4 + \lambda^2)\}}{(x^2 - 4\lambda x + 4)^{5/2}} A_s\,\mathrm{d}x \qquad (s \geqslant 0)$$
$$. \tag{A.16}$$

(Compare (2.09) and (2.10) of chapter 10 [42].) The integration constant in equation (A.16) can be determined upon the condition $A_{s+1} \to 0$ as $x \to \infty$. In the case of $s = 1$ in equation (A.16), we have

$$A_1 = -\frac{\lambda x - 8\lambda^2 + 6}{24(-1 + \lambda^2)(x^2 - 4\lambda x + 4)^{1/2}} + \frac{5(\lambda x - 2)}{6(x^2 - 4\lambda x + 4)^{3/2}}. \tag{A.17}$$

We now identify solutions (A.14) and (A.15) with the modified Whittaker functions by using the asymptotic formula (see (11.05) of chapter 7 [42])

$$W_{\kappa,\mu}(z) \sim \mathrm{e}^{-z/2} z^{\kappa} \left(z \to \infty, |\mathrm{ph}\, z| < \frac{3}{2}\pi\right). \tag{A.18}$$

First, we see that for some constant c_1

$$W_{-\mathrm{i}\kappa,\mathrm{i}\mu}(-\mathrm{i}\mu x) = c_1 \left(\frac{x^2 - 4\lambda x + 4}{4x^2}\right)^{-\frac{1}{4}} W_{n,1}(\mu, \xi), \tag{A.19}$$

since both functions are the solutions of modified Whittaker equations and share the same recessive properties as $x \to +\mathrm{i}\infty$. By comparing both sides as $x \to +\mathrm{i}\infty$, we find that

$$c_1 = 2^{-1/2}\,\mathrm{e}^{-\pi\kappa/2}\mu^{-\mathrm{i}(\mu+2\kappa)}(\mu - \kappa)^{\mathrm{i}\mu}(2\mu - \kappa)^{\mathrm{i}\kappa}. \tag{A.20}$$

In the same manner, we see that for some constant c_2,

$$W_{\mathrm{i}\kappa,\mathrm{i}\mu}(\mathrm{i}\mu x) = c_2 \left(\frac{x^2 - 4\lambda x + 4}{4x^2}\right)^{-\frac{1}{4}} W_{n,2}(\mu, \xi), \tag{A.21}$$

since both functions are also solutions to modified Whittaker equations and share the same recessive properties as $x \to -\mathrm{i}\infty$. By comparing both sides as $x \to -\mathrm{i}\infty$, we find that

$$c_2 = 2^{-1/2}\, \mathrm{e}^{-\pi\kappa/2} \mu^{\mathrm{i}(\mu+2\kappa)} (\mu - \kappa)^{-\mathrm{i}\mu} (2\mu - \kappa)^{-\mathrm{i}\kappa}. \tag{A.22}$$

We see from equations (A.19) and (A.21) that under the time dependence $\mathrm{e}^{-\mathrm{i}\omega t}$, $W_{-\mathrm{i}\kappa,\mathrm{i}\mu}(-\mathrm{i}z)$ and $W_{\mathrm{i}\kappa,\mathrm{i}\mu}(\mathrm{i}z)$ correspond to outgoing and incoming waves, respectively, for $z \to \infty$.

Appendix B. Relation between $M_{\mathrm{i}\kappa,-\mathrm{i}\mu}(\mathrm{i}z)$ and $W_{\pm\mathrm{i}\kappa,\mathrm{i}\mu}(\pm\mathrm{i}z)$

According to section 2 in [51], the standard solutions of the Whittaker differential equation (A.2) are

$$M_{\kappa,\mu}(z) \equiv \mathrm{e}^{-z/2} z^{1/2+\mu} \cdot {}_1F_1\left(\frac{1}{2} + \mu - \kappa; 2\mu + 1; z\right), \tag{B.1}$$

$$W_{\kappa,\mu}(z) \equiv \frac{\Gamma(-2\mu)}{\Gamma\left(\frac{1}{2} - \mu - \kappa\right)} M_{\kappa,\mu}(z) + \frac{\Gamma(2\mu)}{\Gamma\left(\frac{1}{2} + \mu - \kappa\right)} M_{\kappa,-\mu}(z), \tag{B.2}$$

where ${}_1F_1$ denotes the confluent hypergeometric function. Each $M_{\kappa,\mu}(z)$ and $W_{\kappa,\mu}(z)$ is a many-valued function of z. Principal branches correspond to the range $-\pi < \mathrm{ph} z \leqslant \pi$.

From Kummer's first formula [41, 51],

$${}_1F_1(\alpha; \beta; z) = \mathrm{e}^{z} \cdot {}_1F_1(\beta - \alpha; \beta; -z), \tag{B.3}$$

the defining equation (B.1) for $M_{\kappa,\mu}(z)$ can be written in another form:

$$M_{\kappa,\mu}(z) = \mathrm{e}^{+z/2} z^{1/2+\mu} \cdot {}_1F_1\left(\tfrac{1}{2} + \mu + \kappa; 2\mu + 1; -z\right). \tag{B.4}$$

It follows from equations (B.1) and (B.4) that

$$M_{\kappa,\mu}(z \cdot \mathrm{e}^{\pm i\pi}) = \mathrm{e}^{\pm i\pi(1/2+\mu)} \cdot M_{-\kappa,\mu}(z). \tag{B.5}$$

On the other hand, from equation (B.2), we immediately see that

$$W_{\kappa,-\mu}(z) = W_{\kappa,\mu}(z). \tag{B.6}$$

Replacing κ and z by $-\kappa$ and $z \cdot \mathrm{e}^{\pm i\pi}$, respectively, in equation (B.2), and applying equation (B.4), we obtain

$$W_{-\kappa,\mu}(z \cdot \mathrm{e}^{\pm\mathrm{i}\pi}) = \frac{\Gamma(-2\mu)\, \mathrm{e}^{\pm\mathrm{i}\pi(1/2+\mu)}}{\Gamma\left(\frac{1}{2} - \mu + \kappa\right)} M_{\kappa,\mu}(z) + \frac{\Gamma(2\mu)\, \mathrm{e}^{\pm\mathrm{i}\pi(1/2-\mu)}}{\Gamma\left(\frac{1}{2} + \mu + \kappa\right)} M_{\kappa,-\mu}(z). \tag{B.7}$$

Solving simultaneous equations (B.2) and (B.7) for $M_{\kappa,\mu}(z)$ and $M_{\kappa,-\mu}(z)$, we find that

$$M_{\kappa,-\mu}(z) = \frac{\Gamma(1-2\mu)\, \mathrm{e}^{\pm\mathrm{i}\pi\kappa}}{\Gamma\left(\frac{1}{2} - \mu - \kappa\right)} W_{-\kappa,\mu}(z \cdot \mathrm{e}^{\pm\mathrm{i}\pi}) - \frac{\Gamma(1-2\mu)\, \mathrm{e}^{\pm\mathrm{i}\pi(1/2+\mu+\kappa)}}{\Gamma\left(\frac{1}{2} - \mu + \kappa\right)} W_{\kappa,\mu}(z). \tag{B.8}$$

In particular, by considering the upper signs in equation (B.8), we obtain

$$M_{\kappa,-\mu}(z) = \frac{\Gamma(1-2\mu)\, \mathrm{e}^{\mathrm{i}\pi\kappa}}{\Gamma\left(\frac{1}{2} - \mu - \kappa\right)} W_{-\kappa,\mu}(z \cdot \mathrm{e}^{\mathrm{i}\pi}) - \frac{\Gamma(1-2\mu)\, \mathrm{e}^{-\mathrm{i}\pi(1/2+\mu+\kappa)}}{\Gamma\left(\frac{1}{2} - \mu + \kappa\right)} W_{\kappa,\mu}(z). \tag{B.9}$$

Replacing κ, μ and z by $\mathrm{i}\kappa$, $\mathrm{i}\mu$ and $z \cdot \mathrm{e}^{-\mathrm{i}\pi/2}$, respectively, in equation (B.9), we finally arrive at the relation

$$M_{\mathrm{i}\kappa,-\mathrm{i}\mu}(\mathrm{i}z) = \frac{\Gamma(1-2\mathrm{i}\mu)\, \mathrm{e}^{\pi\kappa}}{\Gamma\left(\frac{1}{2} - \mathrm{i}\mu - \mathrm{i}\kappa\right)} W_{-\mathrm{i}\kappa,\mathrm{i}\mu}(-\mathrm{i}z) + \mathrm{i} \frac{\Gamma(1-2\mathrm{i}\mu)\, \mathrm{e}^{\pi(\mu+\kappa)}}{\Gamma\left(\frac{1}{2} - \mathrm{i}\mu + \mathrm{i}\kappa\right)} W_{\mathrm{i}\kappa,\mathrm{i}\mu}(\mathrm{i}z). \tag{B.10}$$

Note that $W_{\mathrm{i}\kappa,\mathrm{i}\mu}(\mathrm{i}z)$ and $W_{-\mathrm{i}\kappa,\mathrm{i}\mu}(-\mathrm{i}z)$ are a complex conjugate pair for κ, μ and z being real; this fact can be proved easily using equations (B.2) and (B.6).

Appendix C. Second-order perturbation solutions for the metallic wedge

Here, we solve problem P_2 (72) for the metallic wedge. The solution procedure is much the same as the one used for problem P_1 (71) in section 7.

C.1. Extended angular functions of the second order for the metallic wedge

According to equations (60) and (61), we have the following second-order extended angular equations for the odd symmetry:

$$\frac{\partial^2 Q_j^{-(2)}(\phi,\rho)}{\partial\phi^2} - \{\hat{\eta}_j(\rho)\}^2 Q_j^{-(2)}(\phi,\rho) = -N_j^{-(2)}(\phi,\rho), \qquad j=1,2 \tag{C.1}$$

with nonhomogeneous terms

$$\begin{aligned} N_j^{-(2)}(\phi,\rho) &= \rho^2 \frac{\partial^2}{\partial\rho^2} Q_j^{-(1)}(\phi,\rho) + \frac{2\rho^2}{\hat{R}_u^{(0)}(\rho)} \left(\frac{\partial \hat{R}_u^{(0)}(\rho)}{\partial\rho}\right) \frac{\partial Q_j^{-(1)}(\phi,\rho)}{\partial\rho} \\ &+ \frac{2\rho^2}{\hat{R}_u^{(0)}(\rho)} \left(\frac{\partial \hat{R}_u^{(1)}(\rho)}{\partial\rho}\right) \frac{\partial Q_j^{-(0)}(\phi,\rho)}{\partial\rho} \\ &- \frac{2\rho^2 \hat{R}_u^{(1)}(\rho)}{\left\{\hat{R}_u^{(0)}(\rho)\right\}^2} \left(\frac{\partial \hat{R}_u^{(0)}(\rho)}{\partial\rho}\right) \frac{\partial Q_j^{-(0)}(\phi,\rho)}{\partial\rho} \\ &+ \rho \frac{\partial Q_j^{-(1)}(\phi,\rho)}{\partial\rho} - \hat{\xi}_u^{(1)}(\rho) Q_j^{-(1)}(\phi,\rho) - \hat{\xi}_u^{(2)}(\rho) Q_j^{-(0)}(\phi,\rho), \qquad j=1,2 \end{aligned} \tag{C.2}$$

subject to the boundary conditions

$$Q_j^{-(2)}(\alpha,\rho) = 0, \qquad j=1,2, \tag{C.3}$$

$$Q_j^{-(2)}(0,\rho) = 0, \qquad Q_j^{-(2)}(\pi,\rho) = 0, \qquad j=1,2, \tag{C.4}$$

$$\frac{1}{\varepsilon_1} \lim_{\phi\to\alpha-0} \frac{\partial}{\partial\phi} Q_1^{-(2)}(\phi,\rho) = \frac{1}{\varepsilon_2} \lim_{\phi\to\alpha+0} \frac{\partial}{\partial\phi} Q_2^{-(2)}(\phi,\rho), \tag{C.5}$$

where equation (C.3) is obtained from equation (63), equation (C.4) from the odd symmetry characteristics and equation (C.5) from equation (64).

The nonhomogeneous differential equations (C.1) can be solved using the Green's function method. For the metallic region $j=1$, by using the Green's function in equation (157), we have the solution

$$Q_1^{-(2)}(\phi,\rho) = \int_0^\alpha \hat{G}_1(\phi,\phi') N_1^{-(2)}(\phi',\rho)\,\mathrm{d}\phi' \qquad (0 \leqslant \phi \leqslant \alpha), \tag{C.6}$$

and hence

$$\begin{aligned} Q_1^{-(2)}(\phi,\rho) &= -\frac{\sinh\{(\phi-\alpha)\hat{\eta}_1(\rho)\}}{\hat{\eta}_1(\rho)} \int_0^\phi \frac{\sinh\{\phi'\hat{\eta}_1(\rho)\}}{\sinh\{\alpha\hat{\eta}_1(\rho)\}} N_1^{-(2)}(\phi',\rho)\,\mathrm{d}\phi' \\ &- \frac{\sinh\{\phi\hat{\eta}_1(\rho)\}}{\hat{\eta}_1(\rho)} \int_\phi^\alpha \frac{\sinh\{(\phi'-\alpha)\hat{\eta}_1(\rho)\}}{\sinh\{\alpha\hat{\eta}_1(\rho)\}} N_1^{-(2)}(\phi',\rho)\,\mathrm{d}\phi'. \end{aligned} \tag{C.7}$$

For the dielectric region $j=2$, by using the Green's function in equation (164), we obtain the solution

$$Q_2^{-(2)}(\phi,\rho) = \int_\alpha^\pi \hat{G}_2(\phi,\phi') N_2^{-(2)}(\phi',\rho)\,\mathrm{d}\phi' \qquad (\alpha \leqslant \phi \leqslant \pi), \tag{C.8}$$

and hence

$$Q_2^{-(2)}(\phi,\rho) = -\frac{\sinh\{(\pi-\phi)\hat{\eta}_2(\rho)\}}{\hat{\eta}_2(\rho)}\int_\alpha^\phi \frac{\sinh\{(\alpha-\phi')\hat{\eta}_2(\rho)\}}{\sinh\{(\pi-\alpha)\hat{\eta}_2(\rho)\}}N_2^{-(2)}(\phi',\rho)\,\mathrm{d}\phi' - \frac{\sinh\{(\alpha-\phi)\hat{\eta}_2(\rho)\}}{\hat{\eta}_2(\rho)}\int_\phi^\pi \frac{\sinh\{(\pi-\phi')\hat{\eta}_2(\rho)\}}{\sinh\{(\pi-\alpha)\hat{\eta}_2(\rho)\}}N_2^{-(2)}(\phi',\rho)\,\mathrm{d}\phi'. \tag{C.9}$$

C.2. Determination of the unified separation quantity of the second order for the metallic wedge

The boundary condition (C.5) is used for determining the second-order unified separation quantity $\hat{\zeta}_u^{(2)}(\rho)$. Substituting equations (C.7) and (C.9) into the left and right sides of equation (C.5), respectively, we find the simple relationship

$$\frac{1}{\varepsilon_1}\int_0^\alpha Q_1^{-(0)}(\phi',\rho)N_1^{-(2)}(\phi',\rho)\,\mathrm{d}\phi' + \frac{1}{\varepsilon_2}\int_\alpha^\pi Q_2^{-(0)}(\phi',\rho)N_2^{-(2)}(\phi',\rho)\,\mathrm{d}\phi' = 0. \tag{C.10}$$

Substituting equation (61) for $s = \mathrm{odd}\,(-)$ into equation (C.10) and rearranging terms, we find for the second-order unified separation quantity that

$$\hat{\zeta}_u^{(2)}(\rho) = \frac{\left[\begin{array}{l} \rho^2\left\{\frac{1}{\varepsilon_1}\int_0^\alpha Q_1^{-(0)}(\phi,\rho)\frac{\partial^2}{\partial\rho^2}Q_1^{-(1)}(\phi,\rho)\,\mathrm{d}\phi + \frac{1}{\varepsilon_2}\int_\alpha^\pi Q_2^{-(0)}(\phi,\rho)\frac{\partial^2}{\partial\rho^2}Q_2^{-(1)}(\phi,\rho)\,\mathrm{d}\phi\right\} \\ +\left\{\frac{2\rho^2}{\hat{R}_u^{(0)}(\rho)}\left(\frac{\partial\hat{R}_u^{(0)}(\rho)}{\partial\rho}\right)+\rho\right\}\left\{\begin{array}{l}\frac{1}{\varepsilon_1}\int_0^\alpha Q_1^{-(0)}(\phi,\rho)\frac{\partial}{\partial\rho}Q_1^{-(1)}(\phi,\rho)\,\mathrm{d}\phi \\ +\frac{1}{\varepsilon_2}\int_\alpha^\pi Q_2^{-(0)}(\phi,\rho)\frac{\partial}{\partial\rho}Q_2^{-(1)}(\phi,\rho)\,\mathrm{d}\phi\end{array}\right\} \\ +\left\{\frac{2\rho^2}{\hat{R}_u^{(0)}(\rho)}\left(\frac{\partial\hat{R}_u^{(1)}(\rho)}{\partial\rho}\right)-\frac{2\rho^2\hat{R}_u^{(1)}(\rho)}{\left\{\hat{R}_u^{(0)}(\rho)\right\}^2}\left(\frac{\partial\hat{R}_u^{(0)}(\rho)}{\partial\rho}\right)\right\}\left\{\begin{array}{l}\frac{1}{\varepsilon_1}\int_0^\alpha Q_1^{-(0)}(\phi,\rho)\frac{\partial}{\partial\rho}Q_1^{-(0)}(\phi,\rho)\,\mathrm{d}\phi \\ +\frac{1}{\varepsilon_2}\int_\alpha^\pi Q_2^{-(0)}(\phi,\rho)\frac{\partial}{\partial\rho}Q_2^{-(0)}(\phi,\rho)\,\mathrm{d}\phi\end{array}\right\} \\ -\hat{\zeta}_u^{(1)}(\rho)\left\{\frac{1}{\varepsilon_1}\int_0^\alpha Q_1^{-(0)}(\phi,\rho)Q_1^{-(1)}(\phi,\rho)\,\mathrm{d}\phi + \frac{1}{\varepsilon_2}\int_\alpha^\pi Q_2^{-(0)}(\phi,\rho)Q_2^{-(1)}(\phi,\rho)\,\mathrm{d}\phi\right\}\end{array}\right]}{\frac{1}{\varepsilon_1}\int_0^\alpha\left\{Q_1^{-(0)}(\phi,\rho)\right\}^2\mathrm{d}\phi + \frac{1}{\varepsilon_2}\int_\alpha^\pi\left\{Q_2^{-(0)}(\phi,\rho)\right\}^2\mathrm{d}\phi}, \tag{C.11}$$

where $\varepsilon_1 = \varepsilon_m$ and $\varepsilon_2 = \varepsilon_d$ are used for numerical calculations.

C.3. Unified radial function of the second order for the metallic wedge

The second-order unified radial equation (67) can be written using equation (100) as

$$\frac{\partial^2\hat{R}_u^{(2)}(\rho)}{\partial\rho^2} + \frac{1}{\rho}\frac{\partial\hat{R}_u^{(2)}(\rho)}{\partial\rho} + \left(\{\hat{k}_{mp}(\rho)\}^2 + \frac{\zeta_u^{(0)}(0)}{\rho^2}\right)\hat{R}_u^{(2)}(\rho) = -\frac{\hat{\zeta}_u^{(1)}(\rho)}{\rho^2}\hat{R}_u^{(1)}(\rho) - \frac{\hat{\zeta}_u^{(2)}(\rho)}{\rho^2}\hat{R}_u^{(0)}(\rho). \tag{C.12}$$

From equation (69), we have the boundary condition

$$\hat{R}_u^{(2)}(\rho) = 0 \qquad (\rho \to 0). \tag{C.13}$$

The differential equation (C.12) subject to the boundary condition (C.13) can be solved in the same manner as the first-order unified radial equation (174), so that we find the solution

$$\hat{R}_u^{(2)}(\rho) = \hat{R}_{\mathrm{in}}^{(2)}(\rho) + \hat{R}_{\mathrm{out}}^{(2)}(\rho), \tag{C.14}$$

where

$$\hat{R}_{\rm in}^{(2)}(\rho) = -\frac{\pi \mathrm{i}}{4} H_{i\nu}^{(2)}(\rho \hat{k}_{mp}(\rho)) \times \int_0^{\rho} \left\{ \hat{\zeta}_u^{(1)}(\rho') \hat{R}_u^{(1)}(\rho') + \hat{\zeta}_u^{(2)}(\rho') \hat{R}_u^{(0)}(\rho') \right\} H_{i\nu}^{(1)}(\rho' \hat{k}_{mp}(\rho')) \frac{\mathrm{d}\rho'}{\rho'} \tag{C.15}$$

and

$$\hat{R}_{\rm out}^{(2)}(\rho) = \frac{\pi \mathrm{i}}{4} H_{i\nu}^{(1)}(\rho \hat{k}_{mp}(\rho)) \times \int_0^{\rho} \left\{ \hat{\zeta}_u^{(1)}(\rho') \hat{R}_u^{(1)}(\rho') + \hat{\zeta}_u^{(2)}(\rho') \hat{R}_u^{(0)}(\rho') \right\} H_{i\nu}^{(2)}(\rho' \hat{k}_{mp}(\rho')) \frac{\mathrm{d}\rho'}{\rho'}. \tag{C.16}$$

The functions $\hat{R}_{\rm in}^{(2)}(\rho)$ and $\hat{R}_{\rm out}^{(2)}(\rho)$ correspond to the incoming and outgoing waves, respectively, for $\rho \to \infty$.

Appendix D. Second-order perturbation solutions for the metallic V-groove

Here, we solve problem P_2 (72) for the metallic V-groove. The solution procedure is much the same as the one used for problem P_1 (71) in section 8.

D.1. Extended angular functions of the second order for the metallic V-groove

According to equations (60) and (61), we have the second-order extended angular equations for the even symmetry

$$\frac{\partial^2 Q_j^{+(2)}(\phi, \rho)}{\partial \phi^2} - \{\tilde{\eta}_j(\rho)\}^2 Q_j^{+(2)}(\phi, \rho) = -N_j^{+(2)}(\phi, \rho), \qquad j = 1, 2 \tag{D.1}$$

with nonhomogeneous terms

$$\begin{aligned} N_j^{+(2)}(\phi, \rho) &= \rho^2 \frac{\partial^2}{\partial \rho^2} Q_j^{+(1)}(\phi, \rho) + \frac{2\rho^2}{\tilde{R}_u^{(0)}(\rho)} \left(\frac{\partial \tilde{R}_u^{(0)}(\rho)}{\partial \rho} \right) \frac{\partial Q_j^{+(1)}(\phi, \rho)}{\partial \rho} \\ &+ \frac{2\rho^2}{\tilde{R}_u^{(0)}(\rho)} \left(\frac{\partial \tilde{R}_u^{(1)}(\rho)}{\partial \rho} \right) \frac{\partial Q_j^{+(0)}(\phi, \rho)}{\partial \rho} \\ &- \frac{2\rho^2 \tilde{R}_u^{(1)}(\rho)}{\left\{ \tilde{R}_u^{(0)}(\rho) \right\}^2} \left(\frac{\partial \tilde{R}_u^{(0)}(\rho)}{\partial \rho} \right) \frac{\partial Q_j^{+(0)}(\phi, \rho)}{\partial \rho} \\ &+ \rho \frac{\partial Q_j^{+(1)}(\phi, \rho)}{\partial \rho} - \tilde{\zeta}_u^{(1)}(\rho) Q_j^{+(1)}(\phi, \rho) - \tilde{\zeta}_u^{(2)}(\rho) Q_j^{+(0)}(\phi, \rho), \qquad j = 1, 2 \end{aligned} \tag{D.2}$$

subject to the boundary conditions

$$Q_j^{+(2)}(\alpha, \rho) = 0, \qquad j = 1, 2, \tag{D.3}$$

$$\frac{\partial}{\partial \phi} Q_j^{+(2)}(\phi, \rho) \bigg|_{\phi=0} = 0, \qquad \frac{\partial}{\partial \phi} Q_j^{+(2)}(\phi, \rho) \bigg|_{\phi=\pi} = 0, \qquad j = 1, 2, \tag{D.4}$$

$$\frac{1}{\varepsilon_1} \lim_{\phi \to \alpha - 0} \frac{\partial}{\partial \phi} Q_1^{+(1)}(\phi, \rho) = \frac{1}{\varepsilon_2} \lim_{\phi \to \alpha + 0} \frac{\partial}{\partial \phi} Q_2^{+(1)}(\phi, \rho) \tag{D.5}$$

where equation (D.3) is obtained from equation (63), equation (D.4) from the even symmetry characteristics and equation (D.5) from equation (64).

The nonhomogeneous differential equations (D.1) can be solved using the Green's function method. For the dielectric region $j = 1$, by using the Green's function in equation (191), we have the solution

$$Q_1^{+(2)}(\phi, \rho) = \int_0^{\alpha} \tilde{G}_1(\phi, \phi') N_1^{+(2)}(\phi', \rho)\, \mathrm{d}\phi' \qquad (0 \leqslant \phi \leqslant \alpha), \tag{D.6}$$

and hence

$$\begin{aligned} Q_1^{+(2)}(\phi, \rho) = &-\frac{\sinh\{(\phi - \alpha)\tilde{\eta}_1(\rho)\}}{\tilde{\eta}_1(\rho)} \int_0^{\phi} \frac{\cosh\{\phi'\tilde{\eta}_1(\rho)\}}{\cosh\{\alpha\tilde{\eta}_1(\rho)\}} N_1^{+(2)}(\phi', \rho)\, \mathrm{d}\phi' \\ &- \frac{\cosh\{\phi\tilde{\eta}_1(\rho)\}}{\tilde{\eta}_1(\rho)} \int_{\phi}^{\alpha} \frac{\sinh\{(\phi' - \alpha)\tilde{\eta}_1(\rho)\}}{\cosh\{\alpha\tilde{\eta}_1(\rho)\}} N_1^{+(2)}(\phi', \rho)\, \mathrm{d}\phi'. \end{aligned} \tag{D.7}$$

For the metallic region $j = 2$, by using Green's function in equation (198), we have the solution

$$Q_2^{+(2)}(\phi, \rho) = \int_{\alpha}^{\pi} \tilde{G}_2(\phi, \phi') N_2^{+(2)}(\phi', \rho)\, \mathrm{d}\phi' \qquad (\alpha \leqslant \phi \leqslant \pi), \tag{D.8}$$

and hence

$$\begin{aligned} Q_2^{+(1)}(\phi, \rho) = &-\frac{\cosh\{(\pi - \phi)\tilde{\eta}_2(\rho)\}}{\tilde{\eta}_2(\rho)} \int_{\alpha}^{\phi} \frac{\sinh\{(\alpha - \phi')\tilde{\eta}_2(\rho)\}}{\cosh\{(\pi - \alpha)\tilde{\eta}_2(\rho)\}} N_2^{+(1)}(\phi', \rho)\, \mathrm{d}\phi' \\ &- \frac{\sinh\{(\alpha - \phi)\tilde{\eta}_2(\rho)\}}{\tilde{\eta}_2(\rho)} \int_{\phi}^{\pi} \frac{\cosh\{(\pi - \phi')\tilde{\eta}_2(\rho)\}}{\cosh\{(\pi - \alpha)\tilde{\eta}_2(\rho)\}} N_2^{+(1)}(\phi', \rho)\, \mathrm{d}\phi'. \end{aligned} \tag{D.9}$$

D.2. Determination of the unified separation quantity of the second order for the metallic V-groove

The boundary condition (D.5) is used for determining the second-order unified separation quantity $\tilde{\zeta}_u^{(2)}(\rho)$. Substituting equations (D.7) and (D.9) into the left and right sides of equation (D.5), respectively, we find the simple relationship

$$\frac{1}{\varepsilon_1} \int_0^{\alpha} Q_1^{+(0)}(\phi', \rho) N_1^{+(2)}(\phi', \rho)\, \mathrm{d}\phi' + \frac{1}{\varepsilon_2} \int_{\alpha}^{\pi} Q_2^{+(0)}(\phi', \rho) N_2^{+(2)}(\phi', \rho)\, \mathrm{d}\phi' = 0. \tag{D.10}$$

Substituting equation (61) for $s =$ even $(+)$ into equation (C.10) and rearranging terms, we find for the second-order unified separation quantity that

$$\begin{aligned} &\tilde{\zeta}_u^{(2)}(\rho) \\ &= \frac{\left[\begin{array}{l} \rho^2 \left\{ \frac{1}{\varepsilon_1} \int_0^{\alpha} Q_1^{+(0)}(\phi, \rho) \frac{\partial^2}{\partial \rho^2} Q_1^{+(1)}(\phi, \rho)\, \mathrm{d}\phi + \frac{1}{\varepsilon_2} \int_{\alpha}^{\pi} Q_2^{+(0)}(\phi, \rho) \frac{\partial^2}{\partial \rho^2} Q_2^{+(1)}(\phi, \rho)\, \mathrm{d}\phi \right\} \\ + \left\{ \frac{2\rho^2}{\tilde{R}_u^{(0)}(\rho)} \left(\frac{\partial \tilde{R}_u^{(0)}(\rho)}{\partial \rho} \right) + \rho \right\} \left\{ \begin{array}{l} \frac{1}{\varepsilon_1} \int_0^{\alpha} Q_1^{+(0)}(\phi, \rho) \frac{\partial}{\partial \rho} Q_1^{+(1)}(\phi, \rho)\, \mathrm{d}\phi \\ + \frac{1}{\varepsilon_2} \int_{\alpha}^{\pi} Q_2^{+(0)}(\phi, \rho) \frac{\partial}{\partial \rho} Q_2^{+(1)}(\phi, \rho)\, \mathrm{d}\phi \end{array} \right\} \\ + \left\{ \frac{2\rho^2}{\tilde{R}_u^{(0)}(\rho)} \left(\frac{\partial \tilde{R}_u^{(1)}(\rho)}{\partial \rho} \right) - \frac{2\rho^2 \tilde{R}_u^{(1)}(\rho)}{\left\{ \tilde{R}_u^{(0)}(\rho) \right\}^2} \left(\frac{\partial \tilde{R}_u^{(0)}(\rho)}{\partial \rho} \right) \right\} \left\{ \begin{array}{l} \frac{1}{\varepsilon_1} \int_0^{\alpha} Q_1^{+(0)}(\phi, \rho) \frac{\partial}{\partial \rho} Q_1^{+(0)}(\phi, \rho)\, \mathrm{d}\phi \\ + \frac{1}{\varepsilon_2} \int_{\alpha}^{\pi} Q_2^{+(0)}(\phi, \rho) \frac{\partial}{\partial \rho} Q_2^{+(0)}(\phi, \rho)\, \mathrm{d}\phi \end{array} \right\} \\ -\tilde{\zeta}_u^{(1)}(\rho) \left\{ \frac{1}{\varepsilon_1} \int_0^{\alpha} Q_1^{+(0)}(\phi, \rho) Q_1^{+(1)}(\phi, \rho)\, \mathrm{d}\phi + \frac{1}{\varepsilon_2} \int_{\alpha}^{\pi} Q_2^{+(0)}(\phi, \rho) Q_2^{+(1)}(\phi, \rho)\, \mathrm{d}\phi \right\} \end{array} \right]}{\frac{1}{\varepsilon_1} \int_0^{\alpha} \left\{ Q_1^{+(0)}(\phi, \rho) \right\}^2 \mathrm{d}\phi + \frac{1}{\varepsilon_2} \int_{\alpha}^{\pi} \left\{ Q_2^{+(0)}(\phi, \rho) \right\}^2 \mathrm{d}\phi}, \end{aligned} \tag{D.11}$$

where $\varepsilon_1 = \varepsilon_d$ and $\varepsilon_2 = \varepsilon_m$ are used for numerical calculations. Note that equation (D.11) becomes equation (C.11) by replacing even $(+)$ by odd $(-)$ and tilde $(\tilde{})$ by circumflex $(\hat{})$.

D.3. Unified radial function of the second order for the metallic V-groove

According to equations (121)–(125), the second-order unified radial equation (67) roughly approximates to

$$\frac{\partial^2 \tilde{R}_u^{(2)}(\rho)}{\partial \rho^2} + \frac{1}{\rho}\frac{\partial \tilde{R}_u^{(2)}(\rho)}{\partial \rho} + \left(\{\tilde{k}_{mp}(\rho)\}^2 + \frac{\nu^2 q_1}{\rho} + \frac{\nu^2}{\rho^2} \right) \tilde{R}_u^{(2)}(\rho)$$
$$= -\frac{\tilde{\zeta}_u^{(1)}(\rho)}{\rho^2}\tilde{R}_u^{(1)}(\rho) - \frac{\tilde{\zeta}_u^{(2)}(\rho)}{\rho^2}\tilde{R}_u^{(0)}(\rho). \tag{D.12}$$

From equation (69), we have the boundary condition

$$\tilde{R}_u^{(2)}(\rho) = 0 \qquad (\rho \to 0). \tag{D.13}$$

The differential equation (D.12) subject to the boundary condition (D.13) can be solved in the same manner as the first-order unified radial equation (174), so that we find the solution

$$\hat{R}_u^{(2)}(\rho) = \hat{R}_{\text{in}}^{(2)}(\rho) + \hat{R}_{\text{out}}^{(2)}(\rho), \tag{D.14}$$

where

$$\tilde{R}_{\text{in}}^{(2)}(\rho) = -\mathrm{i}\mathrm{e}^{\kappa\pi}\rho^{-1/2}W_{\mathrm{i}\kappa,\mathrm{i}\nu}(2\mathrm{i}\rho\tilde{k}_{mp}(0)) \int_0^\rho \left\{ \tilde{\zeta}_u^{(1)}(\rho')\tilde{R}_u^{(1)}(\rho') + \tilde{\zeta}_u^{(2)}(\rho')\tilde{R}_u^{(0)}(\rho') \right\}$$
$$\times\, W_{-\mathrm{i}\kappa,\mathrm{i}\nu}(-2\mathrm{i}\rho'\tilde{k}_{mp}(0))\frac{\mathrm{d}\rho'}{2\tilde{k}_{mp}(0)(\rho')^{3/2}} \tag{D.15}$$

and

$$\tilde{R}_{\text{out}}^{(2)}(\rho) = \mathrm{i}\mathrm{e}^{\kappa\pi}\rho^{-1/2}W_{-\mathrm{i}\kappa,\mathrm{i}\nu}(-2\mathrm{i}\rho\tilde{k}_{mp}(0)) \int_0^\rho \left\{ \tilde{\zeta}_u^{(1)}(\rho')\tilde{R}_u^{(1)}(\rho') + \tilde{\zeta}_u^{(2)}(\rho')\tilde{R}_u^{(0)}(\rho') \right\}$$
$$\times\, W_{\mathrm{i}\kappa,\mathrm{i}\nu}(2\mathrm{i}\rho'\tilde{k}_{mp}(0))\frac{\mathrm{d}\rho'}{2\tilde{k}_{mp}(0)(\rho')^{3/2}}. \tag{D.16}$$

The functions $\tilde{R}_{\text{in}}^{(2)}(\rho)$ and $\tilde{R}_{\text{out}}^{(2)}(\rho)$ correspond to the incoming and outgoing waves, respectively, for $\rho \to \infty$.

References

[1] Novotny L and Hecht B 2006 *Principles of Nano-Optics* (New York: Cambridge University Press)
[2] Brongersma M L and Kik P G 2007 *Surface Plasmon Nanophotonics* (Dordrecht: Springer)
[3] Luo X and Ishijhara T 2004 Surface plasmon resonant interference nanolithography technique *Appl. Phys. Lett.* **84** 4780
[4] Srituravanich W, Fang N, Sun C, Luo Q and Zhang X 2004 Plasmonic nanolithography *Nano Lett.* **4** 1085
[5] Liu Z-W, Wei Q-G and Zhang X 2005 Surface plasmon interference nanolithography *Nano Lett.* **5** 957
[6] Liu Z, Xi D, Pile D, Luo Q, Fang N and Zhang X 2007 Enhanced backward scattering by surface plasmons on silver film *Appl. Phys.* A **87** 157
[7] Doskolovich L L, Kadomina E A and Kadomin I I 2007 Nanoscale photolithography by means of surface plasmon interference *J. Opt.* A **9** 854
[8] Takahara J and Kobayashi T 2004 Low-dimensional optical waves and nano-optical circuits *Opt. Photon. News* **15** 54
[9] Takahara J and Kusunoki F 2007 Guiding and nanofocusing of two-dimensional optical beam for nanooptical integrated circuits *IEICE Trans. Electron.* **E90C** 87
[10] Chang D E, Sørensen A S, Denler E A and Lukin M D 2007 A single-photon transistor using nanoscale surface plasmons *Nat. Phys.* **3** 807
[11] Akimov A V, Mukherjee A, Yu C L, Chang D E, Zibrov A S, Hemmer P R, Park H and Lukin M D 2007 Generation of single optical plasmons in metallic nanowires coupled to quantum dots *Nature* **450** 402
[12] Kawata S 2001 *Near-field Optics and Surface Plasmon Polaritons* (Berlin: Springer)

[13] Tominaga J 2003 *Optical Nanotechnologies: The Manipulation of Surface and Local Plasmons* (Berlin: Springer)
[14] Kneipp K, Wang Y, Kneipp H, Perelman L T, Itzkan I, Dasari R R and Feld M S 1997 Single molecule detection using surface-enhanced Raman scattering (SERS) *Phys. Rev. Lett.* **78** 1667
[15] Nie S and Emory S R 1997 Probing single molecules and single nanoparticles by surface-enhanced Raman scattering *Science* **275** 1102
[16] Hartschuh A, Pedrosa H N, Novotny L and Krauss T D 2003 Simultaneous fluorescence and Raman scattering from single carbon nanotubes *Science* **301** 1354
[17] Pettinger B, Ren B, Picardi G, Schuster R and Ertl G 2004 Nanoscale probing of adsorbed species by tip-enhanced Raman spectroscopy *Phys. Rev. Lett.* **92** 096101
[18] Ichimura T, Hayazawa N, Hashimoto M, Inouye Y and Kawata S 2004 Tip-enhanced coherent anti-Stokes Raman scattering for vibrational nanoimaging *Phys. Rev. Lett.* **92** 220801
[19] Anderson N, Bouhelier A and Novotny L 2006 Near-field photonics: tip-enhanced microscopy and spectroscopy on the nanoscale *J. Opt.* A **8** S227
[20] Kneeipp K 2007 Surface-enhanced Raman scattering *Phys. Today* **60** 40
[21] Gurrev M Y and Mironov M A 2007 Superfocusing of a spherical wave: theory and experiment *Acoust. Phys.* **53** 683
[22] Nerkararyan Kh V 1997 Superfocusing of a surface polariton in a wedge-like structure *Phys. Lett.* A **237** 103
[23] Babadjanyan A J, Margaryan N L and Nerkararyan Kh V 2000 Superfocusing of surface polaritons in the conical structure *J. Appl. Phys.* **87** 3785
[24] Janunts N A, Bagdasaryan K S and Nerkararyan Kh V 2000 Superfocusing of surface polaritons in the system of two touching metallic semicylinders *Phys. Lett.* A **269** 257
[25] Stockman M I 2004 Nanofocusing of optical energy in tapered plasmonic waveguides *Phys. Rev. Lett.* **93** 137404
[26] Gramotnev D K 2005 Adiabatic nanofocusing of plasmons by sharp metallic grooves: geometrical optics approach *J. Appl. Phys.* **98** 104302
[27] Janunts N A, Bagdasaryan K S, Nerkararyan Kh V and Hecht B 2005 Excitation and superfocusing of surface plasmon polaritons on a silver-coated optical fiber tip *Opt. Commun.* **253** 118
[28] Babayan A E and Nerkararyan Kh V 2007 The strong localization of surface plasmon polariton on a metal-coated tip of optical fiber *Ultramicroscopy* **107** 1136
[29] Gramotnev D K and Vernon K C 2007 Adiabatic nano-focusing of plasmons by sharp metallic wedges *Appl. Phys.* B **86** 7
[30] Gramotnev D K, Pile D F, Vogel M W and Zhang X 2007 Local electric field enhancement during nanofocusing of plasmons by a tapered gap *Phys. Rev.* B **75** 035431
[31] Vogel M W and Gramotnev D K 2007 Adiabatic nano-focusing of plasmons by metallic tapered rods in the presence of dissipation *Phys. Lett.* A **363** 507
[32] Vernon K C and Gramotnev D K 2007 Adiabatic nanofocusing of plasmons by a sharp metal wedge on a dielectric substrate *J. Appl. Phys.* **101** 104312
[33] Pile D F P and Gramotnev D K 2004 Channel plasmon-polariton in a triangular groove on a metal surface *Opt. Lett.* **29** 1069
[34] Gramotnev D K and Pile D F P 2004 Single-mode subwavelength waveguide with channel plasmon-polaritons in triangular grooves on a metal surface *Appl. Phys. Lett.* **85** 6323
[35] Pile D F P and Gramotnev D K 2005 Plasmonic subwavelength waveguides: next to zero losses at sharp bends *Opt. Lett.* **30** 1186
[36] Pile D F P, Ogawa T, Gramotnev D K, Okamoto T, Haraguchi M, Fukui M and Matsuo S 2005 Theoretical and experimental investigation of strongly localized plasmons on triangular metal wedges for subwavelength waveguiding *Appl. Phys. Lett.* **87** 061106
[37] Pile D F P and Gramotnev D K 2006 Adiabatic and nonadiabatic nanofocusing of plasmons by tapered gap plasmon waveguides *Appl. Phys. Lett.* **89** 041111, 119901 (erratum)
[38] Pile D F P, Gramotnev D K, Haraguchi M, Okamoto T and Fukui M 2006 Numerical analysis of coupled wedge plasmons in a structure of two metal wedges separated by a gap *J. Appl. Phys.* **100** 013101
[39] Maier S A, Andrews S R, Martín-Moreno L and García-Vidal F J 2006 Terahertz surface plasmon-polariton propagation and focusing on periodically corrugated metal wires *Phys. Rev. Lett.* **97** 176805
[40] Kurihara K, Otomo A, Syouji A, Takahara J, Suzuki K and Yokoyama S 2007 Superfocusing modes of surface plasmon polaritons in conical geometry based on the quasi-separation of variables approach *J. Phys. A: Math. Theor.* **40** 12479
[41] Temme N M 1996 *Special Function: An Introduction to the Classical Functions of Mathematical Physics* (New York: Wiley)
[42] Olver F W J 1997 *Asymptotics and Special Functions* (Natick: A K Peters)

[43] Lebedev N N 1972 *Special Functions and their Applications* (New York: Dover)
[44] Samble J R, Bradbery G W and Yang F 1991 Optical excitation of surface plasmons: an introduction *Contemp. Phys.* **32** 173
[45] Kurihara K, Nakamura K and Suzuki K 2002 Asymmetric SPR sensor response curve-fitting equation for the accurate determination of SPR resonance angle *Sensors Actuators* B **86** 49
[46] Farlow S J 1993 *Partial Differential Equations for Scientists and Engineers* (New York: Dover)
[47] Jackson J D 1998 *Classical Electrodynamics* 3rd edn (Hoboken: Wiley)
[48] Dunster T M 1990 Bessel functions of purely imaginary order, with an application to second-order linear differential equations having a large parameter *SIAM J. Math. Anal.* **21** 995
[49] Whittaker E T and Watson G N 1927 *A Course of Modern Analysis* 4th edn (Cambridge: Cambridge University Press)
[50] Buchholz H 1969 *The Confluent Hypergeometric Function with Special Emphasis on its Applications* (Berlin: Springer)
[51] Dunster T M 1989 Uniform asymptotic expansions for Whittakers's confluent hypergeometric functions *SIAM J. Math. Anal.* **20** 744
[52] Arfken G B and Weber H J 2005 *Mathematical Methods for Physics* 6th edn (Amsterdam: Elsevier)
[53] Abramowitz M and Stegun I A 1972 *Handbook of Mathematical Functions with Formulas, Graphs, and Mathematical Tables* (New York: Dover)
[54] Olver F W 1980 Whittaker functions with both parameters large: uniform approximations in terms of parabolic cylinder functions *Proc. R. Soc. Edinburgh* **86A** 213
[55] Dunster T M 2003 Uniform asymptotic approximations for the Whittaker functions $M_{\kappa,i\mu}(z)M_{\kappa,i\mu}(z)$ *Anal. Appl.* **1** 199